

---

## MORE ADVANCED PROBLEMS

Both of the examples presented in Chapter 7 might be considered simple problems as the material considered was isotropic and homogeneous, and a single type of mesh was used to analyse each structure. In this chapter the use of more advanced modelling techniques will be demonstrated, although still with linear static analysis. First, a beam made of a laminated composite material will be considered and then a steel frame, which will be analysed using the substructuring technique. In both examples parts of their structure are subjected to compressive stresses whose magnitudes have been checked to verify that no buckling instabilities will occur and so this aspect of structural design will not be considered further.

### 8.1 COMPOSITE MATERIAL OPEN-SECTIONED BEAM

The purpose of this example is to illustrate the use of commercial software in providing solutions for the class of engineering structures where the structure is made from laminations of materials that have anisotropic properties. These advanced composite materials have been developed over the last 30 years to have mechanical and other properties that make them attractive alternatives to the conventional structural materials such as metal alloys.

The word 'composite' is used, strictly, to describe a wide range of engineering materials whose essential characteristic is that there is more than one distinct material phase. Consequently, virtually all materials are composites. For example, in a metal alloy the dispersion of two or more phases is brought about by careful heat treatment. Here, however, the discussion of composites will be restricted to two-phase materials having discrete, long, cylindrical inclusions (or continuous fibres) in a continuum of a second phase or matrix. The fibres,  $2\mu\text{m}$  or less in

diameter, are usually of carbon, glass or aramid, although ceramic and metal fibres are being introduced, whereas the matrix can be of a polymer resin, metal or ceramic material.

Here the discussion will also be restricted to those materials of laminated construction where different layers are made up of different or similar composite material with dissimilar orientation of the fibres. Such multi-layered materials, often referred to as laminated composites, consist typically of between 16 and 120 laminae. These materials were initially used in the structures of high-performance aircraft exploiting their high strength-to-weight ratio, but they are increasingly being used in structural applications across all engineering industries.

Before addressing the actual beam problem, the ways in which these laminate composites are built up must be considered, as well as the ways in which the finite element method is adapted to model their material properties. Only after this introductory material can the problem be described and a finite element model be built and analysed.

### 8.1.1 Properties of Laminate and Laminated Materials

Figure 8.1 illustrates a unidirectional fibre-reinforced lamina which is the basic building block of a multi-layered laminate (Halpin, 1992). The material of the lamina is assumed to be homogeneous and orthotropic, i.e. there are only three

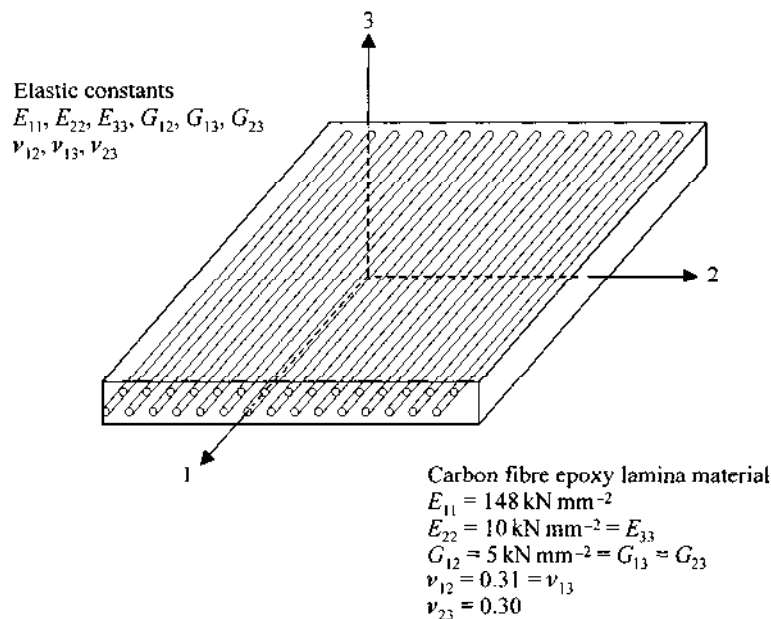


**Figure 8.1** Schematic representation of a unidirectional composite, showing principal axes.

mutually perpendicular planes of symmetry of material properties at any one point. Also, it is assumed that there is a perfect bond between the fibres and matrix, that the composite has linear elastic properties, and that the elastic behaviour of the material in tension and compression is the same. It is often a good assumption to assume that stress-strain relationships are linear elastic up to ultimate failure, as shown in Fig. 2.6(d).

By convention, the principal axes of a lamina are labelled 1, 2 and 3 with the 1-axis parallel to the fibres. Since there is isotropic symmetry in the 23-plane which is normal to the fibres, a unidirectional reinforced lamina is a transversely isotropic material. Hence six independent elastic constants (i.e.  $E_{11}$ ,  $E_{22}$ ,  $G_{12}$ ,  $G_{23}$ ,  $\nu_{12}$ ,  $\nu_{23}$ ) must be used to generate the terms for the full three-dimensional form of Hooke's law, Eq. (2.15). These constants are given in Fig. 8.1 for the carbon fibre epoxy material used here. Note that the  $E$ s are the principal Young's moduli and the  $G$ s are the principal shear moduli. Also note that for the lamina considered here the subscripts on the stresses and strains in (2.15) need to be changed from  $x$ ,  $y$  and  $z$  to 1, 2 and 3, respectively.

Note that there are problems when obtaining material property data for a unidirectional fibre-reinforced lamina material. Owing to anisotropy many standard coupon tests (see Sec. 2.2.6), are needed to determine the six elastic constants and six ultimate strengths. As there are different modes of failure in compression and in tension, these strengths, along and normal to the fibres, are very different.

Table 2.1 gives a range of mechanical properties for unidirectional materials with a polymer matrix. This data can be obtained only after the material has been manufactured and it depends on the volume fraction of fibre, fibre placement and the method of manufacture. Equally, many combinations of fibres and matrix are available and new combinations are appearing all the time, so it is difficult for an analyst to have data for all the materials available. Hence, analysts must check any lamina data and use only values that will ensure a safe design.

Figure 8.2 shows a general laminate which consists of four unidirectional laminae of constant thickness. Here, the fibre directions are not aligned to the principal loading direction, the local laminate  $x$ -direction (i.e. the 0 degree direction). To identify the lamination configuration, a notation derived from the fibre directions, i.e.  $(-45/30/30/-45)$ , is used. In practice, there are several types of lamination configuration and a number of these are used in the example.

When a lamina is orientated at a general angle to the local laminate  $x$ -direction of the laminate, the generalized Hooke's laws (2.15), for the layer are obtained using standard axis transformations. Note that the stresses and strains are now in terms of the Cartesian axis system and the terms in matrix  $[D]$  are functions the lamina stiffness terms. Once the stress-strain relationship for the lamina is known together with its position in a laminate, it is possible to form the relationships between the stress resultants due to axial forces and bending moments and the membrane strains and plate curvatures respectively (Halpin, 1992).

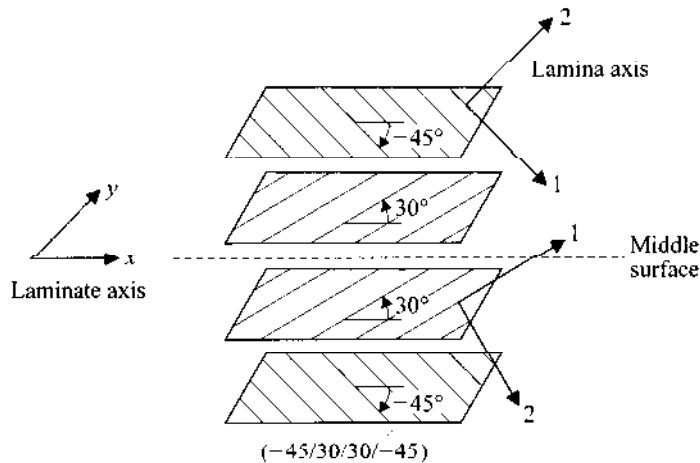


**Figure 8.2** An example of notation for a laminate.

### 8.1.2 Laminated Composites and the Finite Element Method

Here, only a brief introduction to the ways in which the finite element method is used to model anisotropic laminated material properties will be given. Laminated composites are usually represented by a series of equivalent laminated homogeneous plates or shells. Here, the standard form of the element (see Chapter 3) is used, but with the appropriate laminate properties constructed from a compact description of the laminate stacking sequence and lamina material properties, as discussed at the end of Sec. 8.1.1, where relationships for the axial, coupling and bending stiffnesses are produced.

To develop the element properties, the pre-processor is used to define the elastic constants of a lamina and the configuration of the lamination. Then, within the solver, the stiffness matrices for the laminate can be calculated, and assigned to the elements. Hence, when dealing with a laminated composite material as opposed to an isotropic material, it is only the material properties, i.e. the terms in matrix  $[D]$ , that change when element stiffness matrices are formed using (3.9). Note that for all element types, laminate properties may introduce coupling effects between membrane and bending actions that radically change the deformation from what might be expected if the material were isotropic. These coupling effects must be included in the analysis.

Laminated thin-shell elements, both linear and quadratic, are often formulated using approximate solutions to the Mindlin shell theory. This accounts for shear deformation by forcing the normals to a shell to remain straight but then allowing them to rotate such that they are not normal any more. Note that the transverse shear actually causes a normal to become curved. When deformation takes place, if the normals are assumed to remain straight and normal to the surface, which is Kirchhoff's assumption, the laminated shell element is

formulated using classical lamination theory. However, as the inclusion of shear deformation is usually necessary when analysing laminate structures, many solvers do not use classical lamination theory elements at all.

Once nodal displacements have been calculated, the stresses and strains in individual layers have to be recovered and resolved into the appropriate material axes. This data is used to determine a number of layer-by-layer failure criteria, and these are strongly influenced by the method of stress recovery. For laminates this is often the weak link in the analysis. Interpretation of any failure prediction is further hampered by the lack of any general consensus as to the best criterion to use. It is for this reason that failure predictions will not be presented here.

Some solvers allow laminates, and other layered composites, to be constructed of so-called stackable plate and solid elements. This allows a partial three-dimensional analysis to be carried out at a fraction of the cost of a full layer-by-layer analysis with solid elements.

### 8.1.3 Problem Specification

A symmetrical open-section I-beam of length 1600 mm is to be tested in three-point bending; the dimensions of the I-shaped cross-section are given in Fig. 8.3(a). The web and flanges are formed from laminate panels 2 mm thick and consist of 16 laminae of a unidirectional carbon fibre epoxy high-modulus material. Three different lamination configurations for web and flange panels are used and these are detailed later.

The loading arrangement is shown in Fig. 8.3(b), where simple supports are placed 1600 mm apart and a central vertical load of 1 kN is applied to the top

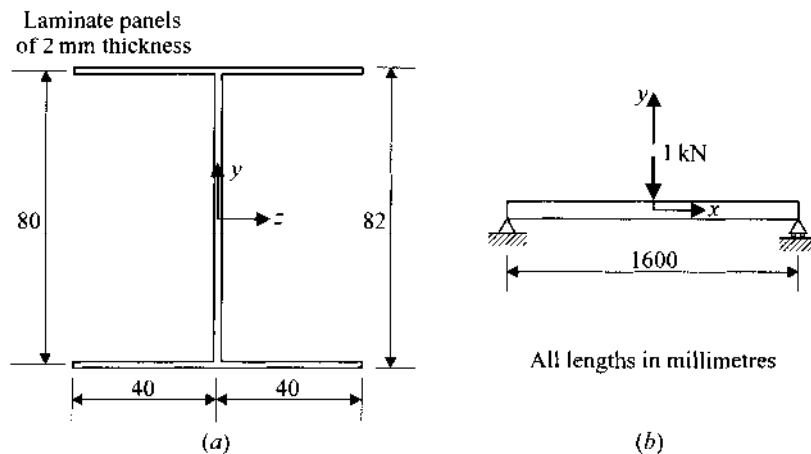


**Figure 8.3** The composite material beam problem: (a) the I-section, (b) the three-point loading arrangement.

flange. This load has been chosen to ensure that any displacements of the beam are small. As well as this configuration, spans of 400, 800 and 1200 mm are also analysed.

The above situations are analysed for the following reasons:

- To illustrate how the deformation of the cross-section is affected by the coupling that can exist between bending and twisting, and membrane and bending actions, when different types of lamination configurations are used.
- To show typical strain and stress output from a finite element analysis for a laminated composite panel.
- To determine the section flexural modulus, and the section shear modulus of the I-section. Note that a given section modulus is not necessarily the same as the corresponding material modulus, as the former will be determined from a theoretical expression for deflection, while the latter is determined using standard material coupon test methods. Both section properties will be found using an extension of beam theory developed in the next section, together with a graphical procedure.

#### 8.1.4 An Extension of Simple Beam Theory

In Sec. 8.1.2 it was stated that laminated structures are often modelled with laminated shell elements formulated using Mindlin shell theory. This is because of the important role that material properties play in determining the deformation of a structure, such that a theoretical model which is acceptable for an isotropic material may not be acceptable for an anisotropic material. Analysts must, therefore, plan a finite element analysis with due regard to the likely deformation behaviour and, when developing the model, choose the best element available.

To illustrate why, for example, shear deformation is not to be ignored when using laminated composites, consider again the simple bending problem of a prismatic beam, introduced at the end of Chapter 2. There, (2.25) gives the general relationship used to analyse bending. It is derived by assuming that the properties of the beam can be lumped along the centroidal axis and that when bending occurs Kirchhoff's assumption holds. For a small displacement analysis, the expression

$$R = \pm \frac{1}{\frac{d^2 v}{dx^2}} \quad (8.1)$$

where  $R$  is the radius of curvature,  $v$  is the deflection of the beam in the  $y$ -direction at the centroidal axis and  $x$  is the local coordinate along the beam's centroidal axis, can be used to form the well-known moment-curvature relationship

$$\frac{M(x)}{EI_a} = \pm \frac{d^2 v(x)}{dx^2} \quad (8.2)$$

Expressions for the deflection at any position along the beam can be obtained using (8.2) if the variation in bending moment along the beam is known together with the boundary conditions for deflection and its slope.

For the three-point bending problem shown in Fig. 8.3, the maximum deflection due to bending is at the mid-span and is given by the well-known expression

$$v_b = \frac{PL^3}{48E_b I_a} \quad (8.3)$$

where  $P$  is the applied load,  $L$  is the span and  $E_b$  is the beam section flexural modulus. Here the negative sign has been ignored for convenience.

Except for the situation where the beam is loaded by a pure moment, shear forces are always present and are transmitted through the cross-section of the beam. These shear forces cause shear stresses that give rise to an additional deflection, known as shear deformation. It can be shown using linear elastic assumptions that this second deflection component is also maximum at mid-span and is given by

$$v_s = \frac{PL}{4K_s G_b A} \quad (8.4)$$

where  $K_s$  is the shear correction factor that accounts for the shear stress distribution not being constant over the cross-sectional area,  $G_b$  is the beam section shear modulus and  $A$  is the area of the cross-section. Values for  $K_s$  are available in the literature for beams with isotropic or orthotropic properties and for a number of cross-section shapes. However, to simplify (8.4) for the purpose of engineering design with I-sectioned beams, it is acceptable to assume that  $K_s \equiv A_w/A$ , where  $A_w$  is the area of the web, implying that the shear force is transmitted by the web alone and that the shear stress distribution is constant.

Combining the deflection components from bending and shear, the maximum deflection is given by

$$v_{\max} = v_b + v_s = \frac{PL^3}{48E_b I_a} + \frac{PL}{4G_b A_w} \quad (8.5)$$

It is usually acceptable, however, when considering isotropic beams to ignore the shear deflection component. To see why, consider the relative magnitudes of the two deflection components. Looking at the terms in (8.5), it can be seen that

$$\frac{v_s}{v_b} = \frac{12E_b I_a}{G_b A_w L^2} \quad (8.6)$$

If the material is isotropic, then the ratio  $E_b/G_b$  (or  $E/G$ ) is 2.6. For this case the shear deformation is small compared to the bending deformation, provided that the beam has a span-to-depth ratio of greater than 5. For typical steel beams this is the case. If not then the beam is termed *stocky* and shear deformation must be accounted for. The situation is, however, very different for an identical beam made of laminated composite material, as  $E_b/G_b$  is much greater than 2.6, possibly 30 or more. Hence, from equation (8.6),  $v_s$  cannot be ignored. As a rule of

thumb the shear deformation contribution to  $v_{\max}$  must be included for a laminated composite beam when the span-to-depth ratio is less than 25.

In Fig. 8.3, the span-to-depth ratio for the beam is 19.5, but this decreases to 4.9 when the span is 400 mm. For all cases, therefore, the shear deformation behaviour is expected to be significant and so this beam problem cannot be modelled using standard one-dimensional beam elements, as would be the case if material were isotropic.

### 8.1.5 Defining the Finite Element Model

Before beginning to build a model of the beam, the problem must be considered a little more. To take advantage of any symmetry in the problem a suitable choice of coordinate system and origin is required. Figure 8.3 shows the global system, where the  $x$ -direction is along the span of the beam, the  $y$ -direction is in the vertical direction and the  $z$ -direction is horizontal across the flanges. For this system, the origin is placed at the mid-span in the  $x$ -direction and at the centroid of the cross-section (i.e. at mid-depth of web).

There are also certain expectations of the deformation of the beam when subjected to three-point bending. Applying symmetry arguments, the cross-section at mid-span will be restrained such that it moves only in the  $z$ - $y$  plane, i.e. it is a plane of mirror symmetry. If the material is isotropic and any displacements are small, then from Kirchhoff's assumption the normals will remain straight and normal, such that any cross-section remains planar. In this situation (2.25) holds and so, given the symmetry in the  $x$ -direction, only one-quarter of the beam need be modelled. However, sections do not necessarily remain planar because of shear deformation and coupling effects, as discussed in the last section, and so the model will be for the half-beam about the mid-span. Finally, if the mid-span plane is restrained to move in the  $y$ - $z$  plane, then one of the simple supports must be free to move in the  $x$ -direction to prevent membrane action being induced in the flanges.

**Geometry and mesh description** The geometry of the physical beam is shown in Fig. 8.3. As the panels have a thickness of only 2 mm relative to a minimum width of 40 mm, they can be considered to be thin plates. This leads us to use elements known as thin laminated shell elements to model the beam. These elements are placed such that they are at the mid-plane of the panels, and so care is needed to ensure their correct location. Each of the three rectangular panels of the beam must be modelled as shown in Fig. 8.3, but the depth of the model will be only 80 mm to account for the 'zero' thickness of the elements. Only when the laminate properties are defined for the elements will the model simulate the correct depth of the beam. Note also that quadratic elements are used because they provide the best solution of all the element types available.

Meshing the beam is relatively simple in this case as there are three flat areas to mesh, each 800 mm long and 80 mm wide. Lines in three-dimensional space can be used to define simple flat surfaces for each side of the upper flange and the



upper half of the web, and these surfaces are meshed with a run of 20 quadrilateral elements which are 40 mm square. There will be no distortion from the parent element shape. This mesh can then be mirrored in the  $x-z$  plane to produce the final mesh of the half-beam. This mesh is shown in Fig. 8.4 and consists of 120 elements, 413 nodes and 2478 nodal degrees of freedom.

**Materials** As the element type has been specified as a shell, the laminate material properties must be assigned to each element. For each element there is a local coordinate system which, as the elements are essentially planar, is just  $x$  and  $y$ . Here the local  $x$ -direction for a laminate element coincides with the global  $x$ -direction of the beam, as shown in Fig. 8.4. These laminate properties consist of axial, coupling and bending stiffnesses which are generated by the pre-processor using a laminate modelling facility. The user has, typically, two options to produce the lamina elastic constants, either entering them directly or entering the fibre and matrix constituent properties and allowing the software to calculate the constants using micromechanical formulae. Then the user supplies the orientation and thickness of each lamina in the stacking sequence, starting at the bottom layer and working to the top layer.

In this case, the former method was used to enter the unidirectional carbon fibre epoxy lamina data given in Fig. 8.1. Then 3 different examples of laminates, each 2 mm thick with 16 layers of this lamina, were constructed. Their laminate

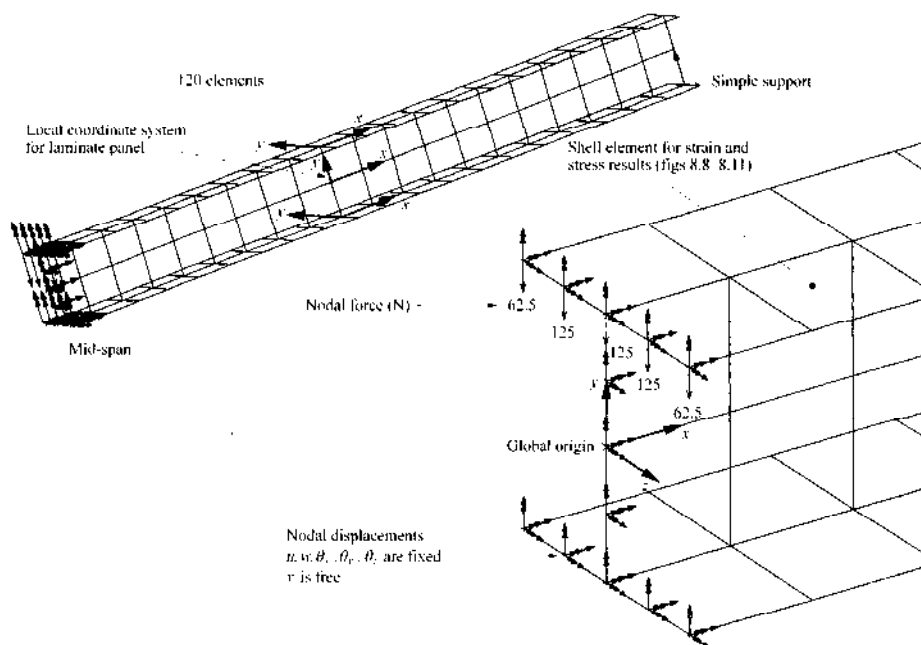


Figure 8.4 Mesh construction and boundary conditions.

**Table 8.1** Examples of laminates used for the beam problem

Label	Lamination notation/type	Description
Laminate 1	(0/90/0/90/0/90/0/90/0/90/0/90/0)	Symmetrical cross-ply
Laminate 2	(0/ - 45/90/45/0/ - 45/90/45/45/90/ - 45/0/45/90/ - 45/0)	Symmetrical quasi-isotropic
Laminate 3	(0/ - 45/90/45/0/ - 45/90/45/ - 45/0/45/90/ - 45/0/45/90)	Antisymmetrical quasi-isotropic

configurations are defined in Table 8.1. Clearly, a large number of laminate configurations could have been used. These three configurations have been chosen because each represents a specific lamination type with a certain deformation behaviour. In reality, it is not easy to produce a beam with any general lamination configuration. One practical option is to manufacture a laminated I-section by joining two 8-layer channel sections back-to-back and then adding one 8-layer plate to each flange to achieve the appropriate thicknesses. Such an option may be used to produce the laminate configurations in the table.

Considering each of the laminate configurations in turn, the following may be seen:

- Laminate 1 has an equal number of  $0^\circ$  and  $90^\circ$  orientation laminae, stacked symmetrically about the mid-plane. Hence, the laminate stiffnesses for a thin-shell element are those of an equivalent orthotropic material, i.e. there is no coupling between bending and twisting and membrane action and bending. It can therefore be expected that a beam made of this material will behave in a way similar to an isotropic beam.
- Laminate 2 is a quasi-isotropic laminate, as it has an equal number of layers with orientations of  $0^\circ$ ,  $90^\circ$ ,  $45^\circ$ , and  $-45^\circ$ . It also has a stacking sequence that is symmetrical. Such a laminate, when produced with carbon fibre reinforcement, is known as *black aluminium*, because all its stiffnesses do not change significantly with angle. The presence of the  $45^\circ$  laminae introduce bending coupling stiffness terms that cause the material to bend as it twists and twist as it bends. However, when such a panel is subjected to membrane deformation there is no coupling with bending deformation. This feature of the deformation is due to the symmetrical stacking sequence.
- Laminate 3 has the same layer orientations as laminate 2 and is of the quasi-isotropic type. However, the stacking sequence about the mid-plane is what is termed 'antisymmetrical'. Now the laminate has coupling between membrane and bending deformations, but the terms which denote bending-twisting coupling are zero.

**Loads and restraints** Remembering that the load applied at the mid-span is 1 kN (see Fig. 8.3), and that symmetry has been applied such that only half of the beam is modelled, only 500 N need be applied at the mid-span for the model. This load

can be assumed to be uniformly distributed across the upper flange. To calculate the load that is applied at each node, consider the length over which the load acts. Figure 8.4 shows that the inner nodes along the line at the mid-span of the upper flange act over twice the length when compared to the edge nodes, and so twice the load is applied to the inner nodes. Hence, the two nodes at the free edges have point loads of  $-62.5 \text{ N}$  in the  $y$ -direction applied to them and the three internal nodes have point loads of  $-125 \text{ N}$  in the same direction applied to them. Here, the minus sign indicates that the load is acting in the negative  $y$ -direction. Note also that the arrows which denote the loads shown in Fig. 8.4 are all of one length and so the graphical display cannot be used to check the accuracy of the model in this case.

Applying the correct restraints to the nodes that are on the mid-span plane of the beam must ensure that the nodes stay in the  $y$ - $z$  plane and move only in the  $y$ -direction. This involves allowing only the  $v$ -displacement to be free, while setting the  $u$ - and  $w$ -displacements and the  $\theta_x$ ,  $\theta_y$  and  $\theta_z$  rotations to be zero.

To model a simple support, the nodal displacement boundary conditions can be one of two types. If the deformation is such that sections remain planar, then all the nodes across the width of the bottom flange at the support location have their nodal displacement  $u$  and rotation  $\theta_z$  set to be free. A value for  $u$  set to zero represents the situation where axial shortening of the beam is not allowed, and this has not been included when deriving (8.5). If sections do not remain planar, i.e. there is twisting of the section which causes warping of the section, it can be observed that the rotational nodal displacements at the support may be nonzero. To model both cases, the node at the bottom of the web has its nodal displacements  $v$  and  $w$  fixed to be zero, while all other nodes across the width of the bottom flange have their degrees of freedom left free.

In Fig. 8.4, double-arrowheaded vectors are used to show those nodal displacements that are fixed. This can be used to check whether the conditions imposed on the model are those required.

**Analyses** For each of the three laminates in Table 8.1 models have been built, as described, to represent spans of 1600 mm. Also spans of 400 mm, 800 mm and 1200 mm have been modelled by moving the position of the simple support. Linear static analyses have been carried out for each case.

### 8.1.6 Results of the Analysis

Once an analysis is run the raw data is checked to make sure that the stresses and displacements are acceptable. This is done visually using a graphics terminal and, for the cases run here, both the stress and displacement values are found to be small. Hence, the underlying assumptions of small displacements and linear elasticity are seen to be valid. Now, the results can be analysed in more detail.

**Displacement contour plots** To illustrate how the deformation of the beam alters with different laminate configurations, Figs 8.5 to 8.7 present displacement contours for the three laminates on the model of half-beam span. The contours are of constant  $v$ -displacement, i.e. in the global  $y$ -direction, and are drawn on the deformed geometry so that the global deformation is visible. For reasons of clarity the undeformed geometry and the mesh are not shown here. However,

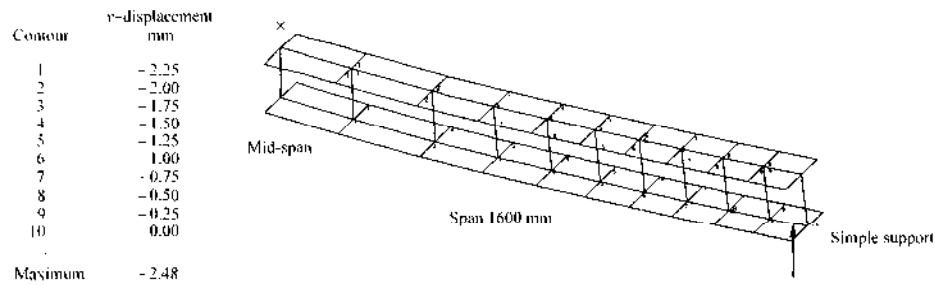


**Figure 8.5** Contours of  $v$ -displacement on the deformed beam with laminate 1 (cross-ply).

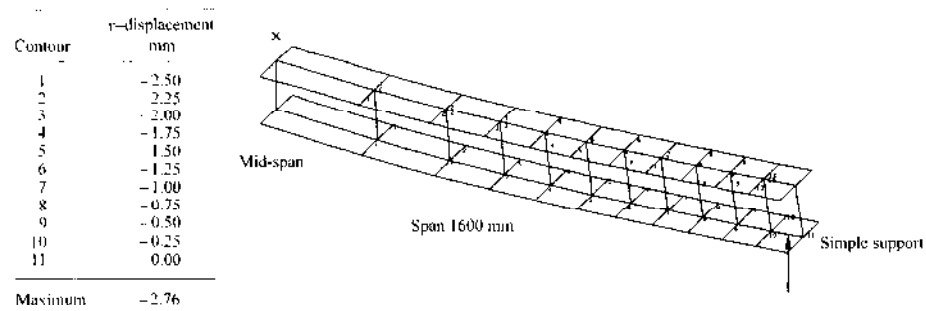


**Figure 8.6** Contours of  $v$ -displacement on the deformed beam with laminate 2 (symmetrical quasi-isotropic)

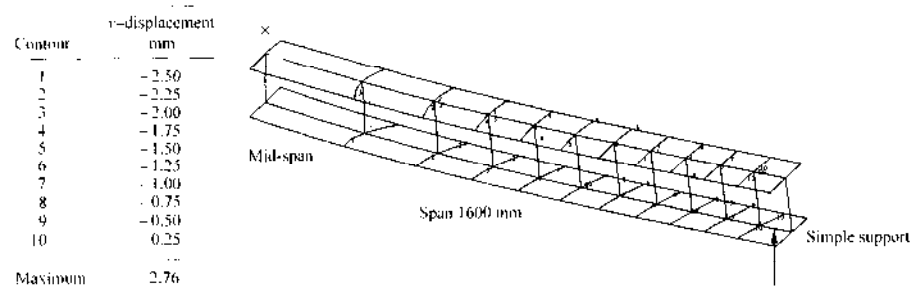


**Figure 8.7** Contours of  $v$ -displacement on the deformed beam with laminate 3 (antisymmetrical quasi-isotropic).

to show that it is correct to allow the  $u$ -displacement to be free at the simple support, the original location of the support is shown. In all the figures, the contours have a uniform interval chosen by the analyst.

From the figures it can be seen that the displacement component  $v$  is negative as the beam deflects in the negative  $y$ -direction. In design the minus sign is ignored as it is the magnitude that is required, the direction being unimportant for safe design. Next, note that the contours are not uniformly spaced along the beam; they become closer together when moving from the mid-span to the end of the beam. This is indicative of a parabolic variation in  $v$  along the beam, which is expected from the moment-curvature expression.

If plane sections of the beam remain plane under loading, then this is shown by the displacement contours being undistorted and at right angles to the centroidal axis of the beam. For the beam made from laminate 1, Fig. 8.5, this is the case as expected. Laminate 2, however, should lead to some twisting, but this cannot be seen in Fig. 8.6. If the raw nodal displacements are interrogated, then some slight twisting of the flanges is found, but that the magnitude of the twisting is too small to be detected from the contour plot. This shows that relying exclusively on visual interpretation of the results can lead to incorrect answers. Figure 8.7 for the beam made with laminate 3 is very different from the other two, as significant distortion of the cross-sections of the beam is visible. Comparing Fig. 8.7 for an antisymmetric laminate with Fig. 8.6 for a symmetric laminate, the membrane-bending coupling of the antisymmetric laminate can be seen to have a large influence on the deformation behaviour. For this reason, in real structures, antisymmetric laminates are not normally used, unless their membrane-bending coupling is desirable.

Also shown in each figure is the maximum vertical deflection. The beams made from laminates 2 and 3 have a similar value, showing that the strong coupling effects do not affect the maximum bending deflection. This has important consequences as (8.5), which has been derived by lumping properties of the beam along the centroid axis, as introduced in Sec. 2.3.1, can be used to determine  $v_{\max}$  for any laminated composite beam subjected to three-point bending. This does not mean, however, that any coupling effects present in the beam can be neglected in the overall design process, because they will undoubtedly have an influence when designing such things as joints and supports.

**Laminate stress and strain output** Having looked at the global deformation of the structure, the stress and strain within the laminate material itself must now be analysed. This is done within a specialist post-processing facility designed to handle multi-layered materials. This facility combines the nodal displacements for the thin-shell elements that represent the laminate, generated by the solver, with the laminate stiffnesses, laminate configuration and lamina elastic constants, to calculate layer stresses, with reference to the local Cartesian coordinate system of the laminate.

Analysts must expect that this process cannot generate accurate results for the individual layer in-plane stresses,  $\sigma_x$ ,  $\sigma_y$  and  $\tau_{xy}$ , and the interlaminar stresses,  $\tau_{xz}$

and  $\tau_{yz}$ . These last two shear stresses are often estimated only approximately, a common method being to use simplified layer-by-layer equilibrium equations. Note also that, normally, the laminate post-processor does not generate output for  $\sigma_z$ , the through-thickness stress, known as the *peel stress*. As laminates are susceptible to delamination damage, caused by such stresses, this lack of information is very serious. These comments on accuracy also apply to the recovery of layer strains.

Examples of the graphical output that can be obtained for a given thin-shell laminate element are shown in Figs 8.8–8.11 for a beam of span 1600 mm made for laminate 1. The stress and strain recovery has been carried out for the element marked in Fig. 8.4. These values are at the centroid of the element.

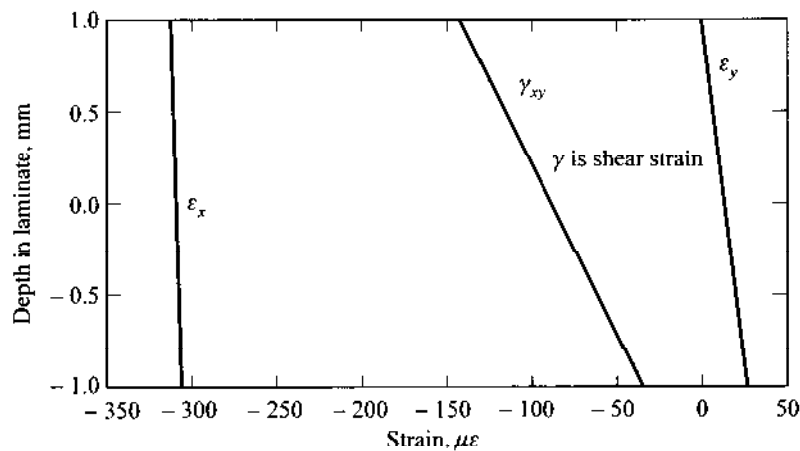


Figure 8.8 In-plane strain profile for the compression flange with laminate 1.

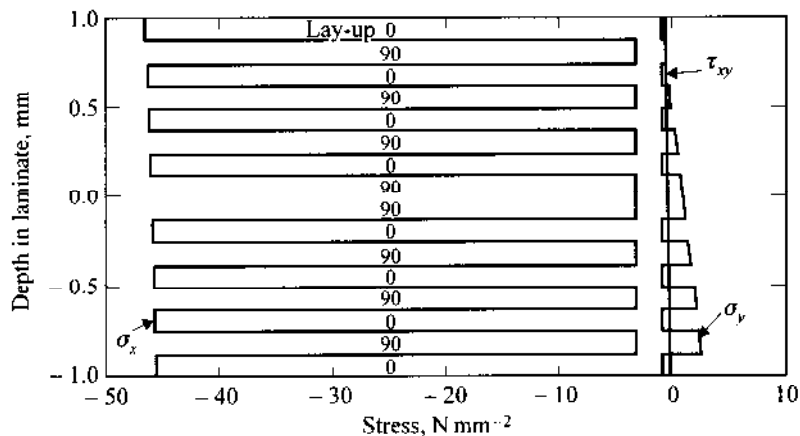


Figure 8.9 In-plane stress profiles for the compression flange with laminate 1.

In Fig. 8.8, the in-plane strain profiles are continuous and vary linearly through the material thickness. This shows that normals have remained straight, a feature of Mindlin shell theory (Sec. 3.8.2), and that the compatibility requirement is satisfied. Using (2.25), with the flexural modulus  $E_b$  for laminate 1 in Table 8.2, it can readily be shown that the top surface strain ( $\varepsilon_x$ ) is  $-300\mu\varepsilon$  and that the bottom surface strain is  $-315\mu\varepsilon$ , a difference of only  $15\mu\varepsilon$ . The finite element results are in good agreement with this strain due to bending about the horizontal  $z$ - $z$  axis. Such an observation indicates that the flanges resist the bending by membrane action, this being the general situation when the walls of an I-section beam are thin. The nonzero values for  $\varepsilon_y$ , the strain perpendicular to the longitudinal axis of the beam, show that there is the expected deformation in the plane perpendicular to the beam's length, as introduced in Sec. 2.3.1.

In-plane stresses are plotted in Fig. 8.9. Although the stress profiles vary linearly through the thickness of a lamina the values are different from layer to layer because of the different material properties in each layer. The stress  $\sigma_x$  is highest in the stiffer  $0^\circ$  layers of the cross-ply laminate and, as expected because of the inherent errors in the finite element model, the results for  $\sigma_y$  and  $\tau_{xy}$  are not exactly zero, but oscillate around this value. In each layer, the in-plane stress distribution in each layer satisfies the equilibrium requirement.

Transverse shear strain and shear stress profiles through the top flange laminate are presented in Figs 8.10 and 8.11. Through thickness shear values are very small because the majority of the shear force is transmitted by the web. Both strain and stress profiles are close to the parabolic shape that is predicted by conventional elastic theory. The deviation of the results from the expected shape is a consequence of using simplified equilibrium considerations to calculate the shear values.

Having obtained the above profiles in Figs 8.8–8.11 it is usually possible to plot them on a layer-by-layer basis having transformed the laminate local axis strains and stresses to be in the principal axis system (see Fig. 8.2). These principal values are then used for the prediction of failure. Von Mises' equivalent stress is no longer relevant here, since failure of a lamina, and hence the laminate, is directionally dependent. The anisotropy of the material also tends to mean that

**Table 8.2** Section moduli of beam compared to in-plane and flexural moduli of laminate

Laminate	Modulus values, $\text{kN mm}^{-2}$ (GPa)				
	Section		Laminate in-plane		Laminate flexural
	$E_b$	$G_b$	$E_x$	$G_{xy}$	$E_{xzz}$
1	79.8	4.46	77.9	5.35	92.5
2	57.6	20.8	63.0	21.6	80.7
3	57.1	18.2	63.0	21.6	66.0

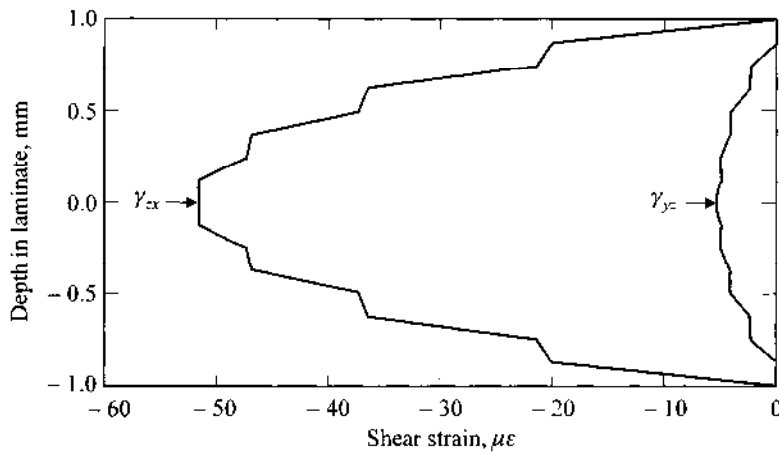


**Figure 8.10** Transverse shear strain profiles for the compression flange with laminate 1.

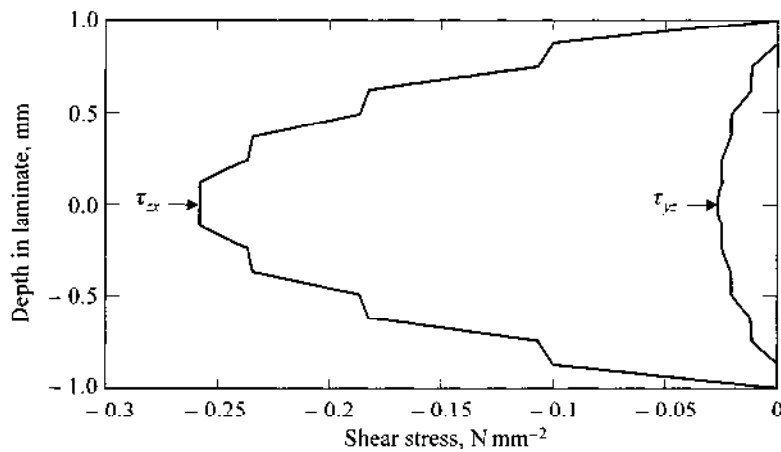


**Figure 8.11** Transverse shear stress profiles for the compression flange with laminate 1.

the individual stress components are more likely to cause failure and this is one reason why post-processors have the options discussed here. However, note that there can be difficulties associated with using finite element analyses to predict such failures.

Often the actual stress causing failure is at a free edge of the material and the calculations are carried out at the centroid of the element. Also, it is not necessarily the largest stress that causes failure. It has been established that the error in any stress component is 5 per cent of the maximum stress component. This indicates that if a stress component causing failure is an order of magnitude less than the maximum component, then the error in this stress can be 50 per cent, and as such is not useful in predicting failure.



**Determination of section moduli** When developing (8.5) for the mid-span deflection, it was stated that  $E_b$  and  $G_b$  were those of the section. To determine their values for a laminated composite I-beam there are a number of alternative procedures; one of these uses solutions from finite element analyses and will be demonstrated here.

Rearranging (8.5) gives

$$\frac{v_{\max}}{PL} = \frac{1}{48E_b I_a} L^2 + \frac{1}{4G_b A_w} \quad (8.7)$$

which is the equation of a straight line if  $v_{\max}/PL$  is plotted against  $L^2$ , with gradient  $1/48E_b I_a$  and intercept  $1/4G_b A_w$ . For the beam section being considered here, the second moment of area  $I_a$  is  $5.91 \times 10^5 \text{ mm}^4$  and the web area  $A_w$  is  $160 \text{ mm}^2$ . Hence by plotting  $v_{\max}/PL$  against  $L^2$  for various span lengths, the gradient and intercept can be found, giving the section moduli.

While the location of  $v_{\max}$  may be at any point within the mid-span section, to be consistent with (8.5) the value of deflection at the centroid of the section has been used. Figure 8.12 shows the results from the beam made of laminate 1. Note that the four data points give an approximation to a straight line, and so the gradient and intercept are determined using the least-squares method to fit the best straight line through the data.

Results for the section moduli produced using this graphical method are given in Table 8.2 together with the equivalent axial moduli for the laminate panels. As the I-section is thin-walled, when the section is flexed the flanges are subject to mainly membrane action as the strain variation through their thickness because of bending is small, as shown in Fig. 8.8. It is not surprising, therefore, that  $E_x$  of the laminate is, for the purpose of design, a conservative approximation to  $E_b$ . Here, the difference is due to the actual location of the layers with respect to the axis of bending. Similarly,  $G_{xy}$  is a conservative approximation to  $G_b$ . Such a favourable

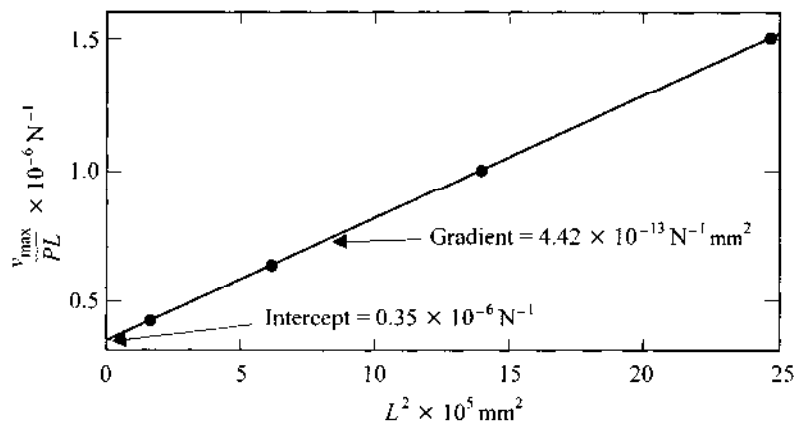


Figure 8.12 Determination of the section modulus with laminate 1.

comparison is not found if the section has thicker walls, and so it is always sensible to use the graphical procedure demonstrated here, with data either from a series of computations or from laboratory testing, to determine the section moduli.

The laminate itself also has its flexural moduli. One of these,  $E_{xzz}$  is the modulus in the  $x$ -direction when a single laminate is bent about the  $z$ - $z$  axis. This flexural modulus is much higher than the equivalent flexural modulus for the section, and this comparison illustrates, yet again, the importance of material properties in the analysis of structures. Note that all three  $E$  values are the same for an isotropic beam—the Young's modulus of the material.

This I-beam example has introduced a number of features that are relevant when analysing structures made from laminated composite materials. There are many more features that can be studied, and those requiring additional information on the analysis of composite material structures are recommended to study the comprehensive work by Taig (1992). This NAFEMS publication is a very practical document, exploring all aspects of those commercial packages available at the time of publication, together with a discussion of their weaknesses and degree of applicability of their features.

## 8.2 DESIGN EXAMPLE WITH SUBMODELS

### 8.2.1 Overview of the Problem

In all analyses, the aim is to have as few elements and spatial dimensions as possible, so that both the overall cost of the analysis and the numerical manipulation errors are kept to a minimum. One way of doing this for complex problems is to carry out a variety of analyses using, where necessary, one-, two- and three-dimensional elements to determine the results required. To illustrate this, consider the design of a frame made up of thin-walled steel tube members, the ends of which are welded together to form the joints. This frame supports a vibrating machine, but as an approximation only time-independent loads are assumed to be transmitted through the joints into the frame.

When analysing such a frame, a first step is to model the skeletal structure as either a series of one-dimensional bars with pin joints or as a set of beam elements with fully rigid joints. The mesh is generated by hand and the range of member stresses and/or forces and of joint and member deflections in the frame are obtained from a series of analyses carried out with static loads applied. Joint behaviour, however, for this practical situation is not predicted in any detail. For example, in this case, the analyst may need to know the local stresses in the vicinity of the connections so that the welds can be designed to avoid a fatigue failure.

It can be seen that to model this situation the use of one-dimensional elements alone is not appropriate. Such a one-dimensional analysis may, however, still be useful if the information it generates can be used for further local analyses of the

joints. This is an example of what is known as substructure (or subregion) modelling, as described by Knight (1993). Here, results from the frame analysis can be used as boundary conditions for the subsequent analysis of a joint, where both the joint and a length of each the members attached to it can be modelled with two-dimensional shell elements. This allows both in-plane and bending behaviour of the joint system to be modelled. If this second-level model does not provide stresses suitable for design purposes then a third-level model of solid three-dimensional elements, with or without shell elements, may be necessary.

Note that only through experience will an analyst know how to formulate the subregion models such that an appropriate number and types of element are used to determine the required deformations and stresses with the degree of accuracy necessary to meet the design requirements.

### 8.2.2 Problem Definition

This example is used solely to illustrate a number of features of the finite element method and so it does not correspond exactly to a real design situation. Hence, the type of frame and loading arrangement is not typical of those used in practice. However, property data for commercially available steel members has been used. Interested readers are referred to any of the available design guides for the construction of frames with hollow steel sections, such as that by Packer, Wardenier, Kurobane *et al.* (1992).

For this example, a space frame of nominal dimensions  $3000 \times 1500 \times 1500$  mm is constructed from steel sections. Members are chosen from a range of welded tubes of rectangular and square section. As is typical of these steel frames, the method of connection at the joints is welding and, to achieve full strength, full-penetration butt welding is used.

This frame is to support a static or dead load, a machine that weighs 72 kN (equivalent to about 7 tonnes), above ground level and so the base of the frame is attached to the ground. At this stage in design the dead load of the frame itself is unknown, but it is not expected to be more than 5 per cent of the machine's dead load. A number of components on the machine move such that the frame is subjected to dynamic loading in addition to the dead load. It is therefore one of the design requirements that the welded connections have an adequate fatigue life. To model the structural behaviour it can be assumed that loading is of constant amplitude and of low frequency such that the dynamic loading can be modelled in the finite element analyses by a quasi-static loading, thus enabling results to be obtained from a purely static analysis.

It is known that the motion of the components provides a dynamic magnification to the dead load of 1.25, making the maximum total vertical load 90 kN and the minimum load 54 kN. In addition, there is a horizontal dynamic load component equal to 0.2 of the dead load. Both dynamic induced loads act in the plane parallel to the longer side of the frame which is illustrated in Fig. 8.13. The dynamic loading perpendicular to this plane is found to be sufficiently small such that it can be neglected.

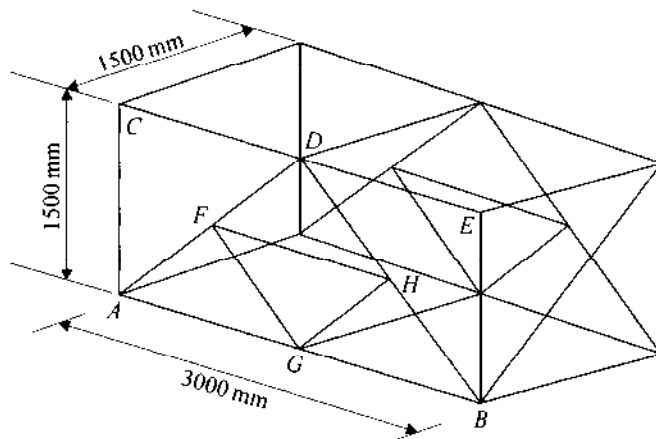


Figure 8.13 The nominal geometry of the frame.

Preliminary design studies show that the frame has the geometry shown in Fig. 8.13, where the joints on one side of the frame have been labelled to aid the following discussion. To simplify the design process advantage is taken of symmetry and so only the plane frame that is labelled and which is subjected to only half of the loading need be considered. In the preliminary design studies account has been made of the way in which the machine is mounted to the frame at points along the horizontal member  $FH$ . From this, the maximum quasi-static load distribution is known and is shown in Fig. 8.14. The vertical component of load is represented by a linearly varying distributed load of value  $12 \text{ N mm}^{-1}$  at joint  $F$  and  $48 \text{ N mm}^{-1}$  at joint  $H$ . This load distribution is equivalent to a resultant concentrated vertical force of  $45 \text{ kN}$  acting between joints  $F$  and  $H$  at a distance  $0.9 \text{ m}$  from joint  $F$ . The horizontal component can be considered to

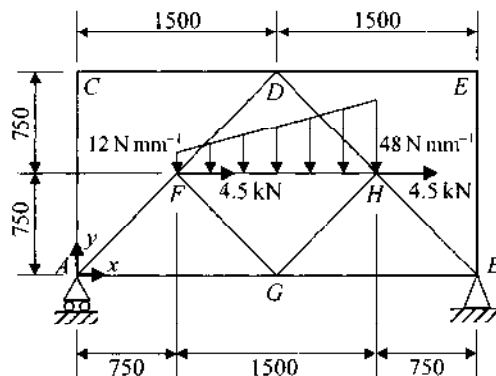


Figure 8.14 Loading on one plane frame section.

consist of two equal concentrated forces of 4.5 kN that act at joints  $F$  and  $H$ . The loading from the machine is considered to be transferred at the joints into the frame as shear forces only. For this situation to be realized the connections between the machine and the frame have to be pinned, ensuring that there are no moments.

To perform the fatigue design of the welded joints it is necessary to conduct four analysis types of increasing complexity:

1. a pin-jointed frame analysis to determine the axial forces in the members and so to allow the appropriate sections to be chosen from a range of commercially available welded tubes
2. a rigid frame analysis to determine the overall response of the structure and to check the suitability of each of the members in terms of peak stresses and deflections
3. a local analysis of the critical joint  $H$ , using a thin-shell finite element model, to obtain estimates of the peak stresses at the welded connections
4. a more refined local analysis of joint  $H$ , using a solid finite element model, to obtain more accurate peak stresses in the vicinity of the welds.

Note that analyses 1 and 2 use frame models where the members are modelled as one-dimensional members placed along their longitudinal centroidal axis. These analysis types are often considered as forerunners of the finite element method (Coates *et al.*, 1988). All four analyses can be performed using the finite element method but in this case results will be presented only for types 2 and 3. Also note that the stress results from analyses of types 3 and 4 are used to design the welds against fatigue failure, but there is not the scope in this text to detail the procedure.

### 8.2.3 Analysis of Pin-jointed Frame

Prior to conducting a finite element analysis to determine the displacements and stresses it is necessary to choose the steel sections to fabricate the frame. To do this the designer needs to know the forces in the members and the simplest technique is to model the frame as a pin-jointed structure. Note, however, that for the frame shown in Fig. 8.14, the distributed loading along member  $FH$  induces bending in that member which is transmitted throughout the frame by the joints. This could be important when choosing the section sizes, but will not be predicted by the pin-joint analysis as only axial member forces are determined.

Figure 8.15 shows the plane frame where it is assumed that all joints are pinned, that all members are struts, i.e. they can transmit only axial forces and that, at each joint, the centrelines of the members are coplanar and concurrent. For this analysis the vertical loading is been modelled as acting only at ends of member  $FH$ , with the values of 18 and 27 kN determined from an application of static equilibrium to the distributed loading. It is assumed that the loading has a line of action coinciding with the centroid plane of the frame. In practice, there will be eccentricity causing a moment about the  $x$ -axis. Our ideal assumption

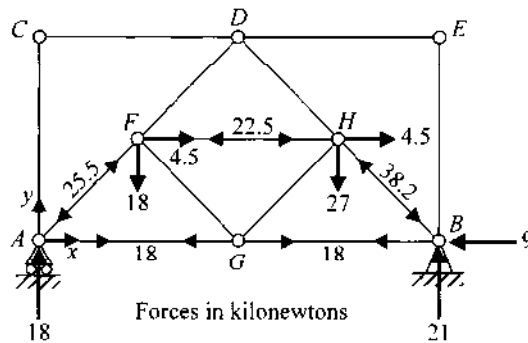


Figure 8.15 Analysis of the plane frame with pin joints.

simplifies the analysis and is valid provided that the resultant out-of-plane moment is small. This is yet another situation where engineering judgement is used to reduce the complexity of the model. If the effect of the out-of-plane moments is to be included, then the model needs to be three-dimensional.

Next, the supports for the frame are modelled such that the whole problem is statically determinate and the reaction forces can be determined from considerations of static equilibrium alone. Joint *B* is assumed to be fixed in space and joint *A* is assumed to be free to move in only the horizontal direction, hence joint *A* is shown in Fig. 8.15 fixed to a roller support.

Some discussion of the choice of these ideal support conditions is necessary. In practice, the frame may be supported by the strong floor of a factory via elastomeric bearings placed at its four corners. These bearings are used to reduce the transmission of the dynamic excitation through the floor into the fabric of the building and, commonly, they are produced from viscoelastic rubber. To work effectively, the bearings must have a stiffness much smaller than that of the frame and its members, but this leads to problems if the bearings are modelled as spring elements in the full finite element analysis as a result of ill-conditioning, as described by Cook *et al.* (1989). To prevent occurrence of this problem, which is not easily remedied, ideal rigid support conditions are used.

By considering the static equilibrium of each joint in turn (Coates *et al.*, 1988), the forces in the members can be determined and these are shown in Fig. 8.15. From these forces the choice of section can be made. Here, sections from the British Steel COLDFORM range of hollow rectangular and square sections are used. To aid the designer, technical data sheet TD 341/20E/91 (available from British Steel's advisory service) provides data for each section, giving an axial tension and compression resistance to prevent buckling. Note that the grade of steel is 50/45 having, for the purposes of structural design, a yield strength ( $\sigma_Y$ ) of  $350 \text{ Nmm}^{-2}$  and an ultimate tensile strength ( $\sigma_U$ ) of  $430 \text{ Nmm}^{-2}$ . Also, the isotropic homogeneous material has the following elastic constants: Young's modulus,  $205 \text{ Nmm}^{-2}$  and Poisson's ratio, 0.3.

As all members in the frame have to resist a combination of stresses due to axial forces, shear and bending it was decided to choose section sizes that have an axial resistance at least three times the axial force given in Fig. 8.15. Members *AF*, *FD*, *FH*, *DH* and *HB* are thus fabricated from rectangular section material which is 80 mm deep by 40 mm wide and has a wall thickness of 4 mm. All other members are made from square section material 40 mm deep and 40 mm wide, with a wall thickness of 4 mm. This smaller section material is also to be used for the members that connect the two plane frames shown in Fig. 8.13. Note that the deeper section has a tension capacity of 294 kN and a maximum axial compression resistance of 135 kN (minor axis buckling), while the values for the shallower section are 182 and 72 kN, (major and minor axis buckling respectively).

When assembling the frame, the members are connected such that the centroidal axes are coplanar and concurrent, as was assumed for the pin-joint analysis, and so there is no joint eccentricity to make subsequent analyses more difficult. Note also that using just two section sizes, each of width 40 mm, ensures that the fabrication process is straightforward and that the joints have the full section strength. Finally, the actual dimensions of the frame are now  $3040 \times 1540 \times 1540$  mm.

#### 8.2.4 Rigid-frame Finite Element Model

If the frame is to be loaded solely at the joints and has a construction such that it is statically determinate then the pin-jointed analysis can be used to determine accurately the joint strengths and deflections (Packer *et al.* 1992). However, this frame has to transmit some bending due to the distributed loading on member *FH*. Hence, to determine a statically admissible set of moments, shear and axial forces throughout the frame, a finite element beam analysis of the rigid-jointed frame can be made.

In Sec. 3.8.1 a linear bending beam element was developed that did not model the effect of shear deformation. Such an element models the prismatic member subject to a loading normal to the centroidal axis by lumping all the properties along this axis and assuming that the bending deformation causes the normals to this axis to rotate but remain normal. These elements have two nodes, each possessing two degrees of freedom and, in standard texts, such an element is referred to as the beam element. Commercial packages generally do not include such a simple two-dimensional beam element alone, rather they include a three-dimensional beam element that possesses six degrees of freedom per node. This element is the combination of four simple elements: a torsional element, an axial element, a major-axis bending element and a minor-axis bending element.

These beam elements are defined within the pre-processor, usually in a module specifically provided to handle beam elements, by specifying the geometry of the section. Geometrical properties for a section are then calculated and are assigned to the appropriate beam elements within a mesh during the solution phase. Here, two structural sections are used and so two sets of element properties need to be defined.

Next, a mesh of these beam elements has to be created to model the geometry of the plane frame in the  $x$ - $y$  plane of a global Cartesian axis system, where the origin has been chosen to be at joint  $A$ . For a frame structure it is not necessary to consider meshing areas or volumes as the continuum is modelled by one-dimensional elements. To model this frame, the mesh shown in Fig. 8.16 has been constructed by first defining the positions of the 24 nodes and then connecting them with beam elements to which the correct section properties have been attached. Note that the positions of the nodes in the vicinity of joint  $H$  have been chosen carefully, as the calculated nodal forces and moments at these positions are used as boundary conditions for the substructure analysis presented in Sec. 8.2.5.

Then the isotropic material properties of the beam elements can be defined. These are taken from technical datasheet TD 341/20E/91 for British Steel's steel Grade 45/50. Note that the analysis needs only the elastic constants for the steel as the stress results from a beam model cannot be readily used in a failure prediction.

Boundary conditions are then entered to define the loading arrangement and support conditions of the model and these are shown in Fig. 8.16. Here, the support conditions at joints  $A$  and  $B$  are the same as those for the pin-jointed truss model shown in Fig. 8.15. To enforce these restraints the nodal displacements  $u$  and  $v$  are zero at joint  $B$  and the displacement  $v$  is zero at  $A$ . With the loading acting in the  $x$ - $y$  plane there is no requirement to specify, at each node, that the nodal displacement  $w$ , and the rotations  $\theta_y$  and  $\theta_x$  are zero. These nodal displacements remain inactive automatically.

The loading defined in Fig. 8.14 is modelled in two separate parts. First, the horizontal concentrated forces at joints  $F$  and  $H$  are entered as nodal forces of 4.5 kN in the  $x$ -direction and zero in the  $y$ - and  $z$ -directions. Then the vertical distributed loading along the length of member  $FH$ , shown in detail in Fig. 8.17 as a distributed load with a linear variation, is allocated to each of the five beam elements representing the member  $FH$ . This is usually done using a general beam

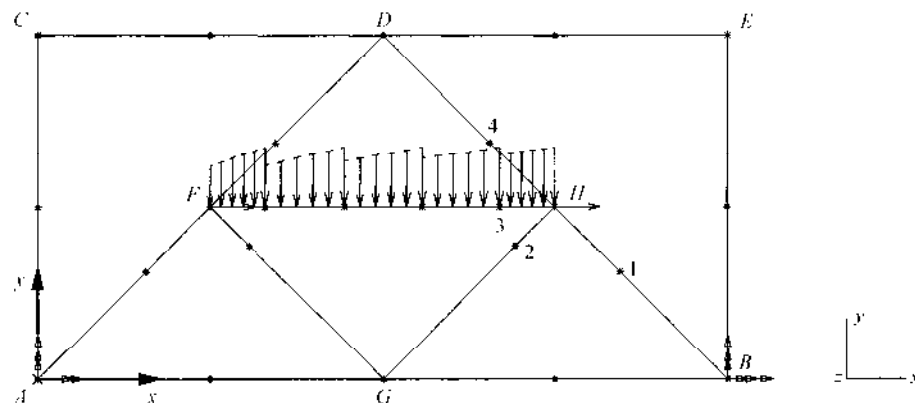


Figure 8.16 A beam element model for a rigid-joint analysis.



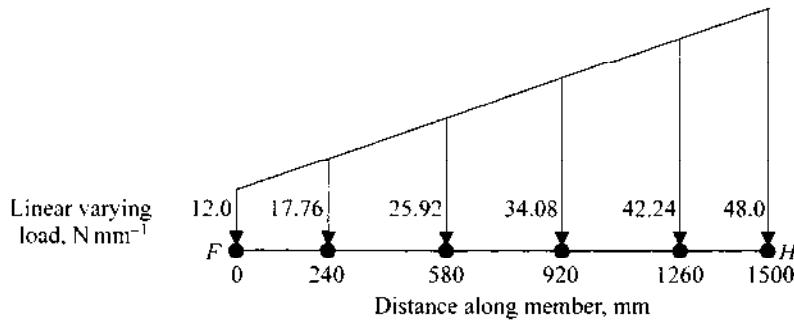


Figure 8.17 The load distribution for the elements along member  $FH$ .

loading facility where distributed loadings of any variation can be applied. Finally, before the displacements and stresses are calculated, a check is made on the reaction forces to see that they balance the applied external loading.

Figure 8.18 shows the deformed shape of the frame together with the undeformed shape. As anticipated, the largest deflections occur in the horizontal member  $FH$ . In fact, the maximum deflection is about 5 mm, which is  $\frac{1}{300}$  of the span, and this is considered to be within the design specification. By comparing the deformed and undeformed shapes of the frame, it is apparent that joint  $H$  is experiencing the highest deformations and so is the critical joint in the frame.

Results from the static analysis can also be presented in the form of displays of the beam forces and stresses along the length of the beam elements superimposed on the mesh. Figures 8.19–8.22 show the information for the bending moment ( $M_z$ ) and axial force ( $F_a$ ) distributions and their stress distributions. Solutions for the shear force and stress are not given here because shear does not influence decisions in the design of the frame. Note that the bending stresses

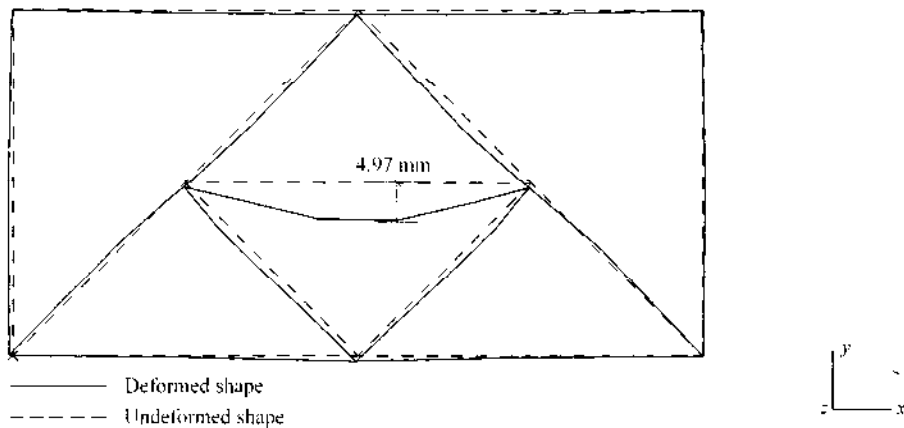


Figure 8.18 Displacement of the frame calculated using beam elements.

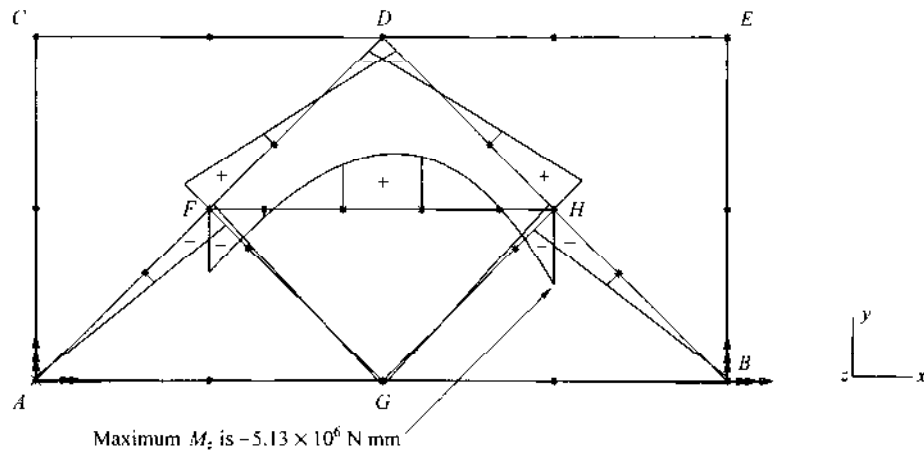


Figure 8.19 Bending moment distribution in the frame.

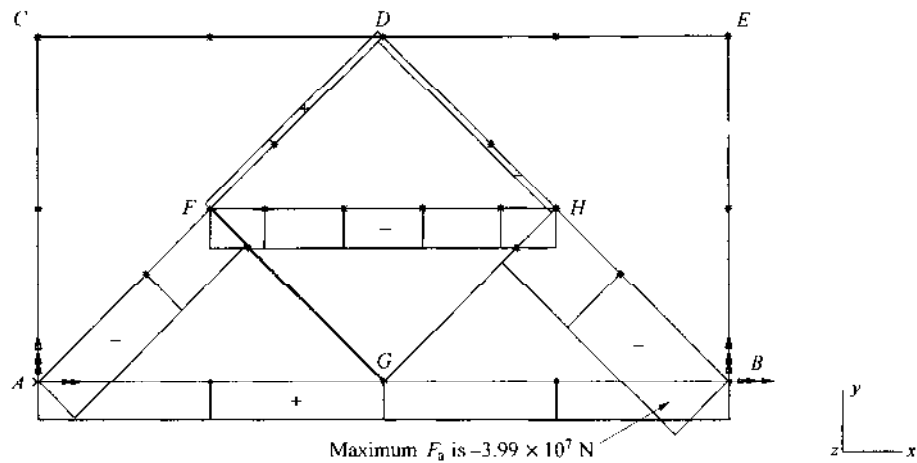


Figure 8.20 Axial force distribution in the frame.

are calculated from the bending moments using the bending formula of (2.25), and they are calculated as the maximum value, that is at the surface of the section. For example, the maximum direct stress at the mid-span of member  $FH$  as a result of bending is at a distance of  $\pm 40 \text{ mm}$  from the centroidal axis. Clearly, the axial stress in Fig. 8.22 is calculated by dividing the axial force by the cross-sectional area of the beam member, and this geometric property is determined when the section is constructed in the beam creation facility.

Combining the two direct stress components gives the stress output displayed in Fig. 8.23. Note that this combined stress may be given as a magnitude only.

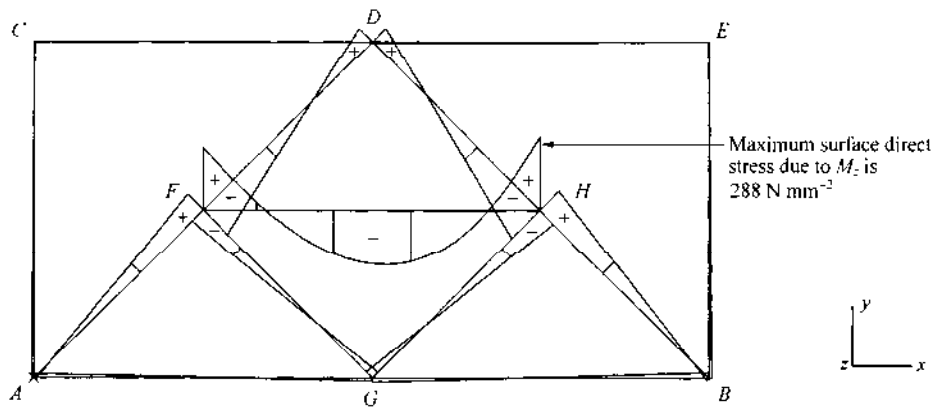


Figure 8.21 Distribution of maximum bending stress in the frame.

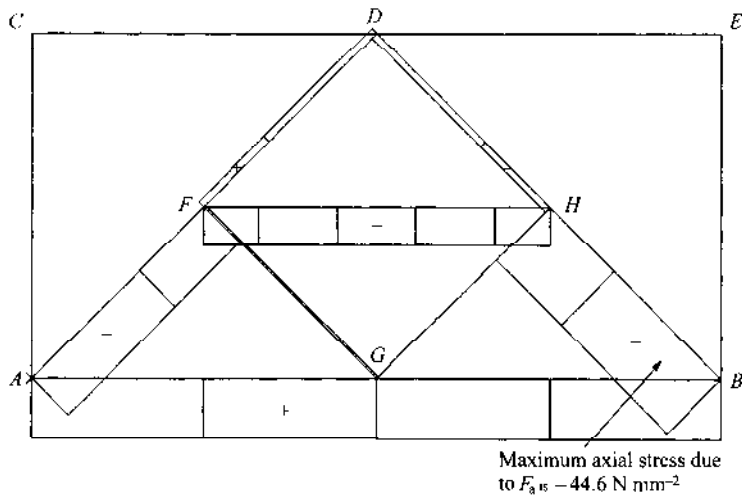


Figure 8.22 Distribution of axial stress in the frame.

This stress can be used to check the suitability of the beam section sizes. Disregarding the areas of the joints, the maximum tensile and compressive stresses are 0.6 of the yield stress given and this is considered to be a safe design.

Focusing on the critical joint, joint *H*, Fig. 8.24 gives the combined stress values at this joint calculated from the element forces for the four beam elements that meet at this joint. The variation in the values is very high, such that it is impossible to establish the maximum stresses that the butt welds of the joint need to transmit. As it is these stresses that are needed for the fatigue design, they have to be modelled using a substructuring technique. This requires that the boundary

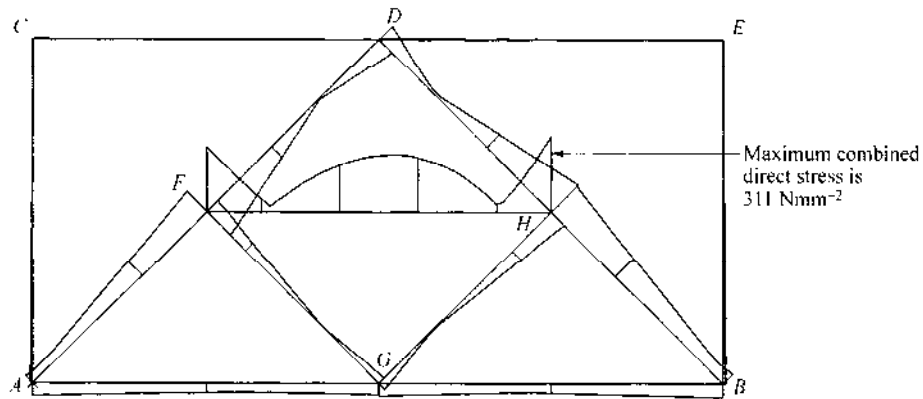
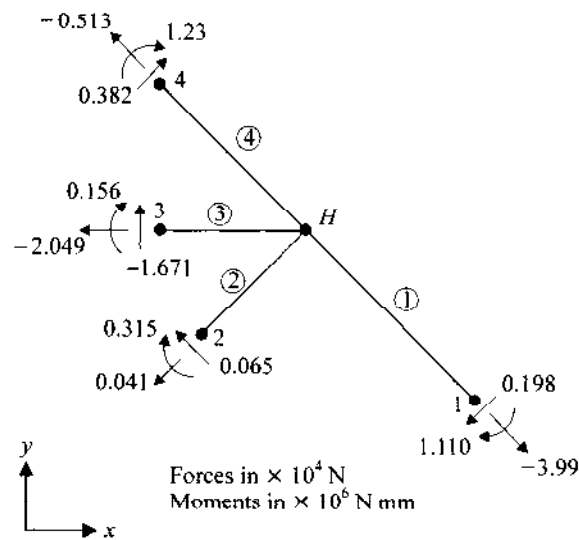


Figure 8.23 Distribution of maximum combined direct stress in the frame.



Nodal displacements				Surface direct stresses at joint H		
Node	$u$ mm	$v$ mm	$\theta_z$ mrad	Element	Top, $\text{Nmm}^{-2}$	Bottom, $\text{Nmm}^{-2}$
1	0.398	0.197	0.92	①	-159	151
2	0.201	-1.158	1.39	②	75	75
3	-0.290	-2.577	8.72	③	265	-311
4	-0.842	-1.175	0.40	④	62	-151

Figure 8.24 Stresses and displacements at joint H from beam model.

conditions are provided by the frame analysis; these are presented in Fig. 8.24 as the forces and displacements at nodes 1 to 4.

### 8.2.5 Modelling the Substructure with Shell Elements

As was observed above, the stress output from a rigid frame analysis cannot be readily used to design the joints. One approach to obtaining an improved stress solution is to model the hollow sections of the complete frame with thin-shell elements but there are several reasons why this is not an attractive option. First, this analysis takes a lot of effort and does not necessarily provide all the information required. Second, it is clear from the frame analysis that joint  $H$  is the critical joint, and so if it can be demonstrated that this joint design is acceptable in terms of its fatigue performance, then the rest of the butt-welded joints will be acceptable. Finally, as the real purpose of this particular example is to explain how real engineering problems can be modelled, it is more appropriate here to illustrate the important modelling technique known as substructuring.

Occasionally, a finite element analysis will produce a solution which is good over most of the continuum but which lacks accuracy and convergence in one or more local regions. On other occasions, the model may be complex and contain many components such that mesh refinement in all regions becomes impractical, leading to the exhaustion of the computational resources or the limits of the numerical accuracy being exceeded. These common situations call for the ability to model a substructure or subregion alone but subject to the influence of the overall problem under consideration.

There are a few methods available that can be classed as substructure modelling and these are introduced by Knight (1993). Here, an approach will be used that takes the output at specific nodes of the overall frame model and, from this output, establishes the boundary conditions for a substructure model of joint  $H$ , where thin-shell elements are used to represent the walls of the hollow sections.

Note here that it is expected that a thin-shell finite element model of the joint will give an improved stress prediction in the vicinity of the welds. However, modelling of the welds themselves is largely ignored. For example, the mechanical properties of the weld material are not accounted for, nor is the actual geometry, as the actual weld thickness is greater than the wall thickness modelled and also fillet radii at the welds are ignored. These factors must be allowed for when interpreting the results of the substructure analysis. If further refinement is necessary to take proper account of the welds, then the solution for the thin-shell element model can be used to provide the boundary conditions for a more localized substructure model of solid elements. Any such solid model will have many elements and degrees of freedom, if element aspect ratios are to be sensible, with one or two elements through the walls of thickness 4 mm being unlikely to give accurate stress predictions. Hence, such an analysis will be very costly both in the time taken to build the model and in the computing resources needed to produce a solution.

Before the mesh can be specified, the geometry of the substructure needs to be defined. As the boundary conditions are generated from the nodal values of the rigid-frame model, the lengths of the members in the region of the joint are predetermined by the beam element mesh. This is shown in Fig. 8.25, where the finite element mesh is shown superimposed on the local beam elements of the frame analysis. To simplify the behaviour of the joint, and to make both the pinned and rigid-frame models correct, the members have their centre lines concurrent. It is often the case, however, that members are offset such that eccentricity is present.

The shell mesh is constructed within a new global axis system which is chosen with its origin at the point where the centre lines of the four members intercept, i.e. point  $H$ . Coordinates for the ends (i.e. nodes 1 to 4) of the substructure are calculated from the frame model, and trigonometry is used to determine the coordinates of the 14 separate areas of the surface where the thin-shell elements will be placed. Simple distributions of elements are then created on these areas of the surface to give the mesh shown in Figs 8.25 and 8.26. Clearly, this is an example of a mapped mesh. Some element distortion has occurred but this is well within the limits imposed by the element formulation. Note, however, that the geometry used here defines the middle surface of the elements and so the depth and breadth of each member are each some 4 mm, i.e. the wall thickness, narrower than the nominal section size.

To assist in fabrication of the physical frame and to improve structural performance, the member joining nodes 1 and 4 is a single continuous length of section  $80 \times 40 \times 4$  mm. The other members consist of a length from node 2 of

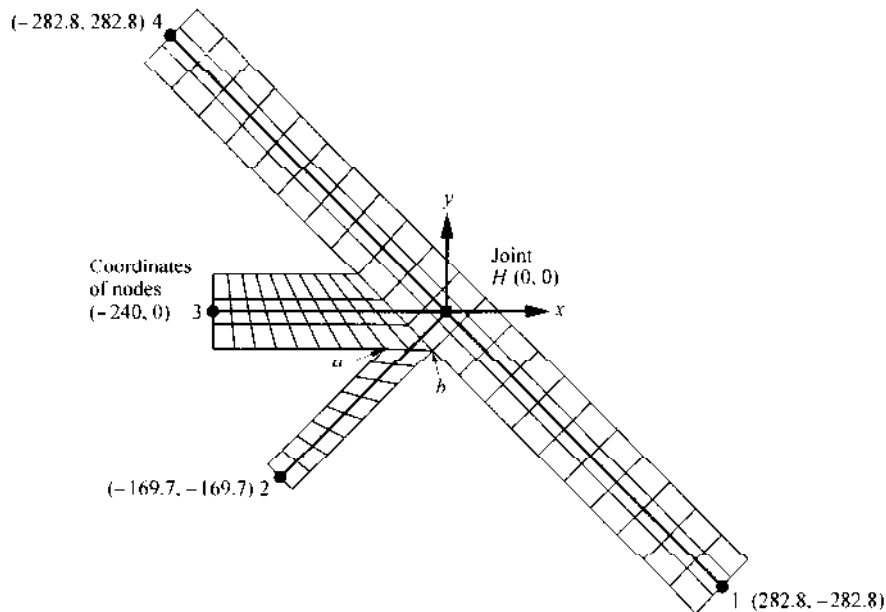


Figure 8.25 Mesh of thin-shell elements superimposed on beam mesh.

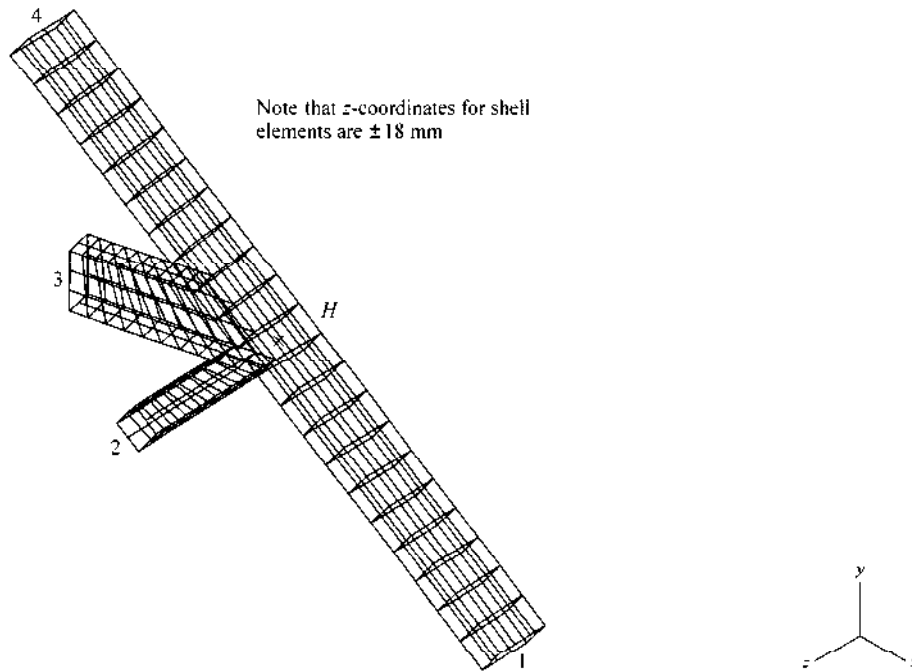


Figure 8.26 Isometric view of thin-shell element mesh.

section  $40 \times 40 \times 4$  mm and a length from node 3 of section  $80 \times 40 \times 4$  mm. In the model the connection between these sections has been approximated as can be seen in Fig. 8.25. Looking at the surface labelled *ab*, it is found that it is not horizontal and has a downward inclination of  $1.9^\circ$ . This slight modification to the mesh prevents the model from having elements of widely different aspect ratios. Such a modification to the geometry is not considered serious here, as this region is in compression and it is the tensile regions of the butt welds that limit the fatigue resistance.

The model was constructed from linear quadrilateral thin-shell elements, and there are 374 elements and 384 nodes. Each node has 6 degrees of freedom and so there are 2304 degrees of freedom in total. All elements are assigned a thickness of 4 mm and have the material properties given above. This shell analysis allows von Mises' stress contour plots to be generated and this requires values for the direct yield strength.

### 8.2.6 Applying Boundary Conditions to the Substructure Model

Now the boundary conditions must be specified. The first of these is a restraint on all movement at one node in the frame model, which translates to support restraints for a plane of nodes. Noting, from the frame model, that the smallest

rotation  $\theta_z$  is at node 4 it is decided to fully restrain the nodes at the equivalent plane of nodes, that is all six degrees of freedom are set to zero. This support boundary condition, shown in Figs 8.27 and 8.28, is not physically correct and any stress concentrations that arise near to this region has to be ignored. However, this is a valid assumption if advantage is taken of Saint-Venant's principle. This tells us that any local behaviour dies away quickly away from a local disturbance such that results are unaffected a reasonable distance from where any slightly erroneous boundary conditions are applied. Saint-Venant's principle also allows us to model, at nodes 1 to 3, the loading due to the element forces, be they axial or shear forces or bending moments, given in Fig. 8.24, as a statically admissible set of edge pressures. The word 'admissible' is important here as it means that the loading in the model does not exactly match the true distribution but is acceptable for the purpose of modelling.

To illustrate the modelling procedure for the loading at the ends of members, the calculation of the constant edge pressure, entered into the software as a force per unit length per element thickness (dividing this force by the element thickness gives the pressure loading in  $\text{N mm}^{-2}$ ), shown in Fig. 8.29 for node 1, will now be considered. Note that in the figure the directions used to define the sign of the forces are shown.

There are three element forces to consider. First, the axial load at node 1 is  $-3.99\text{e}+04\text{ N}$ . To determine the axial edge pressure of  $-178.2\text{ N mm}^{-1}$  per

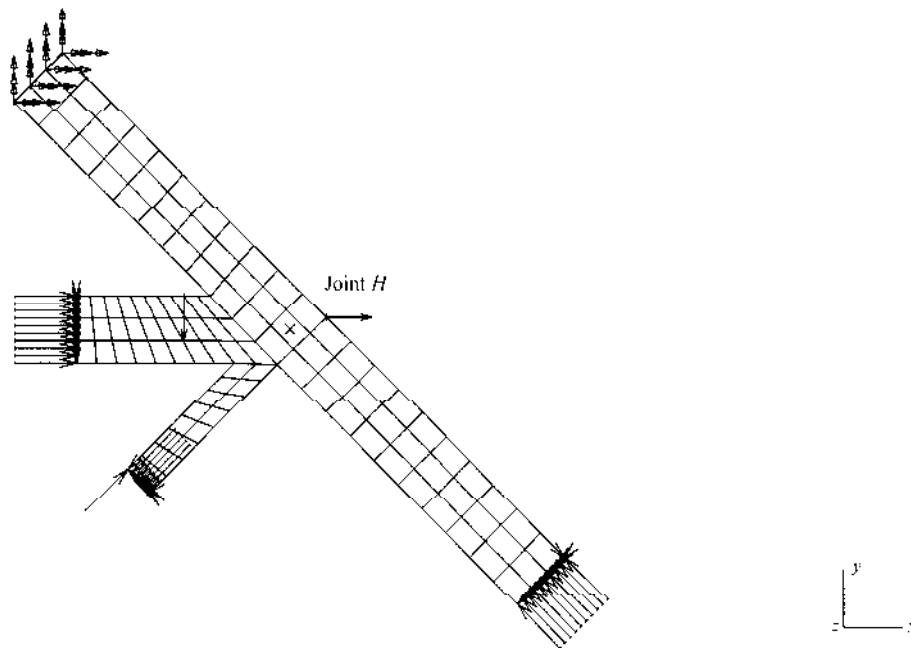
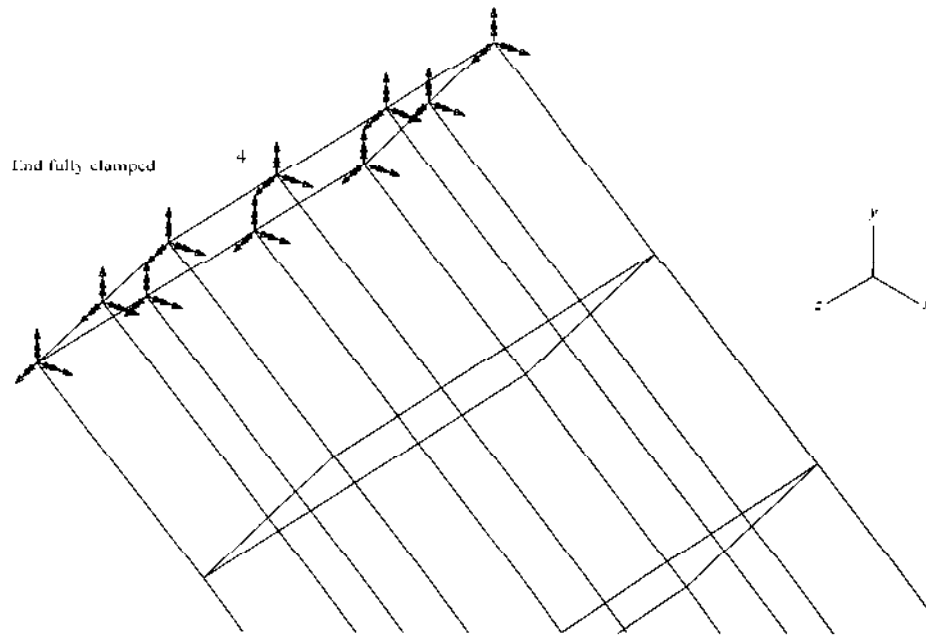
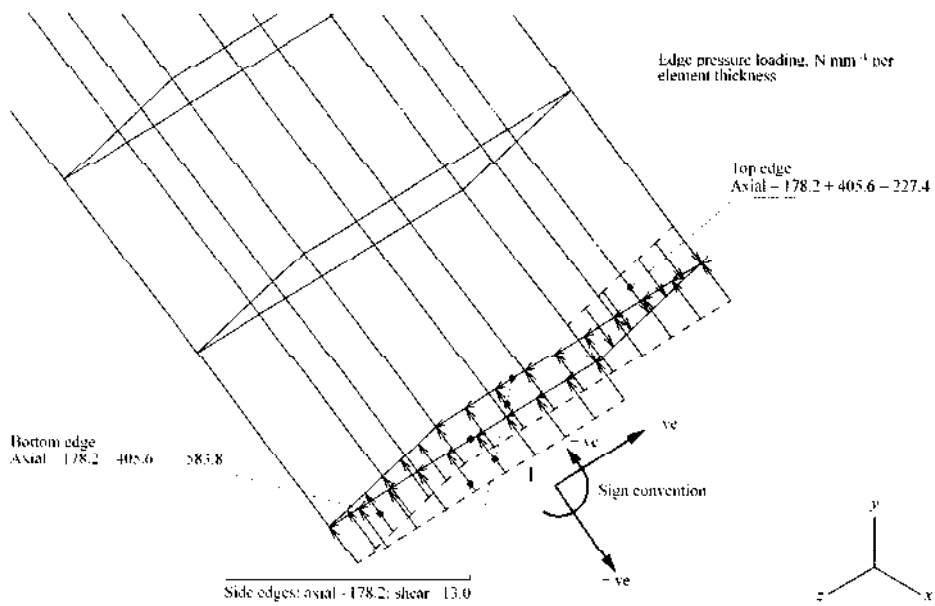


Figure 8.27 Boundary conditions for shell model of substructure.





**Figure 8.28** Fully clamped boundary condition at node 4.



**Figure 8.29** Boundary conditions applied at node 1.

element thickness, the load is divided by the length over which it acts, 224 mm (twice 76 mm plus twice 36 mm). This axial pressure is applied to all four edges. Second, the shear load of  $-1.98 \times 10^3$  N is assumed to act as a constant shear stress of  $-13.0 \text{ N mm}^{-1}$  per element thickness over the two side walls. Finally, the bending moment of  $-1.11 \times 10^6$  N mm must be modelled. The simplest way is to use the fact that the moment is a couple that may be modelled by two equal and opposite parallel forces separated by a distance, i.e.  $M = Fd$ . By taking  $d$  as 76 mm, the distance between the top and bottom edges of the mesh, the value of the force  $F$  is  $1.46 \times 10^4$  N. This force is translated into an axial pressure loading of  $405.6 \text{ N mm}^{-1}$  per element thickness by dividing it by 36 mm, the length of an edge. Following the direction of the moment it is positive at the top edge and negative at bottom edge. The software takes account of the constant wall thickness.

Now that the boundary conditions are known in terms of the data derived from the rigid-frame analysis, this stage of the modelling process can be completed by including the loading due to the external applied loads. This loading consists of two parts:

1. A concentrated force of 4.5 kN acting in the  $x$ -direction with its (assumed) line of action being through the centre of joint. In the real frame this load is applied to the side walls (front and back) of the member  $1H4$ , as shown in Fig. 8.25, and, for example, this may be achieved by having a rigid bar member welded to both front and back walls. Our model of the substructure does not include this level of detail and so the load is modelled in a different way. Here, note that it is important to maintain symmetry in the problem and so to have all of the loading acting in the  $x$ - $y$  plane. This eliminates any out-of-plane deformations which would make the rigid-frame analysis invalid. A statically equivalent concentrated nodal force and moment are, therefore, applied to a mid-position node on the top surface of the member, and this loading condition is, in part, shown by a horizontal arrow in Fig. 8.27.
2. A distributed vertical loading on member  $FH$  (see Fig. 8.17). On studying the geometry of the substructure in Figs 8.25 and 8.26, it can be seen that the length of member  $3H$  is less than the corresponding sections in the frame analyses. This is because of the physical geometry of the members which are now being modelled. Consequently, the distributed load cannot be applied as shown in Fig. 8.17. As an approximation, it has been decided to model this loading as a statically equivalent single vertical force of 10.83 kN at a distance of 122.5 mm from the end of the member, as shown in Fig. 8.27. It was necessary to model this load as a force and compensating moment as the nearest node to this position where the force acts is actually 120.2 mm from the end.

### 8.2.7 Analysing the Results for the Substructure

Having applied all the necessary boundary conditions a static analysis of this finite element model of the substructure is carried out. As a first check of the

results of this analysis, the reaction forces ( $F_x$ ,  $F_y$  and  $M_z$ ) at the restrained end are checked to ensure that static equilibrium is satisfied and so to establish that the loading is that given by the frame analysis. As this simple check shows that the overall position is correct, a more detailed analysis of the results can be made.

By using post-processing facilities the results of the analysis can be viewed. For example, the deformed shape and stress contour plots of any view of the model may be produced. Here, however, it is important to plan the required pictures so that they are meaningful to those who have to interpret them.

For this analysis let us consider the deformed shape, which is shown in Fig. 8.30 together with the undeformed shape. Note that the displacements are greatly magnified and that the display produced here is a two-dimensional view for the  $x$ - $y$  plane and has been chosen to show that the joint is not twisted out of this plane. Comparing the deformed shape calculated from the substructure analysis with that for the same joint calculated from the frame analysis, Fig. 8.18, it is seen that the two analyses predict the same overall behaviour. This positive check between the analyses is another piece of evidence that points to the substructure model being qualitatively correct.

As to the use of the substructure model in the design of the frame, it is the results for stress within the material of the joint that are needed to carry out a fatigue analysis of the butt welds. The designer will want to know the peak stress values when the dynamic loading is a maximum and a minimum and the peak

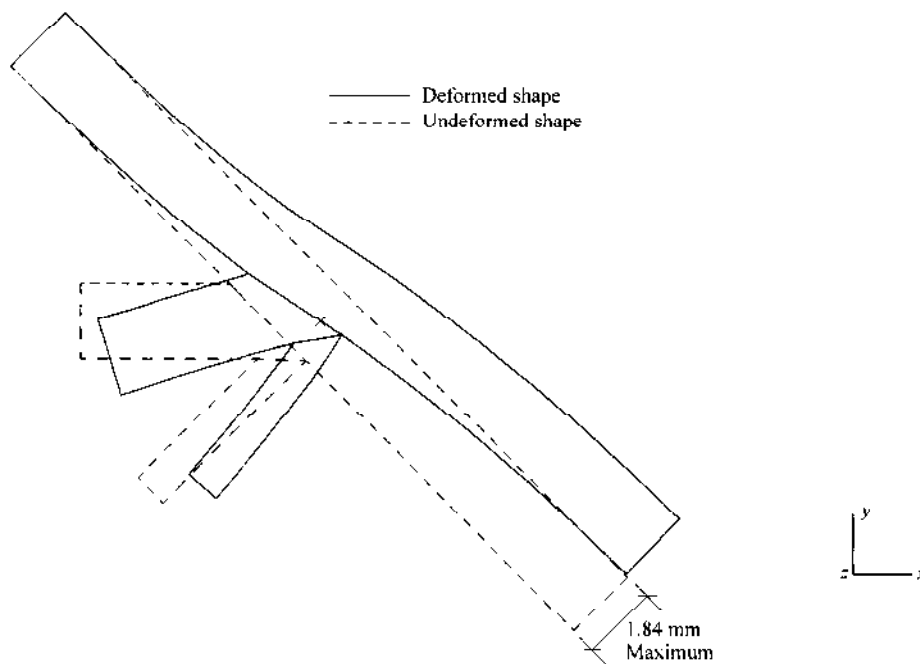


Figure 8.30 Deformed shape of the substructure.

stresses when the machine is not in motion and the frame has to transmit only the dead loads. The finite element model developed above will predict the first of these situations and so further analyses are necessary to predict the other cases.

To illustrate a typical display of stress results, consider the the butt weld in joint  $H$  with the highest tensile stresses. By generating a stress contour plot of the maximum principal stresses, e.g.  $\sigma_{ts}$  at the top surface of the shell elements (see Fig. 7.22), over the whole model and then using the zoom facility, it is a simple task to find that this critical connection occurs where the top surface of the horizontal member  $3H$  meets the bottom surface of member  $4H$ .

To present the contour displays, two areas of elements have been chosen and the elements grouped for display purposes. Figure 8.31 shows that such a display effectively isolates the required butt weld from rest of the mesh. Clarity of the stress contour display is improved by magnifying the region of the weld on the screen and then displaying only the boundaries of the element group. Figures 8.32–8.34 show, respectively, contour plots for:

- the maximum principal stress at the top surface  $\sigma_{ts}$ , which comprises mainly tensile stresses
- the maximum principal stress at the middle surface  $\sigma_{ms}$ , which is mainly axial stress
- the maximum principal bending stress  $\sigma_b$ .

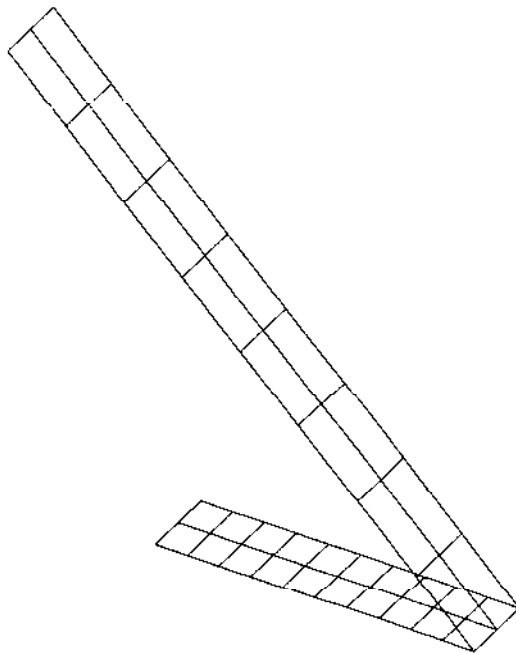


**Figure 8.31** Group of elements for display purposes.

The contours are generated using nodal values from all nodes in the model and not just those nodes associated with the elements shown in Fig. 8.31. If the plots are generated using only those elements in the group shown, then the values displayed are restricted in range, producing a misleading impression. Hence it can be seen that an analyst has to ensure that the contour plots are calculated using all relevant nodal values to give a meaningful display.

Figures 8.32–8.34 also show three nodal stress values along the line representing the welded connection. From this the peak stress value is seen to be about  $150 \text{ Nmm}^{-2}$ . Comparing this with the value calculated using the rigid-frame analysis, i.e.  $265 \text{ Nmm}^{-2}$  shown in Fig. 8.24, and with the yield stress of  $350 \text{ Nmm}^{-2}$ , it can be seen that the shell model produces a peak stress at the weld about one-half of the beam analysis value. Figures 8.33 and 8.34 show that the top surface stress is principally due to an axial component with the bending component being significantly lower. Note that the relationships between the stresses given in Fig. 7.22 do not hold at the location of the butt weld, because not all of the elements are in one plane.

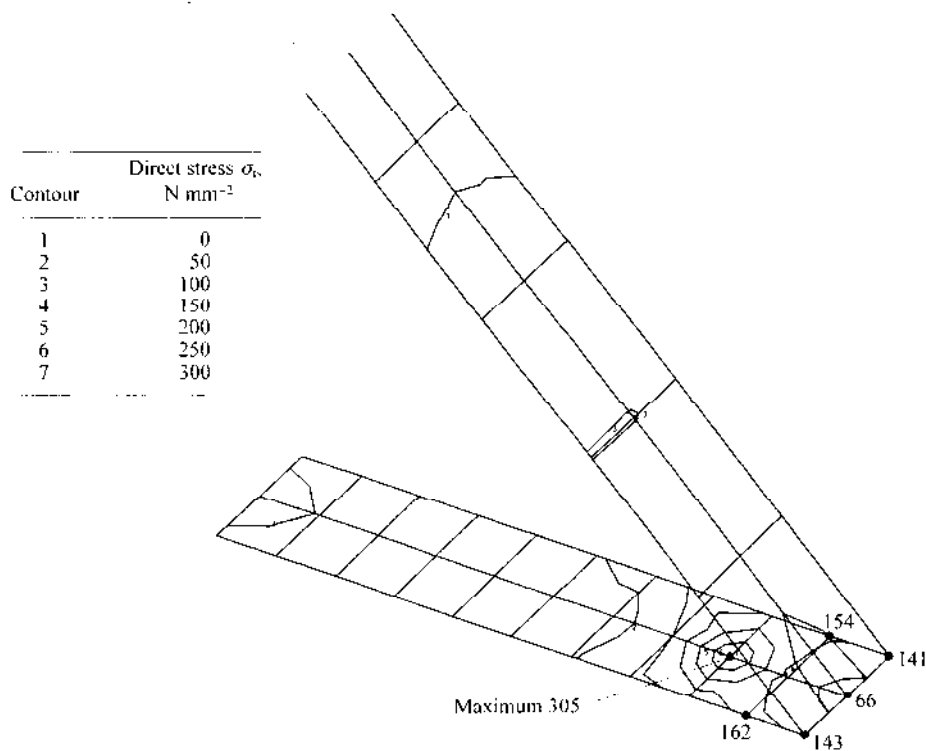


Figure 8.32 Contour plot of maximum principal stress at top surface.

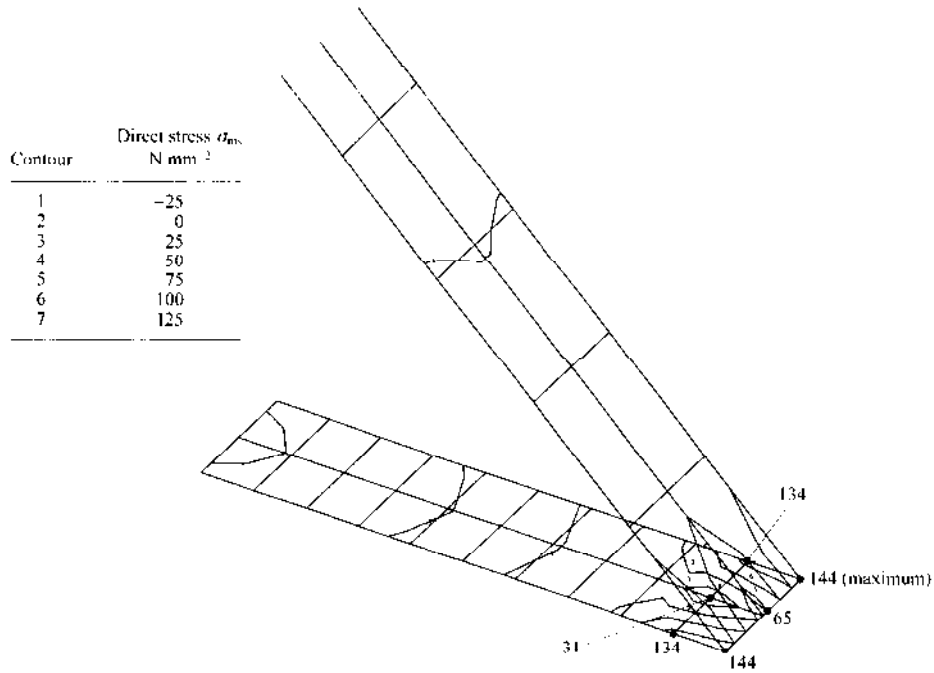


Figure 8.33 Contour plot of maximum principal stress at middle surface.

Finally, Fig. 8.35 is a contour plot of the von Mises' maximum principal stress at the bottom surface of the shell elements, the location where this stress is maximum. This is derived from the standard formula

$$\sigma_{\text{vonMises}} = \sqrt{\frac{1}{2}[(\sigma_1 - \sigma_2)^2 + (\sigma_1 - \sigma_3)^2 + (\sigma_2 - \sigma_3)^2]} \quad (8.8)$$

where  $\sigma_1$  and so on are the principal stresses. The formula predicts that yielding occurs when the value of von Mises' stress in (8.8) exceeds the yield stress in uniaxial tension  $\sigma_Y$  which is  $350 \text{ N mm}^{-2}$  for grade 45/50 steel. It can be concluded that yielding of the material has not occurred in the region of the weld because the peak von Mises' stress there is about  $150 \text{ N mm}^{-2}$ .

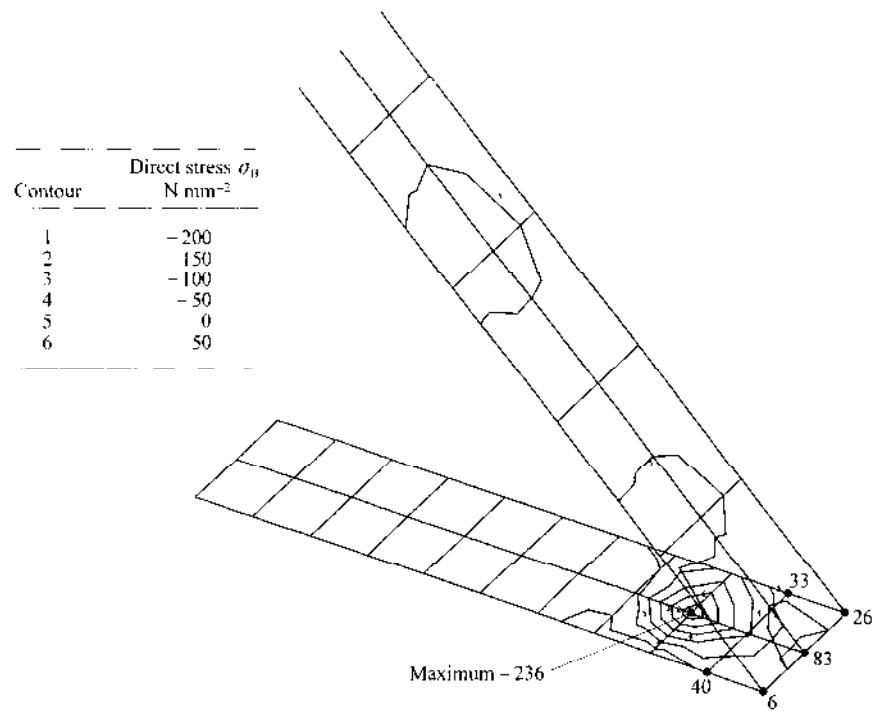


Figure 8.34 Contour plot of maximum principal bending stress.

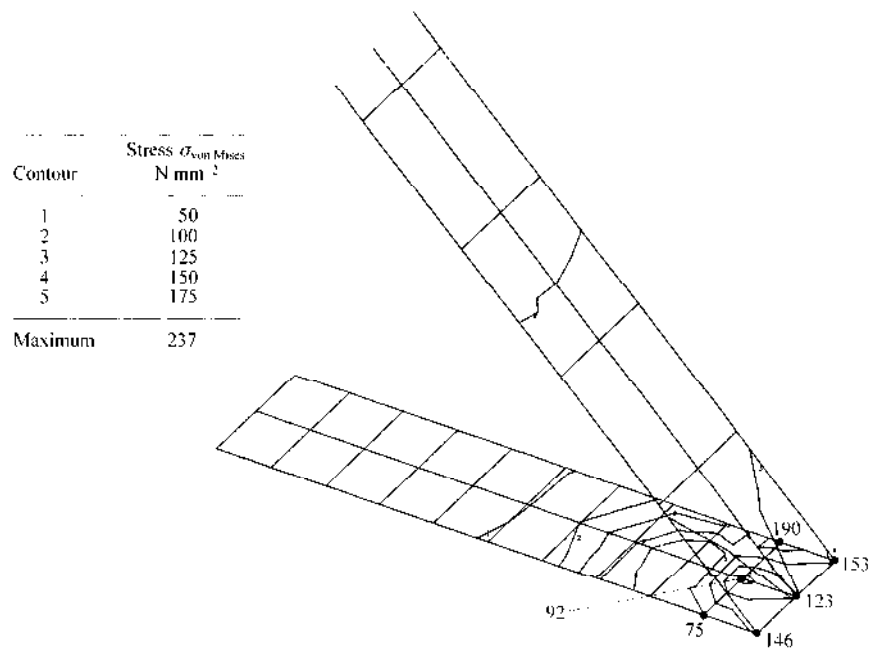


Figure 8.35 Contour plot of von Mises' stress at bottom surface.

Having discussed four examples in detail within Chapters 7 and 8, where minimal computing effort was required, some larger cases can now be considered. These have an automotive flavour, but they are typical of the larger scale studies that are carried out in a variety of industries. While the previous examples enabled discussion of some of the finer points of modelling, these industrial case studies will show how finite element modelling is used for situations with complex geometries where some form of assumption has to be made to progress a solution. It is the use of sensible assumptions in given situations that distinguishes the artistry of truly professional analysts.

The following cases will be studied here:

- a strength and stiffness analysis of the frame of a recumbent bicycle
- an analysis of a connecting rod from a road vehicle engine
- a composite suspension arm from a road vehicle
- a displacement analysis of a passenger vehicle body shell.

## 9.1 ANALYSING A BICYCLE FRAME

In this example the strength of a commercially available recumbent bicycle which has been used as the basis for a variety of undergraduate projects in the area of human-powered vehicles is considered. To define the geometry, a solid model is built and then the surface of this is meshed with thin-shell elements. Realistic load conditions can then be simulated and the strength of the existing frame assessed.



### 9.1.1 Description of the Problem

The generic form of a recumbent bicycle is illustrated in Fig. 9.1, which is a solid model of the major components. It is clear from this figure that the rider sits in a quite unusual position, compared to that for a normal bicycle. In this case the rider sits as if in an armchair and provides motive power by pushing on the pedals which are located directly ahead. With the rider in this position, the aerodynamic drag of the rider–bike combination is reduced and this enables higher speeds to be achieved for a given power input. For this reason, such a riding position has been widely adopted by several manufacturers of human-powered vehicles. As part of a programme of undergraduate project work, ways of improving the design in terms of the aerodynamics, steering, ergonomics and drivetrain of the vehicle have been investigated, together with a study of putting a small engine on the bike to turn it into a low-powered endurance vehicle.

Before making any structural changes to the bike, the strength of the frame needs to be assessed and any weak areas determined. This enables strengthening to be carried out where necessary before any modifications are made that might increase the load on the bicycle frame. Stress results will be produced for this geometry under normal static load conditions.

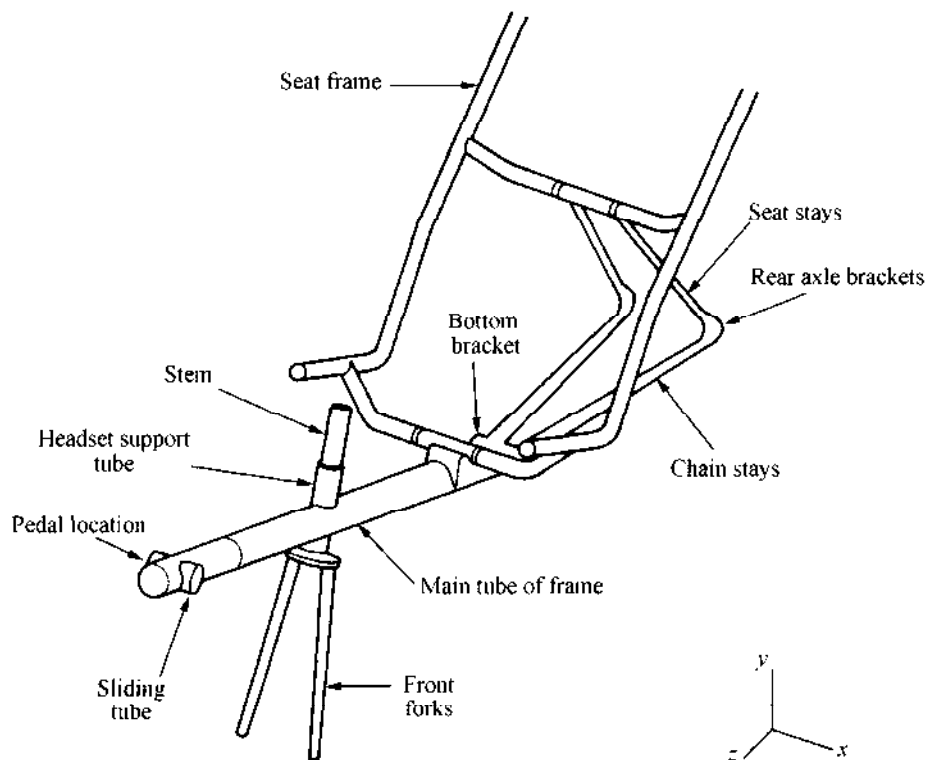


**Figure 9.1** A solid model of a recumbent bicycle frame.

### 9.1.2 The Bicycle Geometry

A detailed study of Fig. 9.1 shows that this bicycle is of extremely simple construction. A conventional bike has a triangular frame with the main triangular section made of a top tube, seat tube and down tube. In the recumbent design studied here, this triangle of tubes is replaced by a single structural member which is a tube of larger diameter than is used on a conventional bicycle. Through this main member is placed a tube which supports the bearings, or headset, for the stem attached to the handlebars and the front forks. For simplicity of manufacture, these two tubes are welded at right angles to each other. Elliptical cross-section forks are used which are straight and welded to a cross-piece, the fork crown. To support the pedals and chainwheel, a smaller tube which holds an axle and bearings is slipped into the front of the larger tube and clamped in place. At the rear of the main tube a conventional, but nonfunctional, bottom bracket supports two chain stays, to which the rear axle and the gear system are clamped. Finally, two seat stays are joined to the top of the tubular seat frame and a bracket clamps the seat frame to the main tube. Note that webbing is slung across the seat frame to support the rider.

Detailed measurements of all of the relevant structural members have been taken manually from the physical frame and from this data the solid model shown in Fig. 9.1 can be created. Note that all the members are of single thickness as no joints have been double-buttet.

### 9.1.3 Creating a Solid Model of the Geometry

Care must be taken when thinking about the creation of the solid model. Yet again, it is seen that the needs of the analysis must be taken into account before producing a computer model. In this case a thin-shell finite element model will ultimately be built; this dictates the approach to be taken in creating the solid model of the geometry. It is perfectly feasible, and probably very obvious, to build a solid model of the exact geometry using tubes for all the components that are tubular. Here, however, as shell elements are to be used which have zero physical thickness, a different approach has to be taken. The mathematical formulation for an element handles the behaviour of the element owing to its thickness and so the elements must be placed with their nodes at the mid-depth position in the out-of-plane direction. This is the same procedure as that used for the pressure vessel in Sec. 7.2 and for the substructure analysis of the frame joint in Sec. 8.2. To ensure that this is easy to do, the physical dimensions of the tubes are not recreated in the solid model, rather the tubes are modelled as solid cylinders with a diameter calculated to allow for the actual material thickness.

First, the main tube is modelled using the primitive shape of a cylinder and is placed in the correct orientation. Then further cylinders to represent the holder for the forks and stem, and the bottom bracket, are created and placed in position. Using the Boolean addition operation typical of solid modelling software that uses constructive solid geometry (CSG), these smaller cylinders can then be

joined to the main cylinder. The chain stays are created using a skinning operation. To do this closed curves, known as profiles, of the appropriate form for the ends of the stays are created and a smooth skin placed between them. The software uses a smooth surface to transform these profiles into solid objects. These stays can then be placed in position and added to the cylinders. To complete the first stage of the geometry modelling, the rear axle brackets are created as a profile in two dimensions and then extruded through the third dimension to give the object depth, before being joined to the rest of the model. Figure 9.2 shows the solid model as a wireframe form at this stage of the process.

Next, skinning operations are used to model the seat stays. Also simple clips and brackets are modelled to support the seat frame, before the two cylinders representing the pedal support are joined and moved into place. Figure 9.3 shows the model at this stage.

A further skinning operation is used to form the seat frame, with a circular profile being swept along a path in three dimensions for each of the four members of the seat frame. In those areas where the seat frame is highly curved, a number of profiles are used to ensure that a smooth surface is created. Finally, skinning is used to create the front forks which are attached to the stem through a cross-piece, the fork crown. With these items added to the model the necessary structure is complete and a wireframe of the complete model is shown in Fig. 9.4.

#### 9.1.4 Obtaining a Mesh of the Geometry

To produce a mesh from the solid model of the geometry an automatic free mesh generator is used. This looks at the solid model, then places a pseudo-triangular

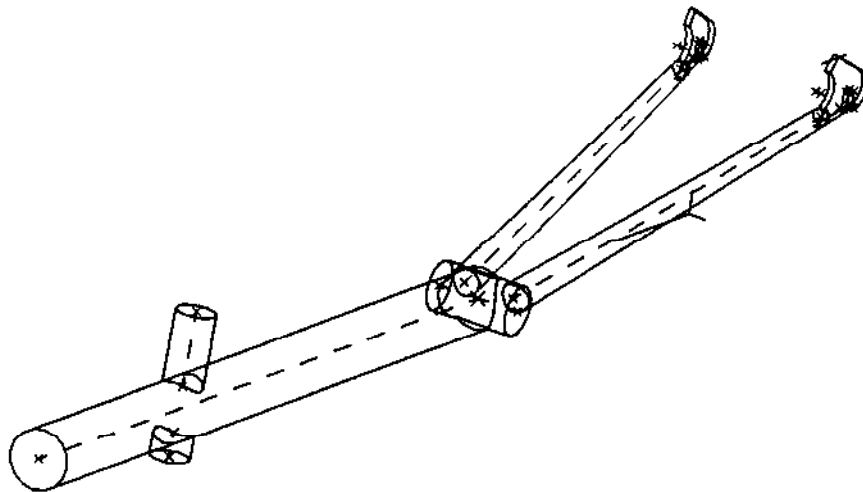


Figure 9.2 First stage in the assembly process.

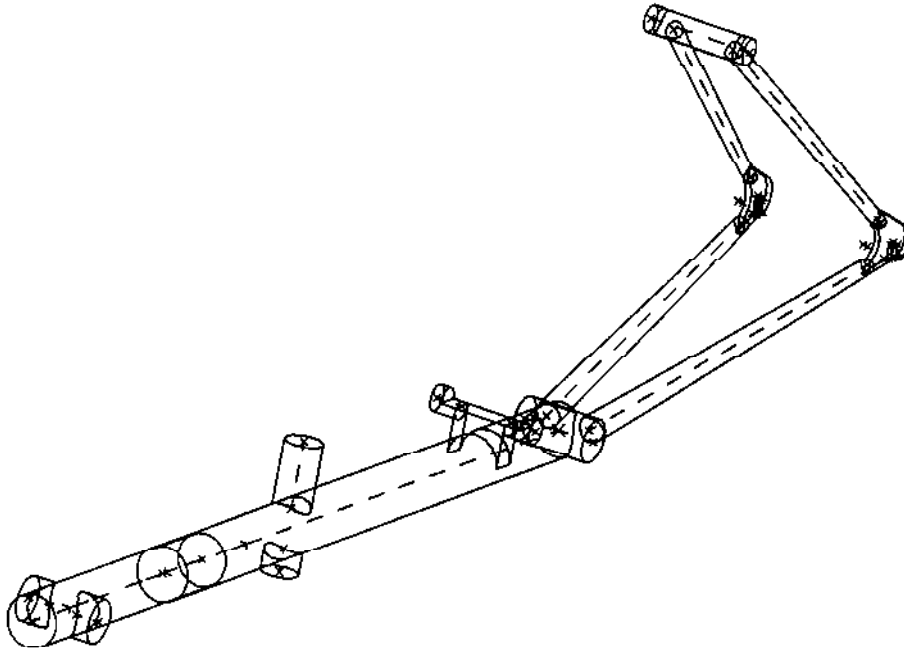
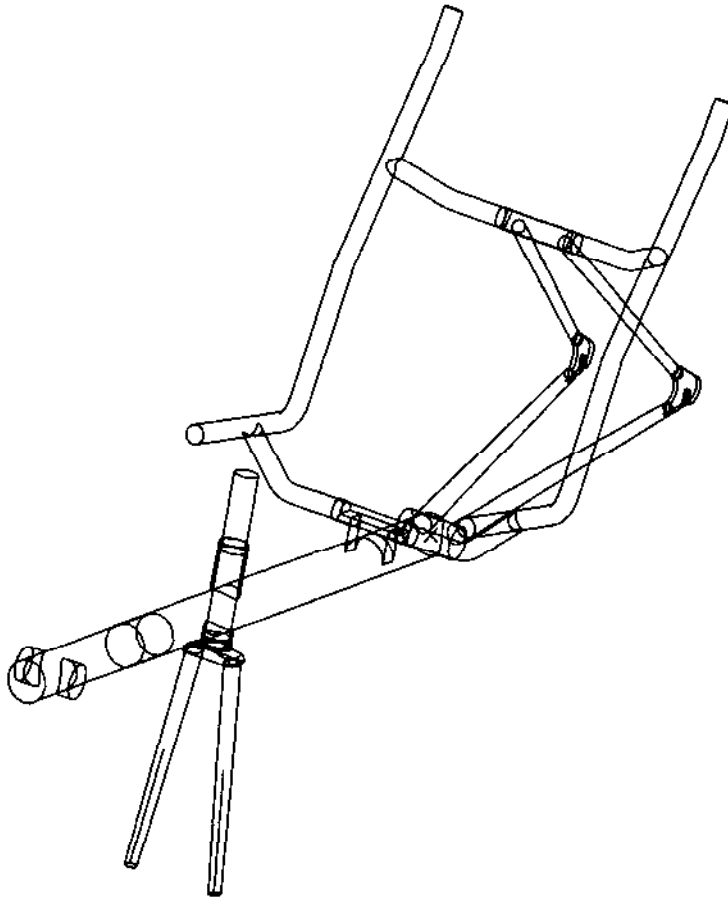


Figure 9.3 Second stage in the assembly process.

mesh on the surfaces of the model before creating a final tetrahedral mesh within the surfaces. In this case the tetrahedral mesh is deleted, as it is not needed for this thin-shell finite element analysis. However, the data defining the surface patches enclosing the volume is retained, so that a thin-shell mesh can be created on these surface patches.

Separate meshes have been created for the forks-stem assembly, the seat frame, the pedal support tubes and the main structure. To control the distribution of the elements, global element lengths of 30 mm on the main tube and 10 mm in other areas have been used. A second mesh control parameter has also been used which ensures that a suitable number of elements are placed on highly curved surfaces. Figure 9.5 shows how this works in the two-dimensional case, where the deviation is defined for a single element as a percentage of the element length. The shorter the element, the more accurate is the description of the surface and the lower the deviation. Here the maximum allowable deviation has been set to 20 per cent.

Figure 9.6 shows the full thin-shell mesh for this problem. Note that, for now, only tubular material has been meshed and the solid metal parts, such as the axle brackets, have been left out of the finite element model. Such solid material is considered to be lightly stressed, with the large stresses of interest being generated only in the thin tubing. For this situation, some 15 000 linear triangular elements have been used together with some 8000 nodes.



**Figure 9.4** Final stage in the assembly process.

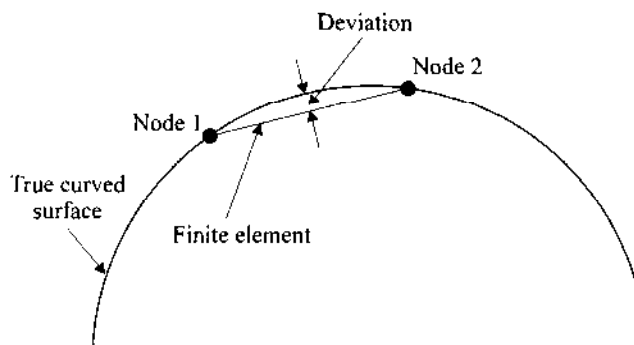


**Figure 9.5** Deviation of an element from a surface.

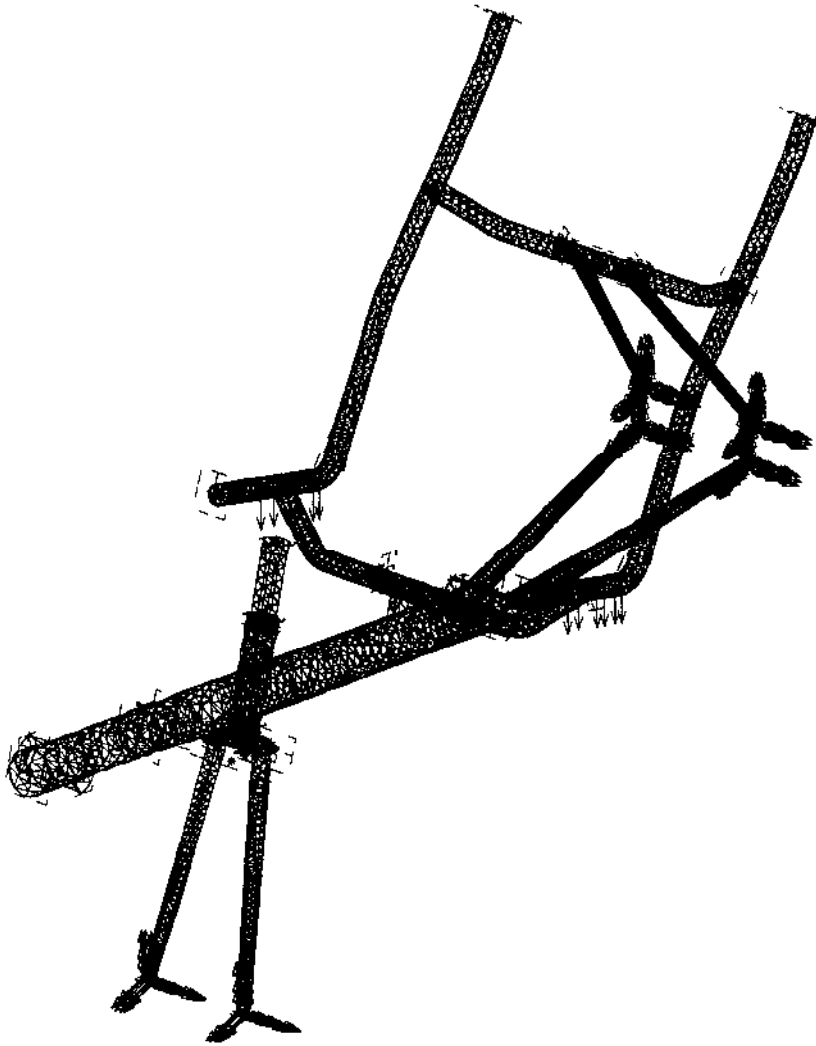


**Figure 9.6** The completed finite element mesh.

### 9.1.5 Material Properties and Application of Boundary Conditions

All of the tubes modelled are of structural steel, as is the seat frame, and appropriate Young's modulus and Poisson's ratio have been defined.

For the strength analysis of the bike only the static load of a rider sitting on the seat will be simulated, i.e. no load is to be applied to the pedals. To do this the nodes that are next to the missing rear axle brackets are restrained such that they have zero displacement in all directions, and the nodes where the front axle is clamped are restrained to have no vertical or sideways movement, from the rider's viewpoint, but they are left free to move forwards and backwards.

The dead weight of the rider is applied by splitting a total load equivalent to 80 kg across 20 nodes along the seat frame. This is shown in Fig. 9.6 by the single-headed arrows, together with the other restraints. Such an approximation is considered to be valid as the area of concern is the bike frame itself not the seat frame. Hence any load applied to the seat should be diffused through the seat frame, ensuring that the load transfer from the seat into the main structure is realistic.

Finally, the seat frame is connected to the clips by rigid bar elements. These are also used to join the pedal support to the main tube and to join the forks–stem assembly to the main tube system.

### 9.1.6 Analysing the Results

Once the model has been run, the results can be analysed. To do this the graphical post-processor is used, as the large quantity of data produced prevents the raw information being used in the first instance. A useful starting point is to analyse the results for displacement. Figure 9.7 shows a typical view of the structure with a displaced side elevation. Note that the displacements have been magnified and that they show the basic form of the deformation. The frame acts by the load on the seat deforming the main member in a downwards direction in the middle forcing the front end to rise up. This bending is opposed by bending in the forks. Also, the chain stays and seat stays bend to oppose the bending of the seat frame and main member.

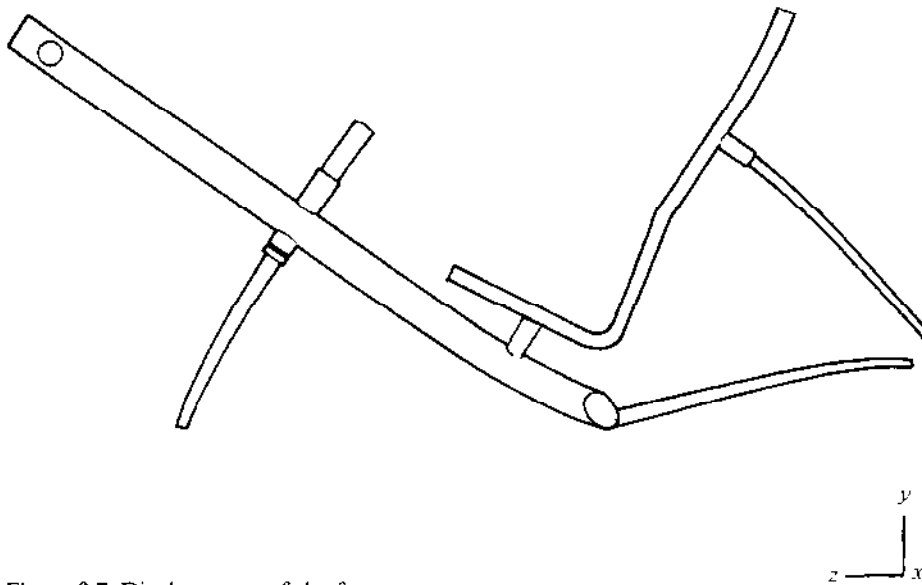


Figure 9.7 Displacement of the frame.

For quantitative data about the behaviour of the structure, contour plots of stress magnitude are shown in Figs 9.8 and 9.9, where the von Mises' stress for certain areas of the mesh are plotted. In reality colour plots would be used but, for reasons of clarity in monochrome, labelled contours are shown here. In Fig. 9.8, the von Mises' stress on the bottom surface of the shell elements are shown in the region of the seat, main tube and stays. Similar plots are obtained for the stresses at the top and middle surfaces of these elements as well. From this figure stresses at contour level 4 (200 MPa) can be seen to occur where the main tube meets the chain stays and where the seat is attached to the main tube. In Fig. 9.9 a close-up of the area around the tube-stay junction is shown where contours of level 6 (300 MPa) occur. As typical values for the ultimate tensile strength of steel vary from 400 to 700 MPa, the finite element model seems to be predicting that failure is close in this case. This analysis shows that strengthening needs to be considered in this area of the structure.

## 9.2 DESIGN OF A CONNECTING ROD

All piston engines use a connecting rod (con-rod) to convert the reciprocating motion of a piston to the rotary motion of a crankshaft. Traditionally, con-rods have been made of steel, but with the pressure on vehicle manufacturers to reduce the mass of vehicles and so make them more fuel efficient, other lighter materials are now being used.

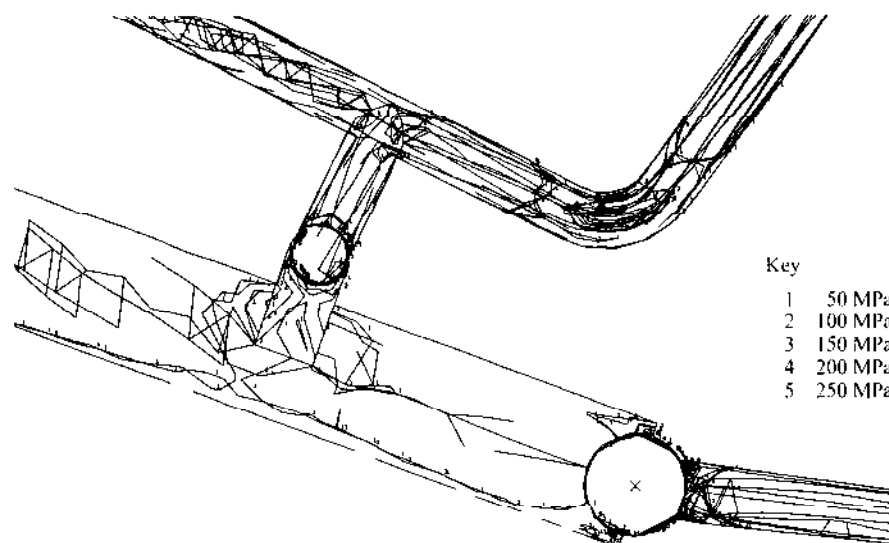


Figure 9.8 Contour plot for stress—side view.



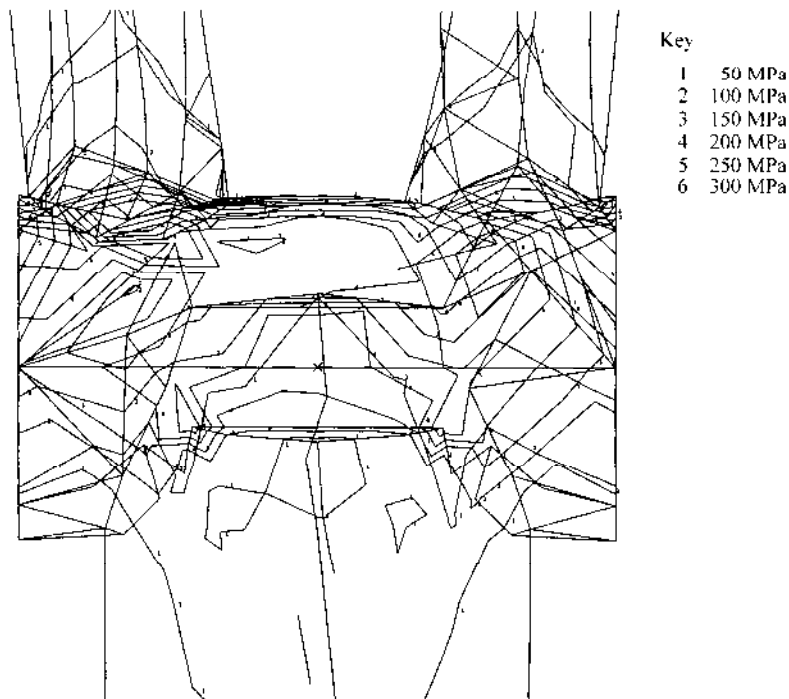


Figure 9.9 Contour plot for stress where stays meet main tube.

This example has been provided by Jaguar Cars and is concerned with the early development of an experimental aluminium alloy con-rod during the late 1980s. During fatigue testing of an initial prototype design, the con-rods were failing well before their specified design life. Investigations were carried out using finite element analysis with the goals of understanding the reasons for these failures, of improving the design before further testing was carried out and of producing appropriate design rules.

### 9.2.1 The Problem Statement

Finite element analysis is to be used to investigate the fatigue life of a prototype aluminium alloy connecting rod. Modifications to the design can also be considered to ensure that the fatigue life is acceptable. By using such a computational tool near the start of the design cycle, the amount of physical testing required to achieve a successful design should be reduced.

### 9.2.2 The Geometry of the Con-rod

From engineering drawings of the con-rod a simple solid model can be built, as shown in Fig. 9.10. This shows the shank and little end of the rod together with

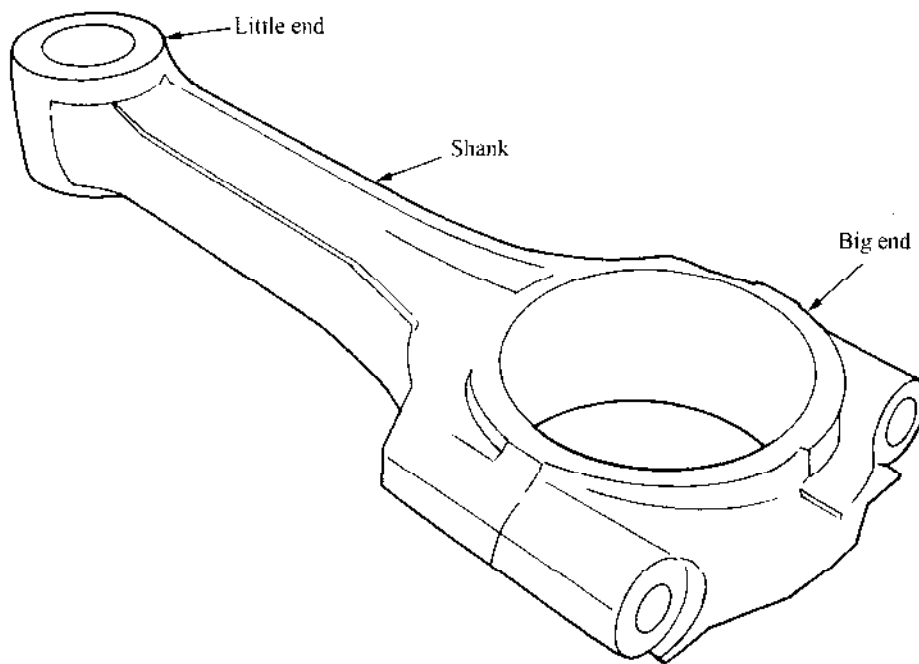


**Figure 9.10** Solid model of the connecting rod.

the big-end cap modelled as a single piece, although in fact they are split at right angles to the plane of symmetry of the con-rod along the axis of the crankshaft. Note the holes for the gudgeon pin at the little end, for the crankshaft at the big-end and for two bolts (at the bottom right of the figure). Also extensive use of filleting has been made.

### 9.2.3 Producing a Mesh

For this design, all the loading cases will be along the longitudinal axis of the rod, and so from symmetry only one-quarter of the physical artefact need be modelled. Hence only one-quarter of the solid model needs to be transferred between the solid modelling program and the finite element pre-processor. Simple mapped meshes can be built to represent the little end and shank of the rod together with the small-end bearing bush and the gudgeon pin. In the big-end region, the geometry is too complex for a mapped mesh and so a mesh has been created manually from the geometry of the solid model. Mapped meshes can, however, be used for the big-end shells and the con-rod bolts, with a manual mesh being used for the crankshaft to match the mesh on the con-rod and cap.

Throughout the model 20-noded parabolic solid elements have been used. Figures 9.11 and 9.12 show the completed mesh with the latter figure showing detail near the bolt. Note that this model was produced before the widespread

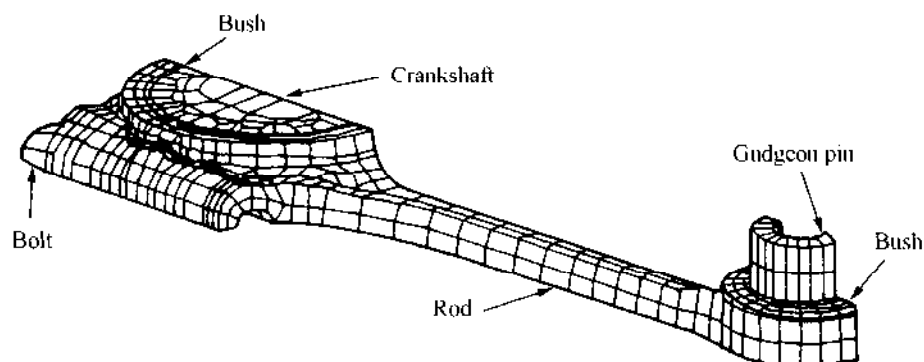


**Figure 9.11** Mesh of the connecting rod.

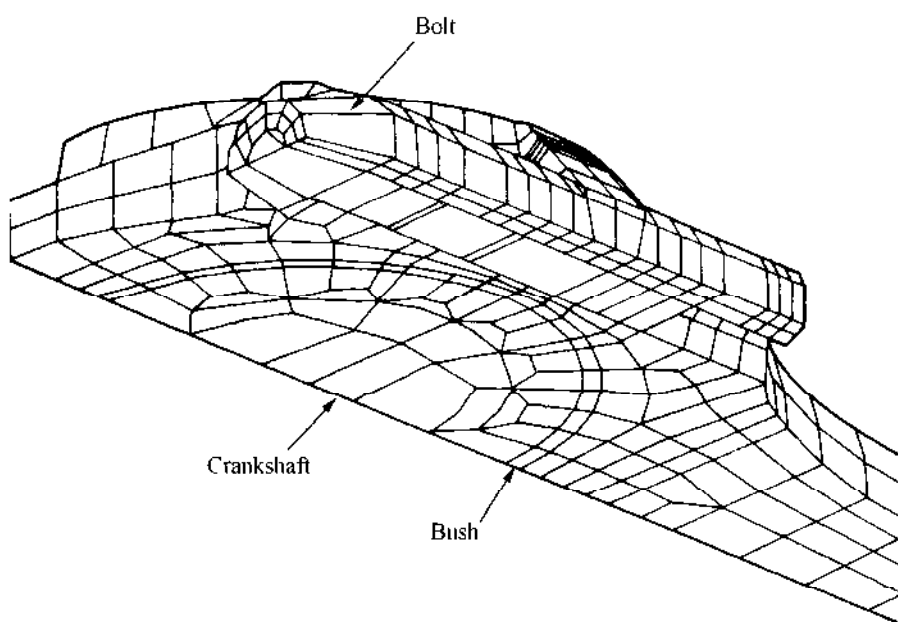


**Figure 9.12** Mesh of rod in the region of the bolt.

availability of automatic meshing procedures. Meshing this combination of objects is much simpler now, as was seen with the bike example in Sec. 9.1.

#### 9.2.4 Material Properties and Application of Boundary Conditions

Aluminium alloy is used for the con-rod with steel for the bolt, gudgeon pin, crankshaft and bearings. Appropriate material properties have been used for the elements in these areas.

As the connecting rod assembly is made up of several parts, complex nonlinear interactions govern how these parts transmit forces. Solving the full nonlinear model is prohibitively expensive, and so a series of well-proven engineering assumptions are used to model the interactions while still using only a static analysis. In all cases friction forces are assumed to be zero where metal-to-metal contact occurs. Hence the big-end cap is joined to the con-rod by axial ties which allow lateral movement along the plane of the joint. Similarly, bearings are tied in the radial direction only.

At the bolt the thread is simulated by tying the bolt to the con-rod and cap in the axial direction and the bolt head is tied axially to the cap. Also the bolt is coupled laterally at two points in the thread region and at the head to allow bending loads to be transmitted to the bolt. To simulate the pre-load on the bolt which draws the con-rod and cap together, the bolt is split into three sections with constraint equations used to pull the sections together and so load the whole structure. This load was adjusted until the stress in the bolt after solution was correct. Hence several solutions had to be run to achieve this initial situation. The temperature effects used to do this will be mentioned in Chapter 10.

Contact areas between the gudgeon pin and small-end bush and between the crankshaft and big-end shells are modelled as a contact patch of constant area some  $60^\circ$  to each side of the loading line. This is done with constraint equations, which are different for the contact patches for the different loading cases. Further, interference fits are used to pre-tension the physical bearings at both the big and little ends. This has been simulated using temperature effects again to produce an initial size for the bearings consistent with the interference.

Symmetry conditions have also been applied along the symmetry planes as was explained for the pressure vessel in Sec. 7.2.

The following three simulations have been run with this model:

1. An assembly case where only the effects of the interference fit of the bearings and of the bolt clamping load are simulated. A tightening torque of 50 Nm giving an axial load of 33.3 kN was applied by trial and error, as mentioned previously.
2. A tensile load applied at the crank-pin centre line with all the nodes along this line being constrained to move together. The gudgeon pin was restrained here to provide the necessary reaction to the applied load. This simulates the physical fatigue test not the actual running condition of the engine. The maximum tensile load during the fatigue test was estimated as 15.71 kN and so an assumed load of 20 kN has been simulated by applying a load of 5 kN to the model of one-quarter of the geometry.
3. A compressive load applied at the crank-pin centre line to give the opposite loading situation to that above.

### 9.2.5 Some Results

Plots of the displacement for the three test cases of assembly, compression and tension are shown in Figs 9.13–9.15, respectively. The displacements have been

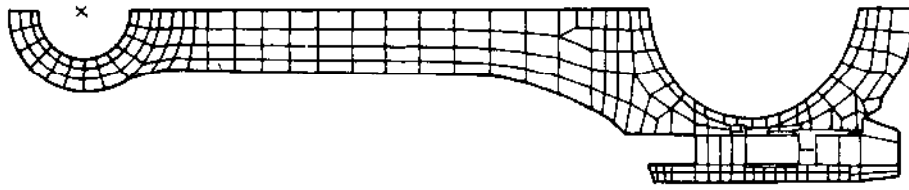


Figure 9.13 Displacement of the model for assembly loading.

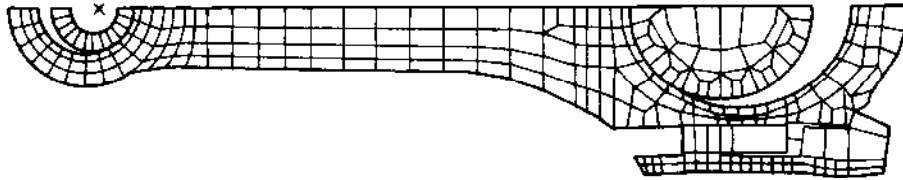


Figure 9.14 Displacement of the model for compressive loading.

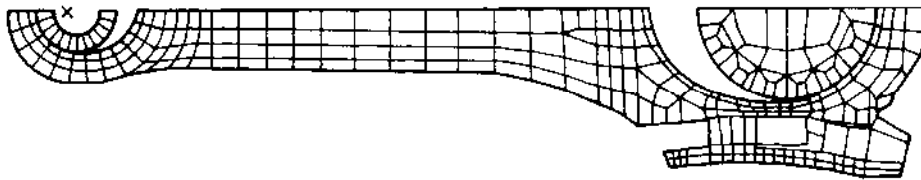
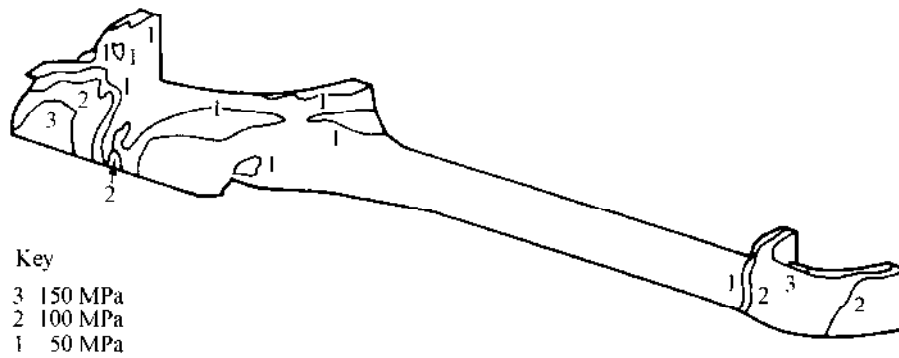


Figure 9.15 Displacement of the model for tensile loading.

magnified by 50 times in all cases. Note that in the assembly case some distortion of the cap and the bolt can be seen. Under compression the little-end eye distorts, as do the cap and bolt yet again, while under tension the eye is stretched severely and the cap-bolt combination distort even more.

Von Mises' stress is shown in the contour plots in Figs 9.16–9.18. The vulnerable areas, i.e. the small-end eye and the cap near the bolt hole can be identified. Note that the compressive load does not alter stresses much from those with just the assembly load at the cap, but the tensile load makes the stresses much larger in this area. Also, the stresses in the eye area are large for both compressive and tensile cases.

Given the results from these three stressing cases, a fatigue analysis can be carried out as the alternating stresses and mean stresses are available for the whole geometry. Such a fatigue analysis predicts a low fatigue life of one million cycles compared to a design expectancy of one hundred million cycles. By increasing the thickness of the material within the rod and repeating the analysis, all the vulnerable areas can be eliminated and the fatigue life improved. Also, design rules for future designs can be derived from these analyses, enabling engineers to design aluminium alloy con-rods in future with the benefit of this piece of work.



**Figure 9.16** Von Mises' stress from assembly loading.

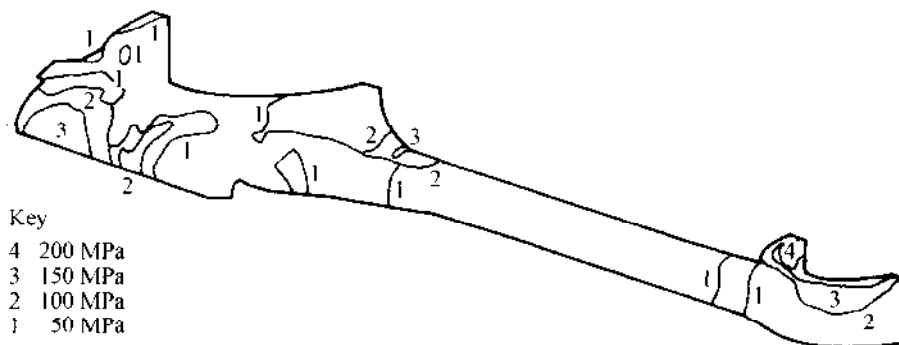


**Figure 9.17** Von Mises' stress from compressive loading.

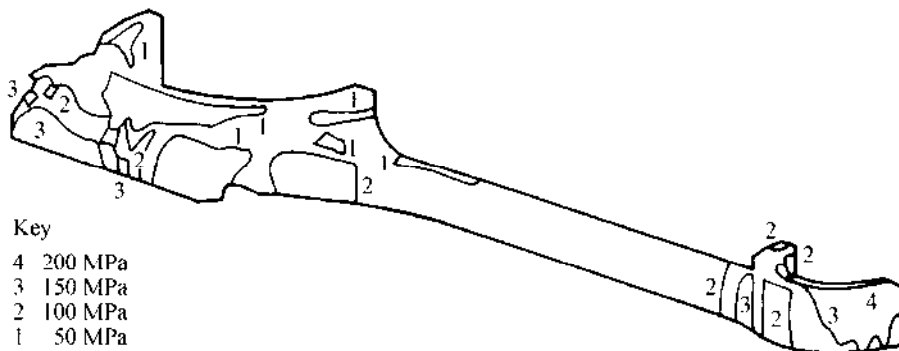


**Figure 9.18** Von Mises' stress from tensile loading.

### 9.3 A COMPOSITE SUSPENSION ARM

#### 9.3.1 Objectives of the Simulation

There is a growing interest across many fields of engineering in the use of new materials, such as composites, as a replacement for traditional steels. The driving force is the intention to develop components that are lighter than those made with traditional materials. As with all design problems, some means of assessing the suitability of a component has to be made, and in this case finite element analysis may be able to predict the behaviour of components before the testing of prototypes takes place. If this can be proven, then such analysis can be used routinely in the design process.

As an example of the analysis of a composite material, a finite element analysis of the suspension arm shown in Fig. 9.19 will be described. This is part of a large program where the results derived from computational methods have been compared with the results gained by a variety of experimental methods. The arm is attached to the vehicle subframe through rubber bushes placed at the body mounts shown in Fig. 9.19, with the load applied at the ball-joint housing. The material used for the arm is sheet moulding compound (SMC). This numerical experiment has been summarized by Pinfold and Calvert (1994).

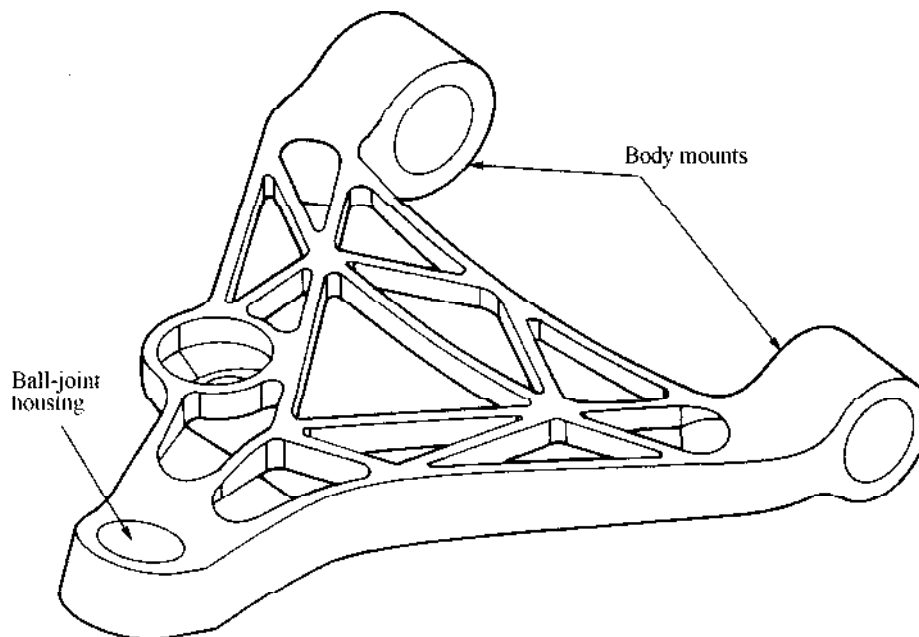
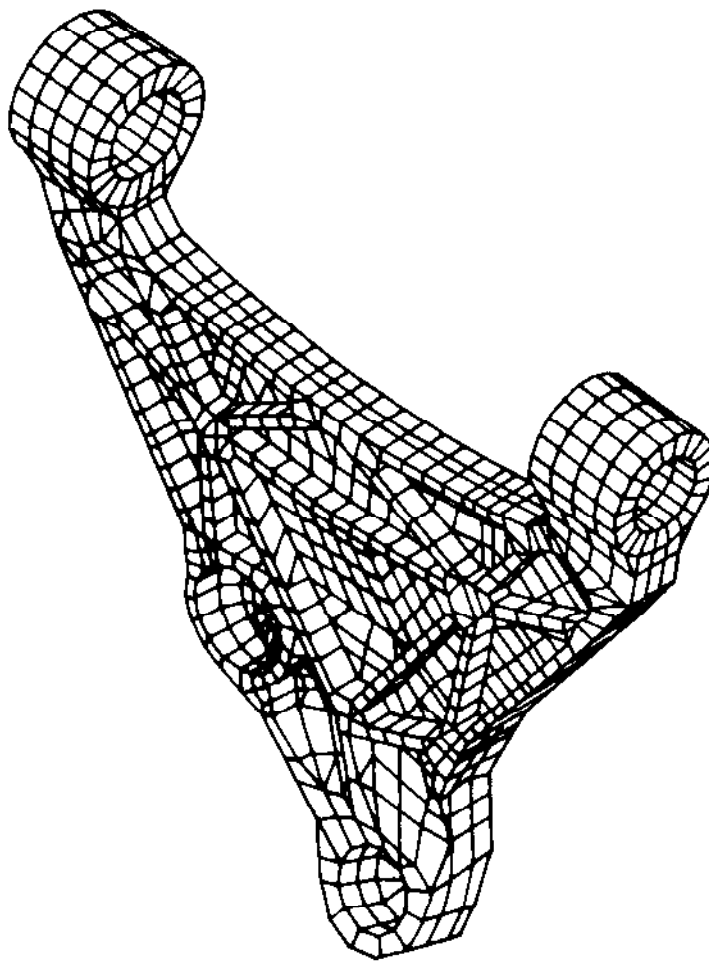


Figure 9.19 The suspension arm.

### 9.3.2 Building the Finite Element Model

The geometry of the arm was initially defined within a CAD system as a wireframe model. To build the mesh shown in Fig. 9.20, sections of the wireframe model were taken such that, where possible, regions of the mesh could have a regular structure. This is clearly the case in the regions of the body mounts and the webs of the structure. Owing to the complexity of the geometry, this strategy could not be applied everywhere and so these regular blocks of elements were joined together manually to form the final mesh. Hence the finished mesh has 1267 solid linear elements of which the majority are bricks, but with some wedge and tetrahedral elements. This is, of course, a relatively coarse mesh.

Compression moulding was used to manufacture the component and despite this the material properties were assumed to be isotropic. Further, from



**Figure 9.20** The mesh of the arm.



laboratory tests, the SMC has a Young's modulus of 10.5 GPa, a Poisson's ratio of 0.26 and a density of  $1800 \text{ kg m}^{-3}$ .

To provide loading boundary conditions, the design case known as the *pot-hole brake* condition is used. This simulates a vehicle travelling at 30 mph, where one wheel falls into a pot-hole with the brakes fully applied. From this situation and the vehicle and suspension geometry, the resultant fore and aft loads and also lateral loads on the arm at the ball-joint housing can be calculated. These are applied at the nodes near the housing, with restraints being applied at the body mounts. Note, however, that spring elements have been added to simulate the rubber bushes and that the forces have been applied at the ball joint using beam elements.

Two other load cases were also run to simulate the experimental tests carried out on the component. These experiments were carried out at a reduced load of approximately one-quarter of those at the design condition.

### 9.3.3 Some Results and Comparison with Experiment

Figure 9.21 shows the predicted stress distribution on the arm. Areas of high stress can be seen in the ball-joint region and near the upper right-hand body mount. These values can also be compared to the results determined through strain gauges placed on the physical arm and through photoelastic techniques. Table 9.1 details

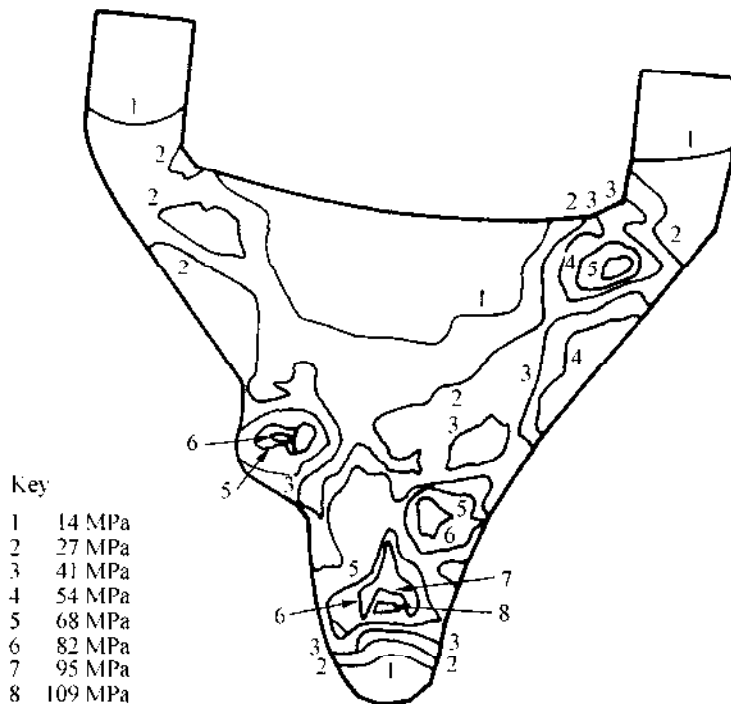


Figure 9.21 Stress distribution on the arm.

**Table 9.1 Comparison of finite element analysis and experimental results**

Position	Finite element analysis, MPa	Strain gauges, MPa	Photoelastic, MPa
Ball-joint housing	165	176	176
Inner radius body mount (with bushes)	20	25	Not available
Inner radius body mount (without bushes)	Not available	22	25

this comparison: the predictions are very good with only small errors between the computational and experimental results. From these results the validity of the finite element method for this case can be demonstrated, and now further work is ongoing to determine its validity in other more demanding circumstances.

## 9.4 DISPLACEMENT ANALYSIS OF A VEHICLE BODY SHELL

### 9.4.1 The Problem

In this final example a simple displacement analysis will be investigated for the monocoque structure of a typical saloon vehicle. Such an analysis is desirable as these structures are designed to have a given stiffness in both bending and torsion. High values of stiffness within the body shell enable accurate assembly to be carried out on the production line and are necessary for the vehicle to have good ride and handling qualities when being driven. Further, a high stiffness reduces the possibility of so-called NVH (noise, vibration and harshness) problems. These NVH problems include the amplification by the body shell of noise generated by the tyres moving over the road surface and by the air moving over the vehicle as well as the noise transmitted from the engine itself, together with extraneous noises caused by the resonant vibration of parts of the vehicle such as the exhaust or loose fittings. On the other hand, if the stiffness is low, not only will the ride, handling and NVH qualities be poor, but also other problems can arise such as vehicle doors not opening when the vehicle is parked with one wheel on a kerb or the front or rear window glass cracking or being forced out of the weather seals.

As with all engineering design problems the solution may well have to be a compromise. High cost or profit vehicles such as luxury saloons require excellent ride, handling and NVH properties and hence high stiffness in the structure. Conversely, lower cost or profit vehicles such as volume production hatchbacks and small saloons have lower standards applied to them in terms of structural stiffness as the functional requirements are much lower.

### 9.4.2 Building a Model of the Vehicle Body

Within the vehicle design process, external details such as the shape of the vehicle are the first things to be decided. This is done by the styling team for the vehicle.

Once the shape is decided then engineers take this shape, probably from a full-size clay model of the proposed vehicle, and produce a CAD model of the external panels. This is used to drive the design of the internal structure of the body shell. At this point a first-shot analysis to predict the stiffness of the body shell can be made.

A coarse finite element mesh is built from the CAD model, taking into account the known lines of the pressed steel panels and information based on experience, which gives a feel for the critical cross-sections where nodes must be placed for a successful analysis to be carried out. Figure 9.22 shows a coarse mesh in its displaced shape for a typical vehicle thin shell structure. This mesh consists of some 5000 linear triangular and quadrilateral elements, and the full body shell is modelled. The mesh has been created manually from the CAD data, but current practice is to use either a fully automatic mesh generation procedure or a combination of automatic and manual mesh generation methods. Note that the mesh models the vehicle roof and supporting pillars (known as the A, B, C and D posts from front to rear), the main external steelwork at the rear (i.e. rear wings), the boot floor and internals, the floor pan and the structural steel around the engine (i.e. front bulkhead, suspension mountings and main beams).

Material properties are applied to the elements and in this case data for a typical steel has been used. Next the boundary conditions can be applied. This is done by restraining the geometric location of the body shell where the rear axle is attached to the body shell by the suspension mounts as shown by the double-headed arrows in Fig. 9.23. This simple schematic illustrates the application of the boundary conditions. Then equal and opposite vertical forces of magnitude  $F$  are applied at the front suspension mounting points, which are a distance  $L$  apart, as shown in Fig. 9.23. Hence a torque of magnitude  $FL$  is applied to the body shell. Note that these boundary conditions simulate the actual physical tests that are carried out on the body shell when the first prototypes are manufactured, and that the force  $F$  need only be a nominal force as the linear model will generate displacements which are proportional to the force.

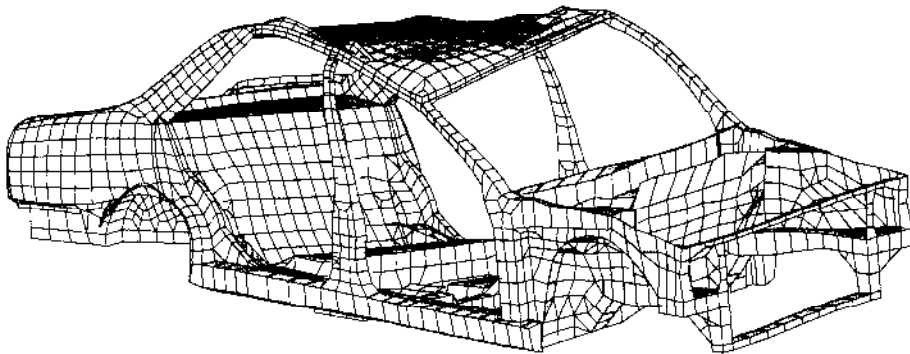


Figure 9.22 Displaced mesh for the vehicle body shell.

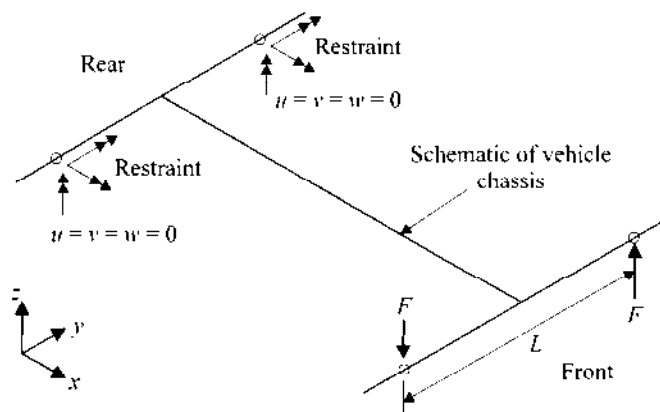


Figure 9.23 Loads applied to the vehicle body shell.

### 9.4.3 Analysing the Results for the Vehicle

The key result that is obtained from the analysis of this coarse model is the twist of the body shell per unit length of the body per unit loading. From experience this simple quantity can be used to decide if the actual body shell will have an acceptable level of stiffness. Figure 9.22 shows the displaced shape for this case, with the displacements much magnified of course. Note that the front offside of the roof is displaced downwards whereas the rear is displaced upward, and note that the opposite happens at the nearside.

This mesh is too coarse for the stress results to be of much use, but the analyst can use the stress data to identify key areas where high stresses may be expected. Either a more detailed model can be built of the whole structure or a model of some part of the structure (a submodel) can be built and analysed. This is another example of the use of substructuring as was discussed in Sec. 8.2.

A more detailed mesh is seen in Fig. 9.24, where a crash simulation has been carried out. This involves a nonlinear analysis of the structure, which will be dealt with in Sec. 10.4.

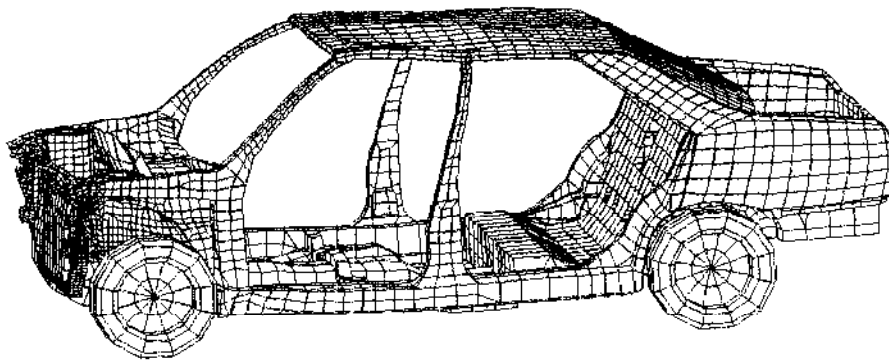


Figure 9.24 A simulation of a vehicle crash.

---

SOLVING MORE COMPLEX PROBLEMS

Throughout this book there has been a concentration on the development and application of the finite element method to linear static problems. In these problems complex geometrical structures can be analysed to find the small displacement of the structure from the applied loads when the material properties are such that nonlinear effects are negligible and effects over time are not important. While the vast majority of analyses are of this type, increasing use is being made of the finite element method in solving more complex problems. Typical examples are:

- the calculation of the variation in some property, say displacement, over time
- the determination of the mode shapes and frequencies of a vibrating structure
- the inclusion of optimization within a finite element program to allow, for example, either the shape of a structure or the thickness of shells to be modified to minimize the displacement of the structure at some point or to minimize the stress within the structure
- the treatment of material properties in the nonlinear range, such as during metal-forming processes when gross plasticity of the material occurs
- the linking of structural solvers to heat transfer solvers so that the effects of heating a structure in terms of both displacement and stress can be calculated.

This chapter is not intended to be a comprehensive guide to the fundamentals and applications of the finite element method to these problems. Rather, the intention is to give a brief overview of the ways in which such problems are handled, concentrating on the changes to the modelling process that occur which are different from those that have been outlined in previous chapters. Note that because the problems are handled differently to linear static problems, the modelling requires specifying additional parameters which the analyst will need to understand. Such modelling issues are covered in detail in the texts listed in Sec. 10.6.

## 10.1 TRANSIENT PROBLEMS

When considering the time-dependent behaviour of a structure, the motion is considered over a series of steps in time, with the solver calculating the structural motion from step to step. Here, the motion of the structure is described by considering the motion of the degrees of freedom in the finite element model. To model the necessary time-dependent terms describing the motion, i.e. the velocity and acceleration of the structure, a so-called *semi-discrete* form of the equations is produced from approximations to the time derivatives. For example, the first derivative of displacement with time can be approximated by using a truncated Taylor series expansion as

$$\left\{ \frac{\partial \delta}{\partial t} \right\} = \frac{\{\delta\}^{n+1} - \{\delta\}^n}{\Delta t} \quad (10.1)$$

where the superscripts denote time levels labelled  $n+1$  and  $n$  and  $\Delta t$  is the time interval. Use of shape functions and nodal values convert this, for an element, to

$$[N]^T [N] \frac{\{\delta^e\}^{n+1} - \{\delta^e\}^n}{\Delta t} \quad (10.2)$$

When substituted in the governing energy equation for the problem, this leads to a new matrix  $[M^e]$ , which is known as the *element mass matrix*, where

$$[M^e] = \int_{V^e} \rho [N]^T [N] dV \quad (10.3)$$

where  $\rho$  is the density of the material of the element.

When this is integrated over an element, either the full integration can be performed to give the consistent mass matrix or approximations can be made to give a diagonal matrix, the lumped mass matrix. In (10.1) the value  $\Delta t$  acts to control the step-by-step procedure just as the relaxation parameter  $\omega$  is used for the case of material nonlinearity. If  $\Delta t$  is very small the solution progresses slowly and convergence is more likely, whereas if  $\Delta t$  is large the time terms have very little effect and divergence is more likely.

As well as the time-dependent terms, those terms that are independent of time must also be discretized across various time levels. Often they are discretized just as they are for steady state problems, with the assumption that they are calculated at time level  $n$ . This leads to an explicit formulation of the equations which does not require the use of a simultaneous equation solver to produce a solution. Equally, though, the time-independent terms could be calculated at time level  $n+1$ , leading to a fully implicit form of the equations. Also, some form of weighted average can be performed between these two extremes as follows:

$$\{\delta\} = \theta \{\delta\}^{n+1} + (1 - \theta) \{\delta\}^n \quad (10.4)$$

Now setting  $\theta$  to unity gives a fully implicit form and setting  $\theta$  to zero gives the explicit form. For all other values an implicit form is produced and with  $\theta$  set to 0.5 the Crank–Nicholson form is produced. If  $\theta$  is 0.5 or greater then the

schemes are unconditionally stable, and when  $\theta$  is less than 0.5 they are conditionally stable. In the conditionally stable cases the time step  $\Delta t$  must be set small enough for stable solutions to be produced.

As far as the analyst is concerned, the following features need to be taken into account when a time-dependent simulation is produced:

- *The value of  $\theta$  that is to be used* Typically 1.0 or 0.5 are used to ensure stability regardless of the time step.
- *The value of the time step  $\Delta t$*  This is set to provide stability if necessary when  $\theta$  is less than 0.5, and must provide the analyst with a sufficiently detailed time response of the structure. This means that it must be small enough to give an accurate picture of the response.
- *The initial conditions* As the time terms have been discretized in this way a step-by-step procedure is involved that relies on data at time level  $n + 1$  being produced from data at time level  $n$ . Hence to start the calculation at the first time step the values of the variables at time level zero must be known. These might be known from the specification of the problem or they may have to be assumed from experience.
- *The computing effort required* When any iterative procedure is involved, due to time variation or nonlinearity, the computer effort is very important as, effectively, the step-by-step procedure can easily be equivalent to many hundreds of individual static analyses.
- *The storage of data* It may be that the displacements of just a handful of nodes with time are required as the results of the simulation, but it is more likely that the displacement of all nodes at the different time steps will be required so that an animation of the structural response with time can be produced. For complex geometries such as a car body the number of degrees of freedom can be in the tens of thousands and storing this amount of data at several hundred time steps can require vast amounts of secondary disk storage.

## 10.2 VIBRATION PROBLEMS

Typical governing (or global) matrix forms of the time-dependent equation are:

$$[\mathbf{M}] \left\{ \frac{\partial^2 \delta}{\partial t^2} \right\} + [\mathbf{C}] \left\{ \frac{\partial \delta}{\partial t} \right\} + [\mathbf{K}] \{\delta\} = \{\mathbf{F}(t)\} \quad (10.5)$$

where  $[\mathbf{M}]$  is the mass matrix,  $[\mathbf{C}]$  is the damping matrix and  $\{\mathbf{F}(t)\}$  is the forcing function due to the load which may vary with time.

If a free vibration problem is considered, then there is no damping and no forcing of the structure, and so both  $[\mathbf{C}]$  and  $\{\mathbf{F}(t)\}$  are zero, giving:

$$[\mathbf{M}] \left\{ \frac{\partial^2 \delta}{\partial t^2} \right\} + [\mathbf{K}] \{\delta\} = 0 \quad (10.6)$$

This situation is similar to the free vibration of a simple spring-mass system with one degree of freedom, which has a natural frequency given by

$$\omega_{\text{nat}} = \sqrt{\frac{k}{m}} \quad (10.7)$$

where  $k$  is the spring stiffness and  $m$  is the attached mass. If the general solution for the motion of the structure can be described in terms of nodal amplitudes  $\{\bar{\delta}\}$  and a frequency  $\omega$ , then

$$\{\delta\} = \{\bar{\delta}\}e^{i\omega t} \quad (10.8)$$

If this is substituted into (10.6), then

$$([A] - \omega^2[I])\{\bar{\delta}\} = 0 \quad (10.9)$$

where  $[A]$  is given by  $[M]^{-1}[K]$  and is known as the *system matrix*. This is a classical eigenvalue problem. Solution of (10.9) for the eigenvalues gives  $n$  values of  $\omega^2$ . Here  $n$  is the dimension of the symmetric matrices  $[M]$  and  $[K]$  and the values of  $\omega$  are the natural frequencies of the system, each of which is associated with an eigenvector of the displacements of the structure. In fact, each eigenvector is a mode of vibration of the structure associated with the corresponding eigenvalue which is the frequency of vibration.

To deal with problems which have many thousands of degrees of freedom, one approach is to choose a limited number of degrees of freedom, known as master degrees of freedom. Through the use of mathematical manipulation the dynamics of the structure can be approximated by the response of these master degrees of freedom.

If damping is present, the damped natural frequency is obtained from

$$\omega_d = \omega_{\text{nat}} \sqrt{1 - \xi^2} \quad (10.10)$$

where  $\xi$  is the damping factor. It is often the physical situation that a structure is lightly damped with  $\xi$  less than 0.1. Under these conditions  $\omega_d$  is within one half of one per cent of  $\omega$  and so the frequencies determined from equation (10.9) can be used to design against resonance in the damped structure. This is done by checking the size of the forcing frequencies to ensure that they are well away from the resonant frequencies. Further, the possible forms of any resonance can be determined from the mode shapes. Typical practical examples include the resonance of a cantilever beam structure such as a turbine blade or the resonance of a vehicle body shell.

### 10.3 OPTIMIZATION

Within the design process engineers have to work to produce a design that meets a given specification. Usually, there are many design solutions that meet the specification and so some sort of decision process must be undertaken to decide which



solution is the *best solution* in some sense. Depending on the situation, determiners such as the cost of a product or the weight of a product may be used to evaluate the range of design solutions, with the so-called best solution being the one with the minimum value of cost or weight. Examples of this include the weight of an aircraft structure which is often minimized or the material cost of a plastic seat.

When the best solution is sought, the process is one of optimization. In this section this process will be considered in broad terms, defining some vocabulary, looking at search techniques and then considering how the process fits in with the finite element method.

### 10.3.1 Vocabulary

The first term that needs a definition is *optimization*. This is defined as the mathematical process of obtaining the set of conditions required to produce the maximum or minimum value of some function. Within the problem, *design variables* are found which are the quantities that can be used to define a product but are not predefined for the problem being considered. These variables may be the thickness of some material, the weight of the product or its cost and so on. One of these variables is minimized in the optimization process. Each problem may also be subject to *constraints* which, typically, are derived from known limits for, say, displacement or stress values in a material.

The entity which is optimized is known as the *objective* or *cost function*, which is a functional form of one of the design variables in terms of the other design variables. For example, if the objective function is  $D$  and the other design variables are  $x_1$  to  $x_n$ , then

$$D = f(x_1, x_2, \dots, x_n) \quad (10.11)$$

### 10.3.2 Seeking a Minimum

If it is considered that seeking the maximum value of a function is the same as seeking the minimum value of the negative of the function, then all optimization can be seen as a minimization process. Differentiation of (10.11) to find the design variables that give a zero value for the derivative may be one way to proceed. However, for complex structural problems, where (10.11) can only be found numerically as there are a large number of design variables, this task is virtually impossible. Numerical methods are, therefore, used to seek the minimum.

The simplest way is the *direct search method* where the value of  $D$  is found for a number of values of each of the design variables  $x_1$  to  $x_n$ . However, a large number of calculations may be required to do this and so, for multi-variable problems, *pattern search* methods can be used. These evaluate  $D$  at a given set of design variables, known as the *base point*, and then consider just one design variable, evaluating  $D$  either side of the original position. Where  $D$  is a minimum, for the three points being considered, a new local search in a second design

variable is made and so on. When all the variables have been considered, the local minimum is found and the process can be repeated from some new base point. This new point is found by moving away from the original base point in the direction of the local minimum by, say, twice the distance between original base point and local minimum. Other methods can also be used and these involve finding the steepest gradient of  $D$  at the base point and moving in that direction before re-evaluating the gradients.

### 10.3.3 The Finite Element Context

When using finite elements for structural design, it is possible to use a manual form of optimization in conjunction with a series of finite element analyses. For example, say an analyst wishes to know the minimum thickness of material that has to be used within a shell structure to achieve a given displacement at some point for a given loading subject to the material not being stressed beyond some value. A finite element shell model can be built and the thickness set to some arbitrary value. Then a linear static analysis can be run and the displacements and stresses can be found. Assuming that the stress constraints are not violated, if the maximum displacement is too large then the thickness must be increased, and if it is too small then the thickness can be reduced. The thickness might be halved or doubled as appropriate and the simulation run again. Repeating this process should lead to the optimum thickness.

However, programs are now available that automate this process. First of all, the relevant design variables must be defined and their initial values set. Then a finite element analysis is performed to calculate the structural behaviour and generate values for the constraints. A so-called *sensitivity analysis* is then performed that calculates the rate of change of the structural behaviour and the rate of change of the constraints with the design variables. From the constraint values and their derivatives a localized model of the constraints as a function of the design variables can be built and a search carried out to improve the design variables such that the cost function is minimized. These design variables are then updated within the finite element model and a second analysis is performed. Repeating the full process results in an optimum design.

## 10.4 NONLINEAR PROBLEMS

### 10.4.1 Nonlinearities in the Material Properties

Here the material properties of the problem lead to what is, at first sight, a small change in the finite element equation. Equation (1.2) becomes:

$$[\mathbf{K}(\boldsymbol{\delta})]\{\boldsymbol{\delta}\} = \{\mathbf{F}\} \quad (10.12)$$

which signifies that the global stiffness matrix  $[\mathbf{K}]$  is now a function of the nodal displacements  $\{\boldsymbol{\delta}\}$ . Here the dependency of the terms in  $[\mathbf{k}]$ , as given by (3.9), is

because the elastic stiffnesses  $C_{ij}$  in  $[\mathbf{D}]$  (2.15) are functions of strain. This change has enormous repercussions when trying to produce a solution to (10.12), as the actual nodal displacements are not known until some complex solution procedure is complete.

To produce a solution, an iterative procedure must be used. To start this procedure, the analyst must provide some guessed values for the displacements to the solver program. These initial values are then used by the solver to calculate an approximate set of coefficients for the matrix  $[\mathbf{K}]$ . Having done this any of the usual linear equation solvers (see Sec. 3.9.3) can be used to solve this initial version of (10.12). This yields a new set of values for the displacements and step one of the process is complete. These updated values can then be used within step two of the process as new estimates for the nodal displacements and the coefficients of matrix  $[\mathbf{K}]$  are calculated, taking account of the changes in the material properties as calculated at the current element stresses and strains (see Sec. 2.2.6). Further solution of (10.12) gives another set of values for the displacements at the end of step two. Further steps in the process are carried out such that the process is repeated many times until the calculated values of the displacement do not change from one step to the next.

Owing to the iterative nature of the process, the displacements may not converge to a given set of values from step to step. Sometimes the displacements can oscillate wildly from step to step, with the magnitude ever increasing in value. When this divergence happens the process is unstable and usually the computer detects that the numbers being generated are outside its range and it stops the process automatically. To assist the process to converge, relaxation techniques can be used where the displacements that are used in the next step are calculated using

$$\{\delta_{\text{next}}\} = \omega\{\delta_{\text{new}}\} + (1 - \omega)\{\delta_{\text{old}}\} \quad (10.13)$$

where the relaxation parameter  $\omega$  can range from zero to unity. Hence, when  $\omega$  is 1.0 the iteration process takes place as originally described, with the displacements being taken as the newly calculated values in the next step, and when  $\omega$  is 0.0 the iteration process is stopped as the displacements are never updated. Taking some intermediate value of  $\omega$  increases the likelihood of convergence where this is necessary, by effectively slowing down the iterative process.

For the analyst the implications of attempting to calculate a nonlinear problem can be immense. Common problem areas include the following:

- *Provision of a guessed set of values for the displacement* If sensible choices are made then the convergence of the process can be improved, but if poor choices are made then divergence is likely. Experience of running similar problems can be a great advantage here.
- *Monitoring the iterative process for divergence* It is useful to check the value of displacement, say at one point, at the end of every step. If the displacements are not oscillating and the change in value from step to step after, say, 10 steps is reducing then the process is probably converging.

- *Setting the number of steps to be run during the iteration process* Here it is sensible to run just a few steps to start with. This enables monitoring to be carried out and convergence to be checked before calculating many more steps. Often several hundred steps may be needed. Usually the solver program allows a restart of the solution from data that has been saved to disk at the end of the last step. This saves rerunning previous steps in the process as the procedure progresses.
- *The choice of relaxation parameter  $\omega$*  Again, experience of running similar problems may well lead to a sensible choice of  $\omega$ .
- *The increase in computer time over a single linear static calculation* It is now clear that many equivalent linear static solutions are calculated during the iterative procedure. Hence the computer effort is magnified by the number of steps run. This may mean that a smaller model in terms of the numbers of nodes and elements may have to be built than would be ideal, in an attempt to solve the problem with a realistic amount of computer effort. It is this increase in computing requirement that has led to an increase in the use of iterative linear equation solvers. While these may be more inaccurate than direct solvers they are much faster. Also, during the initial stages of the iterative process, an inaccurate solution for the displacements is acceptable.

In many ways structural problems that are nonlinear are similar to nonlinear problems in the field of computational fluid dynamics. Analysts in computational fluid dynamics who have to solve problems similar to structural nonlinear problems might find the detailed modelling advice in Shaw (1992) useful.

#### 10.4.2 Geometrical Nonlinearities

With the material nonlinearity problems described above the displacements and strains in a structure may still be regarded as small. However, a second type of nonlinearity, geometrical nonlinearity, is also possible where the displacements are large, and this type nonlinearity is also defined by (10.2). Geometric nonlinear behaviour is introduced into the finite element method by including the third term of a Taylor series expansion in the definition of strains (see Sec. 2.2.4) and constructing the  $[k]$  using the same procedure as in Sec. 3.1.3. A simple example of this behaviour is a buckled strut with imperfections. As a general rule, most buckling problems should be approached as nonlinear problems in which pre-buckling deformations are taken into account. In these problems it is also possible for the material nonlinearity to be present as well.

Buckling can also be solved using an eigenvalue analysis similar to that for free vibration. This type of analysis is often available in packages.

Analysis by the finite element method of problems such as metal forming in a press and impact response of, say, road vehicles requires a combination of material and geometrical nonlinearities. These problems are therefore the most difficult to model and solve with accuracy.

### 10.5 CALCULATING THERMAL EFFECTS WITHIN STRUCTURES

It is often required that the effects of heating or cooling a structure on its stress and strain distribution need to be known. The thermal problem can be, effectively, decoupled from the stress-strain problem through the use of an initial stress and strain field as shown in Chapter 3.

To solve the thermal problem, equations of the form

$$\frac{\partial^2 T}{\partial x^2} + \frac{\partial^2 T}{\partial y^2} + \frac{\partial^2 T}{\partial z^2} + Q = 0 \quad (10.14)$$

are solved. This is Poisson's equation where  $T(x, y, z)$  is the local temperature and  $Q(x, y, z)$  is a local source of heat. A weighted residual form of this equation is easily formed by multiplying the equation by some test function and then by integrating by parts over the volume of an element. By using shape functions and nodal temperatures, a finite element form of this is easily produced:

$$- \int_V \left[ \left[ \frac{\partial \mathbf{N}}{\partial x} \right]^T \left[ \frac{\partial \mathbf{N}}{\partial x} \right] + \left[ \frac{\partial \mathbf{N}}{\partial y} \right]^T \left[ \frac{\partial \mathbf{N}}{\partial y} \right] + \left[ \frac{\partial \mathbf{N}}{\partial z} \right]^T \left[ \frac{\partial \mathbf{N}}{\partial z} \right] + [\mathbf{N}]^T [\mathbf{N}] \right] dV + \int_S [\mathbf{N}]^T \frac{\partial T}{\partial n} dS = 0 \quad (10.15)$$

Here  $V$  denotes the volume of the problem and  $S$  denotes the surface boundary. At the boundary either the temperature  $T$  or the normal derivative of temperature can be the specified boundary conditions. In fact, one nodal value of  $T$  must be given to ensure that (10.15) is not singular. Given a mesh of elements and the boundary conditions, the value of temperature can be found from (10.15) throughout the structure. These can then be converted to initial strains (see Sec. 3.1.1) within the structure and a new calculation can be carried out to find the combined stresses and strains when external loads are applied as well. If the temperature distribution is not constant, then the elastic constants will vary through the body and affect the structural behaviour as defined in (10.12).

## 10.6 REFERENCES AND FURTHER READING

Detailed technical information on the fundamental principles are given in texts such as those by Cook *et al.* (1989), Crisfield (1991), Hinton (1992), Hitchings (1992), Morris (1982) and Zienkiewicz and Taylor (1991). Modelling issues are also discussed in NAFEMS (1986) and Cook (1995). Both fundamental principles and modelling issues are to be found in journals such as: *Computers and Structures*, Pergamon Press; *Finite Element in Analysis and Design*, Elsevier Science BV; *International Journal for Numerical Methods in Engineering*, John Wiley.

---

## REFERENCES AND FURTHER READING

- Ahmad, S., Irons, B. M. and Zienkiewicz, O. C. (1970) Analysis of thick and thin shell structure by curved finite elements, *Int. J. Numer. Methods Engng.*, vol. 2, 419–451.
- Airy, G. B. (1863) On the strains in the interior of beams, *Phil. Trans. Roy. Soc.*, vol. 153, 49–80.
- Argyris, J. H. and Kelsey, S. (1960) *Energy Theorems and Structural Analysis*, Butterworth, London.
- Ashby, M. F. (1992) *Materials Selection in Mechanical Design*, Pergamon, London.
- Bézier, P. (1986) *The Mathematical Basis of the UNISURF CAD System*, Butterworth, London.
- Burnett, D. S. (1987) *Finite Element Analysis From Concepts to Applications*, Addison-Wesley, Reading, Mass.
- Calladine, C. R. (1983) *Theory of Shell Structures*, Cambridge University Press, Cambridge.
- Calladine, C. R. and Christopher, R. (1985) *Plasticity for Engineers*, Ellis Horwood, Chichester, England.
- Cavendish, J. C., Field, D. A. and Frey, W. H. (1985) An approach to automatic three-dimensional finite element mesh generation, *Int. J. Numer. Methods Engng.*, vol. 21, 329–47.
- Charles, J. A. and Crane, F. A. A. (1989) *Selection and Use of Engineering Materials*, 2nd edn, Butterworth, London.
- Cheng, J. H., Finnigan, P. M., Hathaway, A. F., Kela A. and Schroeder, W. J. (1988) Quadtree/Octree meshing with adaptive analysis, in Senegupta, S., Thompson, J. F., Eisman, P. R. and Hauscr, J. (eds.), *Numerical Grid Generation in Computational Fluid Dynamics*, Pineridge Press, Swansea, pp. 633–42.
- Clapeyron, B. P. E. and Lamé, G. (1833) *Mémoire sur L'équilibre Intérieur des Corps Solides Homogènes*, Mem. Savans Etrang. Paris, IV, 463–562.
- Clough, R. W. (1960) The finite element in plane stress analysis, *Proc. 2nd ASCE Conf. on Electronic Computation*, Pittsburgh, Pa., September 1960.
- Coates, R. C., Coutie, M. G. and Kong, K. F. (1988) *Structural Analysis*, 3rd edn, Van Nostrand Reinhold, Wokingham.
- Cook, R. D. (1995) *Finite Element Modelling for Stress Analysis*, Wiley, New York.
- Cook, R. D., Malkus, D. S. and Plesha, M. E. (1989) *Concepts and Applications of Finite Element Analysis*, 3rd edn, Wiley, New York.
- Courant, R. (1943) Variational methods for the solution of problems of equilibrium and vibration, *Bull. Am. Math. Soc.*, vol. 49, 1–23.

- Crisfield, M. A. (1991) *Non-linear Finite Element Analysis of Solids and Structures, Vol. 1: Essentials*, Wiley, New York.
- Cross, H. (1930) The analysis of continuous frames by distributing fixed-end moments. *Proc. Amer. Soc. Civ. Engrs.*, vol. 56, 919–28.
- Cuthill, E. and McKee, J. (1969) Reducing the bandwidth of sparse symmetric matrices, *Proc. 24th ACM National Conference*, New York, pp. 157–72.
- Desai, C. S. and Abel, J. F. (1972) *Introduction to the Finite Element Method*, Van Nostrand Reinhold, New York.
- Deutschman, A. D., Mitchels, W. J. and Wilson, C. (1975) *Machine Design*, Macmillan, New York.
- Dieter, G. E. (1986) *Mechanical Metallurgy*, 3rd edn, McGraw-Hill, New York.
- Donnell, L. H. (1933) Stability of thin-walled tubes under torsion. *NACA Report 497*, National Advisory Committee for Aeronautics, Washington D.C.
- Encarnacao, J. and Schlechtendahl, E. G. (1983) *Computer Aided Design—Fundamentals and System Architectures*, Springer-Verlag, Berlin.
- Fenner, R. T. (1986) *Engineering Elasticity: Applications of Numerical and Analytical Techniques*, Ellis Horwood, Chichester, England.
- Flügge, W. (1973) *Stresses and Strains in Shells*, 2nd edn., Springer-Verlag, Berlin.
- Galerkin, B. G. (1915) Series solution of some problems of elastic equilibrium of rods and plates (in Russian), *Vestn. Inzh. Tech.*, vol. 19, 897–908.
- George, P. L. (1991) *Automatic Mesh Generation—Application to Finite Element Methods*, Wiley, Chichester (Masson, Paris).
- Gere, J. M. and Timoshenko, S. P. (1991) *Mechanics of Materials*, 3rd edn, Chapman & Hall, London.
- Gibbs, N. E., Poole, W. G. and Stockmeyer, P. K. (1976) An algorithm for reducing the bandwidth profile of a sparse matrix, *SIAM J. Numer. Anal.*, vol. 13(2), 236–50.
- Gordon, J. E. (1976) *The New Science of Strong Materials*, 2nd edn, Penguin, Harmondsworth, England.
- Halpin, J. C. (1992) *Primer on Composite Materials Analysis*, 2nd edn, Technomics, Lancaster, Pa.
- Hinton, E. (ed.) (1992) *NAFEMS Introduction to Non-linear Finite Element Analysis*, NAFEMS, Glasgow.
- Hinton, E. and Owen, D. R. J. (1979) *An Introduction to Finite Element Computations*, Pineridge Press, Swansea.
- Hirsch, C. (1988) *Numerical Computation of Internal and External Flows, Volume 1: Fundamentals of Numerical Discretisation*, Wiley, New York.
- Hitchings, D. (ed.) (1992) *A Finite Element Dynamic Primer*, NAFEMS, Glasgow.
- Hoffman, J. D. (1992) *Numerical Methods for Engineers and Scientists*, McGraw-Hill, New York.
- Holmes, D. G. and Lanson, S. H. (1986) Adaptive triangular meshes for compressible flow solutions, in Hauser, J. and Taylor, C. (eds.), *Numerical Grid Generation in Computational Fluid Dynamics*, Pineridge Press, Swansea, pp. 413–24.
- Hordeski, M. F. (1986) *CAD/CAM Techniques*, Reston Pub. Co., Reston, Va.
- Hrenikoff, A. (1941) Solution of problems in elasticity by the framework method, *J. Appl. Mech.*, vol. A8, 169–75.
- Hughes, T. J. R. and Hinton, E. (1986) *Finite Element Methods for Plate and Shell Structures. Vol. 1 Element Technology*, Pineridge Press, Swansea.
- Irons, B. M. (1966) Engineering applications of numerical integration in stiffness methods, *AIAA J.*, vol. 4(11), 2035–7.
- John, V. (1992) *Testing of Materials*, Macmillan, Basingstoke.
- Kaye, G. W. C. and Laby, T. H. (1983) *Tables of Physical and Chemical Constants*, 14th edn, Longman, London.
- Knight, C. E. (1993) *The Finite Element Method in Mechanical Design*, PSW-Kent, Boston, Mass.
- Lamit, L. G. (1994) *Technical Drawing and Design*, West, St Paul, USA.
- Levy, S. (1953) Structural analysis and influence coefficients for delta wings, *J. Aero. Sci.*, vol. 20(7), 449–54.
- Lewis, P. E. and Ward, J. P. (1991) *The Finite Element Method—Principles and Applications*, Addison-Wesley, Wokingham.



- Love, A. E. H. (1944) *A Treatise on the Mathematical Theory of Elasticity*, 4th edn, Dover.
- Martin, H. C. and Carey, G. F. (1973) *Introduction to Finite Element Analysis, Theory and Applications*, McGraw-Hill, New York.
- Maxwell, J. C. (1872) On reciprocal figures, frames, and diagram of forces, *Edinburgh Roy. Soc. Trans.*, vol. XXVI, Edinburgh, 1–40.
- McHenry, D. (1943) A lattice analogy for the solution of plane stress problems, *J. Inst. Civ. Engrs.*, vol. 21, 59–82.
- McMahon, C. and Browne, J. (1993) *CAD/CAM From Principles to Practice*, Addison-Wesley, Wokingham.
- Mindlin, R. D. (1951) Influence of rotary inertia and shear on flexural motions of isotropic, elastic plates, *J. Appl. Math.*, vol. 18, 31–8.
- Morris, A. J. (ed.) (1982) *Foundations of Structural Optimization: A Unified Approach*, Wiley, Chichester, England.
- NAFEMS (1986) *A Finite Element Primer*, NAFEMS, Glasgow.
- NAFEMS (1992) *Benchmark*, NAFEMS, Glasgow (from 1988 to present).
- Norrie, D. and de Vries, G. (1976) *Finite Element Bibliography*, IFI/Plenum, New York.
- Onwubiko, C. (1989) *Foundations of Computer-Aided Design*, West, St Paul, USA.
- Packer, J. A., Wardenier, J., Kurobane, Y., Dutta, D. and Yeomans, N. (1992) *Design Guide for Hollow Rectangular Section (RHS) Joints Under Predominantly Static Loading*, CIDECT ed. Verlag TUV Rheinland, Germany.
- Pahl, G. and Beitz, W. (1988) *Engineering Design, A Systematic Approach* (Trans. A. Pomerans and K. Wallace), The Design Council, London.
- Pinfold, M. and Calvert, G. (1994) Experimental analysis of a composite automotive suspension arm, *Composites*, vol. 25(1), 59–63.
- Rayleigh, J. W. S., Lord (1870) On the theory of resonance, *Trans. Roy. Soc. (London)*, vol. A161, 77–118.
- Reddy, J. N. (1984) *An Introduction to the Finite Element Method*, McGraw-Hill, New York.
- Richardson, L. F. (1910) The approximate arithmetical solution by finite differences of physical problems, *Trans. Roy. Soc. (London)*, vol. A210, 305–57.
- Ritz, W. (1909) *Über eine neue Methode zur Lösung gewisser Variations—Probleme der mathematischen Physik*, *J. Reine Angew. Math.*, vol. 135, 1–61.
- Robinson, J. (1985) *Early FEM Pioneers*, Robinson & Associates, Dorset, England.
- Rooney, J. and Steadman, P. (1987) *Principles of Computer-aided Design*, Pitman and The Open University, London.
- Shaw, C. T. (1992) *Using Computational Fluid Mechanics*, Prentice Hall, London.
- Shigley, J. E. and Mitchell, L. D. (1983) *Mechanical Engineering Design*, McGraw-Hill, New York.
- Smith, G. D. (1985) *Numerical Solution of Partial Differential Equations: Finite Difference Methods*, 3rd edn, Oxford University Press, Oxford.
- Southwell, R. V. (1940) *Relaxation Methods in Engineering Science: Treatise on Approximate Computation*, Oxford Clarendon Press, Oxford.
- Stasa, F. L. (1986) *Applied Finite Element Analysis for Engineers*, CBS Publishing, New York.
- Szmelter, J. (1958) The energy method of networks of arbitrary shape in problems of the theory of elasticity, *Proc. IUTAM Symposium on Non-homogeneity in Elasticity and Plasticity* (ed. Olszak, W.), Warsaw 2–9 September 1958, Pergamon Press, London.
- Taig, I. C. (1992) *Finite Element Analysis of Composite Materials*, NAFEMS, Report R0003, Glasgow.
- Taylor, C. and Hughes, T. G. (1981) *Finite Element Programming of the Navier-Stokes Equations*, Pineridge Press, Swansea.
- Thompson, J. F., Warsi, Z. U. A. and Mastin, C. W. (1982) Boundary-fitted coordinate systems for numerical solution of partial differential equations—A review, *J. Comput. Phys.*, vol. 47(1), 1–108.
- Timoshenko, S. P. (1953) *History of Strength of Materials*, McGraw-Hill, New York.
- Timoshenko, S. P. and Goodier, N. J. (1988) *Theory of Elasticity*, 2nd edn, McGraw-Hill, New York.
- Tizzard, A. (1994) *An Introduction to Computer-aided Engineering*, McGraw-Hill, London.
- Turner, M. J., Clough, R. W., Martin, H. C. and Topp, L. J. (1956) Stiffness and deflection analysis of complex structures, *J. Aero. Sci.*, vol. 23(9), 805–33.

- Vlasov, V. Z. (1964) *General theory of shells and its applications to engineering*. (Translated from Russian in 1949.) Nasa Technical Translation TTF-99, US National Aeronautical and Space Administration, Washington D.C.
- Washizu, K. (1982) *Variational Methods in Elasticity and Plasticity*, Pergamon Press, Oxford.
- Watson, D. F. (1981) Computing the  $n$ -dimensional Delaunay tessellation with application to Voronoi polytypes, *Comput. J.*, vol. 24(2), 167–72.
- Yerry, M. A. and Shephard, M. S. (1984) Automatic three-dimensional mesh generation by the modified-octree method, *Int. J. Numer. Methods Engng.*, vol. 20(11), 1965–90.
- Young, W. C. (1989) *Roark's Formulas for Stress and Strain*, 6th edn, McGraw-Hill, New York.
- Zienkiewicz, O. C. and Cheung, Y. C. (1967) *The Finite Element Method in Structural and Continuum Mechanics*, McGraw-Hill, New York.
- Zienkiewicz, O. C. and Taylor, R. L. (1989) *The Finite Element Method, Volume 1: Basic Formulation and Linear Problems*, 4th edn, McGraw-Hill, New York.
- Zienkiewicz, O. C. and Taylor, R. L. (1991) *The Finite Element Method, Volume 2: Solid and Fluid Mechanics Dynamics and Non-linearity*, 4th edn, McGraw-Hill, New York.

---

## INDEX

- Accuracy, 12, 16, 36, 49, 54, 57, 71, 81, 108, 119–125, 142, 150  
  checking, 159  
  estimation of, 16  
  of consistent element force vector, 76–77  
  of different elements, 56  
  of element stresses, 77–78  
  of examples, 166–169, 172–173, 180, 183, 185, 202, 205, 210, 213, 220  
  of integration, 64, 69–75  
  of solution, 134–136, 152, 259
- Acquisition of technology, 4, 91, 101  
  hardware, 106  
  software, 42–43, 102
- Admissible functions, 12, 49, 50–51, 214, 223
- Advancing front method, 133
- Aircraft design, 5, 6, 10, 12, 192, 256
- Airy stress functions, 6, 14, 17, 41–42, 162
- Aluminium, 29, 30, 35, 107, 240, 242, 244  
  black, 201
- ASCII files, 107, 149, 151–153
- Analysis process:  
  for structural problems, 43, 91–92, 94, 105, 108, 112, 130, 140, 149, 164–165, 175  
  goals, 108, 240  
  initial thinking, 92, 140, 164, 175  
  mesh generation, (*see* Mesh, generation)  
  numerical problem specification, 92, 142, 160  
  numerical solution, 8, 47, 90, 93–94, 98, 140, 147  
  results analysis, 43, 53, 78, 81, 93–94, 96, 108–110, 122–124, 135, 141, 152–154, 157–158, 160–251  
  troubleshooting, 140, 150
- Analyst:  
  team, 108, 191  
  skills, 4, 17, 91, 108, 110, 112
- Anisotropy, 30, 34, 44, 46, 81, 192–195, 197, 206, 209
- Architecture:  
  computer, 91, 97, 100  
  novel, 98
- Assembly of equations, 7, 52, 58, 61, 82–84, 86
- Axial load, 31–32, 38–39, 45, 61, 212, 214, 216, 217, 223, 243
- Axisymmetric elements, (*see* Element, axisymmetric)
- Backup of data, 98, 100, 107
- Bandwidth, 56, 86  
  algorithm, Cuthill–McKee, 137  
  reduction, 136–137
- Bar, 9–10, 15, 19, 30–32, 36, 39  
  element, (*see* Element, bar)
- Beam, 9–10, 15, 19, 37, 40, 182, 192–204, 208–209, 254  
  element, (*see* Element, beam)
- Benchmarks, 16, 42, 71, 120
- Bending, 15, 19, 40, 64, 66, 120, 124, 177, 184–185, 188, 192–210, 209–230, 238, 243, 249  
  element, Element, beam, plate, shell  
  moment, 40, 79, 194, 198, 214–217, 223, 225
- Bezier surface, 114–115, 129
- Bicycle frame example, 231–239
- Biharmonic equation, 41–42
- Binary files, 107, 151–152
- Body forces, 19, 24–25, 38–40, 48–49, 51–52, 77, 92
- Bound:  
  lower, 58  
  upper, 57, 175
- Boundary conditions, (*see also* Restraints)  
  application to faces, 93, 143–146, 148, 180  
  application to global equations, 84–85, 125  
  essential, 14  
  natural, 14  
  symmetry, 118, 165, 182, 201–202, 243
- Boundary element (integral) method, 7
- B-Rep solid model, 115–117
- Brazilian tensile test example, 42, 161–174
- Brick elements, (*see* Element, brick)
- Brittle material, (*see* Material, brittle)
- Duckling, 38, 44–45, 75, 81, 102, 109, 192, 213–214, 259
- Bytes, 106–107, 151–152
- Computer-aided Design (CAD), 44, 74, 103, 113, 115, 129, 247, 250  
  model types:  
    solid:  
      B-Rep, 115–117  
      Constructive Solid Geometry (CSG), 115–116, 233  
  surface:  
    Bezier, 114–115, 129

- Coons patch, 114, 129
- Non-uniform rational B-spline (NURBS), 115, 129
- wireframe, 112-115, 234, 247
- Computer-aided Engineering (CAE) systems, 96-97
- Conjugate gradient method, 89
- Calculus of variations, 9-10, 12
- Carbon fibre composite material. (*see* Material, Carbon fibre composite)
- Checking:
  - data, 96, 144
  - mesh, 134, 137
    - coincident nodes, 138, 150-151
    - exploded mesh, 139
    - free-edge, 139
    - free-face, 138
  - model, 94, 109, 117, 151, 255
  - solution, 93-94, 150, 159
- Command files, 96, 109, 150-151, 153
- Commercial software, 7, 14-16, 36, 54-57, 70-71, 74, 79, 92, 98, 101, 116, 129, 133, 136-137, 167, 179, 184, 192, 209-210, 212, 214, 231
- Communication of design solutions, 3, 100
- Comparison of finite element and classical solutions, 169-173
- Compass point notation, 142
- Compatibility, 6-8, 20, 28-29, 37, 39-42, 49, 53-54, 59, 66, 79, 122, 125, 172, 206
- satisfying, 53-54
- Completeness, 59, 71
- Complementary energy, Principle of minimum 57
- Compliances, 34
- Composite material, (*see* Material, composite)
- Composite material I-beam example, 192-209
- Computer, 97-101
  - aided design, 44, 74, 103, 113, 115, 129, 247, 250
  - hardware, 16, 43, 56, 91, 96-101, 103, 106-108, 145, 152-154, 156, 191, 202
  - graphics, 152-154
    - minicomputers, 98, 101
    - minisupercomputers, 98, 101, 152
    - personal computers, 97, 100, 107
    - parallel, 16, 97-8
    - massively, 98
    - supercomputers, 88, 98, 101, 107
    - workstations, 97-8, 101, 107, 145, 152-153
  - networks, 97-98, 109, 153
- peripherals, 97-100
- software:
  - commercial, 7, 14-16, 36, 54, 56-57, 68, 70-71, 74, 79, 92, 98, 101, 116, 129, 133, 136-137, 167, 179, 184, 192, 209-210, 212, 214, 231
  - for finite element analysis:
    - pre-processors, 16, 94-96, 106, 129-150, 152-153, 160, 195, 200, 214, 241
    - post-processors, 16, 94, 96-98, 103, 106, 109, 137, 150, 153-154, 156, 158, 182, 185-186, 204-205, 207, 226, 238
  - solvers, 85, 94-97, 103, 107-109, 111, 122, 136, 140, 149-153, 159, 167, 182, 195-196, 204, 252-253, 258-259
  - utilities, 94, 96-97
- specifying, 102-106
- speed:
  - millions of instructions per second (mips), 100, 106
  - millions of floating point operations per second (MFLOPS), 100, 106
- Concept design, 3
- Condensation technique, 77
- Conforming element, 59, 63
  - non-, 79
- Connecting rod example, 239-245
- Connections, 9, 53, 113, 209-210, 212
  - semi-rigid, 9
- Connectivity list, 84, 97, 118, 138, 149, 152
- Consistent element force vector, (*see* Element, force vector)
- Consistent transformation, 51-52, 61, 62, 75, 77, 146, 180
- Contour plots, 78, 96, 154, 158-159, 167-173, 182, 191, 203-204, 222, 226-230, 239-240, 244-245, 248
- Control,
  - of solution, 149-152, 253
- parameters, 92, 95, 235
- Convergence, 7, 59, 63, 66, 109, 119-120, 122, 136, 161, 179, 220, 253, 258-259
- Constraints, 77, 81, 85, 108-109, 119, 124-125, 149, 243
  - on design variables, 3, 256-257
  - multi-point, 108
- Coons patch, 114, 129
- Coordinates, 13-14, 21-23, 33, 40, 48, 60, 78-79, 96, 107, 113-114, 118, 129, 148-149, 152, 165, 177, 180, 182, 185, 199, 221
  - generalized, 49-50
  - global, 57, 59, 61-62, 65, 76-77, 125, 128, 156-158, 160
  - local, 57, 63, 125, 128, 142, 154, 197, 200, 204
  - natural, 64-78
  - polar, 162
- Cost function, 256-257
- Coupon test, 31, 38, 175, 194, 197
- Crank-Nicholson method, 253
- Constructive Solid Geometry (CSG) solid model, 115, 116, 233
- Cuthill-McKee algorithm, 137
- Cutting plane, 154, 158
- Damping matrix, 254

- Data:
  - checking, 96, 144
  - files, 96–97, 107, 150–152, 155
  - management, 93–94, 149–150
  - storage:
    - disk, 2, 97–100, 106–107, 149–150, 152, 254, 259
    - primary, 103, 106
    - secondary, 98, 103, 106–107, 254
- Dead load, 19, 161, 189, 210, 227, 237–238
- Decomposition:
  - cell, 117
  - LU, 86
- Deformation, 12–13, 18, 20, 26–35, 47–52, 75, 82, 118, 120, 124
  - of bar, 38
  - of beam, 40, 56, 64, 78, 120
  - of examples, 163, 167, 177, 180, 182, 189–191, 195–206, 210, 214, 216, 225, 238, 259
  - of shell, 80, 120
  - large, 7, 19, 44, 191, 259
- Delaunay triangulation, 130, 133, 135
- Design:
  - analysis, 4, 37
  - communication, 3
  - detailing, 3
  - evaluation, 3–4
  - generation of solutions, 3
  - of frame, 209–230
  - process, 1–6, 9–10, 12, 17, 25, 29, 32, 34–36, 42, 44, 56, 58, 78, 91–93, 109, 175, 204, 232, 240, 255–256
  - situations, 5–6
  - specification, 3, 92, 123, 141
  - of examples, 160, 176, 179, 185, 189, 194, 198, 204, 210, 244, 248–249
  - synthesis, 3
  - variable, 175, 256–257
- Differential operator matrix, 28, 51, 67
- Dimensions, effect on model size, 37, 55–56, 102, 121
- Discontinuities, 108–109, 120, 124–125, 159, 174–175, 183, 185–186, 189, 191
- Discretization of space, (*see* Mesh, generation)
  - effect on solution speed, 103
- Disk storage, 2, 97–100, 106–107, 149–150, 152, 254, 259
- Displacement:
  - distributions, 9–13, 15, 49–51, 53–54, 57–58, 62, 66, 74–75, 80
  - requirements, 58–59
- Display:
  - of geometry, 154, 167, 179
  - of results:
    - contour plots, 78, 96, 154, 158–159, 167–173, 182–191, 203–204, 222, 226–230, 239–240, 244–245, 248
    - deformed geometry, 96, 158, 167–168, 182–184, 203–204, 216, 226, 238, 243–244, 250–251
    - vector plots, 96, 158
- Direct:
  - method:
    - solving simultaneous equations, 9, 16, 85–89, 149, 152
  - search method, 256–257
  - stiffness, 9, 13–15, 85–86
- Divergence, 253, 258
- Domain creation, 129
- Drawings, engineering, 3, 5, 44, 177, 240
- Dynamic magnification, 210
- Dynamics of structure, 4, 43, 81, 101, 109, 127, 210, 213, 227, 249, 254–255
- Eigenvalue, 149, 255, 259
- Eigenvector, 255
- Elastic:
  - constants, 20, 29, 30, 33–34, 44, 81, 142, 165, 175, 194–195, 200, 213, 215, 260
  - range, 32, 34
- Elasticity, 8, 18–46, 53–54, 56, 202
  - classical, 9, 12, 14–15, 21, 108, 161–163, 173
- Element, 54–56
  - aspect ratio, 74, 121–122, 124, 156, 220, 222
  - axisymmetric:
    - formulation, 80
    - use of, 80, 101, 119, 121, 176
  - bar:
    - formulation, 54–55, 59–62, 66–68, 70, 72
    - use of, 112–113, 118–119, 209, 225, 238
  - beam:
    - formulation, 78–79
    - use of, 15, 112–113, 118, 120, 122, 124–125, 209, 214–220, 228, 248
  - brick, (*see* Element, solid)
  - characteristics, 11–15, 51–52, 57, 61–65, 75, 77–78, 80
  - compatibility, 53, 63, 79, 122
  - contact, 122–123
  - crack, 81
  - distribution of, 158
  - distortion of, 74
  - equations, assembly, 7, 52, 61, 62, 82–85
  - force vector, 11–14, 52, 56–57, 61, 82, 83
    - consistent, 51–52, 57–58, 60, 61–63, 72, 75–77, 146, 180
  - gap, 81, 85, 119, 123
  - hierarchical, 66
  - interior angles of, 74
  - lumped mass, 54, 253
  - master, 64–68, 70, 74, 77, 166
  - membrane, (*See* Element, plane stress/strain or membrane)
  - nodal degree of freedom vector, 11–15, 50–54, 56–58, 60–63, 72, 75–79, 82–83, 257

- plane stress/strain or membrane:
    - formulation, 13–14, 54–56, 61–65, 68, 70–75, 77–78, 80
    - use of, 82–85, 119–120, 124, 126–127, 130, 132–133, 136, 161–174
  - plate bending:
    - formulation, 55, 59, 77, 80
    - use of, 115, 121–122
  - requirements of, 53–54
  - shape functions, 11, 13, 51–52, 57–80, 177, 253, 260
  - shell:
    - formulation, 55, 59, 64, 77–81, 177, 195–197, 206
    - Mindlin, 80, 177, 195, 206
    - use of, 119–122, 124–125, 148, 174, 177–184, 191, 195, 199–207, 210, 212, 220–231, 233, 235, 238–239, 250–251
  - solid:
    - formulation, 63, 74–75
    - use of, 80, 119–121, 123, 133, 196, 220, 241–245, 247–249
  - special, 47, 79, 81
  - stiffness matrix, (*see* Matrix, element stiffness)
  - stress-hybrid, 57
  - sub-parametric, 65
  - super-parametric, 65
  - transition, 81, 122
  - types, choice of, 63, 112, 120, 123, 125, 177
- Embodiment design: 3
- Energy:
  - method, 9–12, 15, 38, 47–52, 182, 253
  - Principle of complementary, 57
  - Principle of minimum potential, 10–12, 47–50
- Engineering drawings, 3, 5, 44, 177, 240
- Equations:
  - algebraic, 9, 14–15, 50, 52, 61
  - assembly, (*see* Assembly of equations)
  - compatibility, 28–29, 39–41, 172
  - equilibrium, 37, 40, 53, 172, 205
  - stiffness, (*see* Stiffness, equations)
  - stress-strain, (*see* Stress, -strain relationships)
- Equilibrium, satisfying, 7, 20–25, 37, 53–54, 206, 212–213, 226
- Errors, 93, 107, 137, 150
  - of discretization, 53–54, 70, 74, 79, 120
  - of distorting element, 124, 130, 148
  - estimation of, 15, 36
  - handling of, 5
  - of geometry modelling, 129–130
  - of integration, 64
  - of off-set element, 122
  - residual, 88, 152
  - round-off, 56, 74, 81, 108, 117, 120
  - of solution, 88–89, 135
  - in solving examples, 166, 171, 178–180, 182, 184, 206–207, 209, 243, 249
- Essential boundary conditions, 14
- Evaluation of designs, 3–4
- Examples:
  - bicycle frame, 231–239
  - Brazilian tensile test, 161–174
  - composite laminate beam, 192–209
  - connecting rod, 239–245
  - machine support frame, 209–230
  - pressure vessel, 174–191
  - suspension arm, 246–249
  - vehicle body shell, 249–251
- Explicit methods, 253
- Eye position, 155–156
- Faces, of an element:
  - applying boundary conditions, 93, 143–146, 148, 180
  - finding free faces, 138
- Failure criteria, 5, 23, 35–36, 108, 123, 141, 162
  - Tresca or maximum shear stress, 36
  - von Mises' or distortional, 36, 78, 154, 160, 168, 206, 222, 229–230, 239, 244
- Fatigue, 4, 6, 30, 35, 43, 209–210, 212, 218, 220, 222, 227, 240, 243–234
- Files:
  - ASCII, 107, 149, 151–153
  - binary, 107, 151–152
  - command, 96, 109, 150–151, 153
  - data, 96–97, 107, 150–152, 155
  - EBCDIC, 151
  - neutral, 97, 149
  - results, 151–152
- Finite difference method, 7, 10, 42
- Finite element method,
  - assembly of equations, 7, 52, 58, 61, 82, 84, 86
  - connectivity list, 84, 97, 118, 138, 149, 152
  - Galerkin method, 10, 17
  - research, 7, 14–15, 120, 122, 130
  - shape functions, (*see* Element, shape function)
  - stiffness matrix, (*see* Stiffness, matrix)
  - test (or trial) function, 11, 260
  - variational form, 12, 47–50
- Flexural modulus, 197–198, 206, 209
- Force:
  - body, 19, 24, 25, 38–40, 48–49, 52, 76–77, 92
  - matrix method, 10
  - vector:
    - element, (*see* Element, force vector)
    - global, (*see* Global, force vector)
- Fracture, 30, 35–36, 68, 81
- Free mesh, (*see* Mesh, free)
- Free-face, 138–139, 144–145, 151, 154
- Functional, 12, 48–51, 91, 256
- Functions:
  - admissible, 12, 49, 50–51, 214, 223
  - cost, 256–257
  - objective, 256–257
  - shape, (*see* Shape, function)

- Galerkin method, 10, 17
- Gauss:
  - Legendre quadrature rule, 69, 72
  - points, 69, 72, 75, 77-78, 124, 168, 184
  - rule, 69
  - Seidel method, 87-88
- Generalized:
  - coefficients, 59-60, 62-63
  - coordinates, 49-50
- Generation of design solutions, 3
- Geometry:
  - creation, 129
  - description, choice of, 117
  - models:
    - wireframe, 112-115, 234, 247
    - surface, 114-115, 129
    - solid, 115-117, 233
  - sources:
    - analytical equations, 44
    - Computer-aided Design (CAD), 44, 74, 103, 113, 115, 129, 247, 250
    - engineering drawings, 3, 5, 44, 177, 240
    - measurement of models, 44
  - specification, 44
  - surface, 114-115, 129
- Global:
  - stiffness matrix, (*see* Matrix, global stiffness)
  - nodal degree of freedom vector, 14, 50, 52-53, 61, 77, 84
  - force vector, 12, 14, 52, 77, 84
- Graphics:
  - concepts:
    - cutting plane, 154, 158
    - eye position, 155-156
    - hidden-line display, 145, 157-158
    - magnification, 156, 182
    - target position, 155-156
    - up direction, 155-156
    - view area, 156
    - volume clipping, 157
    - zooming in, 153, 156, 227
  - hardware, 98, 100-101, 103, 107, 145, 152, 154, 202
  - button box, 153, 156
  - mouse, 153
  - Visual Display Unit (VDU), 153
  - software, 97, 100, 107, 141
  - using, 152-155
- Half-bandwidth, 56, 86, 136, 137
- Hardware specification, 43, 56, 96, 101, 103, 106, 108
- Heat transfer, 4, 6, 43, 82, 102
  - links to structure, 252, 260
- Hidden-line display, 134, 145, 157-158
- Hierarchical elements, 66
- Hierarchy of entities, 113, 120, 128-129, 154, 177
- Historical development, 1, 6-16, 47, 50
- Hooke's Law, 29, 32, 194
- Homogeneity, 25, 29-30, 33-34, 195, 213, 141, 161, 163, 174, 192-193
- Ill-conditioning, 74, 121, 124, 213
- Implicit methods, 253
- Inconsistent:
  - loading, 77
- Initial conditions, 13, 32, 44, 48-49, 52, 61, 76-77, 79, 81, 91-93, 95, 109, 149, 254, 257-258, 260
- Instability of mesh, 75, 119
- Integration, 47, 49-50, 61, 64, 79
  - closed-form, 64
  - full, 75, 78, 253
  - numerical, 47, 64, 67, 73, 72-76, 253
    - in one dimension, 68-70
    - in two dimensions, 72
  - points, (*see* Gauss, points)
  - reduced, 75
  - rule:
    - Gauss quadrature, 69
    - Gauss-Legendre quadrature, 69, 72
    - Newton-Cotes, 69
    - Simpson's, 69
    - Trapezoidal, 69
- Interfacing software, 95-96, 103-104, 109, 129
- Irregular mesh structure, (*see* Mesh, irregular)
- Isoparametric elements, 57, 62, 64-67, 70-72, 74-78, 80, 120, 128
- Isotropy, 63
- Iteration:
  - controlling, 149, 258
  - processes:
    - in design, 3, 93-94
    - in mesh generation, 130
    - to resolve nonlinearity, 85, 254, 258-259
    - to solve simultaneous equations, 86-89, 149, 152
    - with time variation, 254, 258-259
  - solution methods:
    - Crank-Nicholson, 253
    - conjugate gradient, 89
    - Gauss-Seidel, 87-88
    - Jacobi, 87
    - line relaxation, 88
    - multigrid, 89
    - point relaxation, 88
    - preconditioning, 89
    - Stone's method, 88
    - successive overrelaxation, 88
- Jacobi method, 87
- Jacobian, 67-68, 72, 124
  - boundary, 76-77
  - matrix, 72
- Joints, 109, 209-210, 246, 248
  - analysis of, 123, 204, 210-222, 243
  - fabrication of, 210, 233

- pin-, 62, 148, 210, 212, 214–215
- rigid-, 210, 212–220, 233
- Keyboard, 153
- Kirchoff's assumption, 195, 197, 199
- Lagrangian:
  - elements, 67, 70–72, 76
  - strain, 25
- Lamina, 193–195, 200
- Laminate:
  - element, 195, 197, 201, 204–205
  - material, 36, 81, 192–198, 200, 202–205
- Line relaxation method, 88
- Load, 18–20, 44–45, 47–49, 80–81, 108–109, 119, 124
  - applied to examples, 85, 161–163, 165–166, 173–174, 176, 183, 189, 196, 201–202, 209, 212,
  - 214–217, 223–225, 231, 237–238, 241, 243, 246, 248, 252, 254
  - axial, 30–32, 35–36, 38–39
  - axisymmetric, 80
  - boundary conditions, 36–37, 143, 146–148
  - dead, (*see* Dead, load)
  - distributed, 13, 52, 61, 75–77
  - element nodal force vector, (*see* Element, nodal force vector)
  - global nodal force vector, (*see* Global, nodal force vector)
  - live, 19
- Locking of mesh, 79, 108, 119, 122
- LU decomposition, 86
- Lumping:
  - load, 77
  - mass, 54, 81, 253
  - properties, 39, 80, 197, 204, 214
- Machine support frame example, 209–230
- Mapped mesh, (*see* Mesh, mapped)
- Mapping, 65, 128
  - from/to master element, 65–68, 72
  - distortion, 70–71, 73–74, 77, 117, 122–124, 178, 200, 221, 244
- Massively parallel computer, 98
- Master:
  - degrees of freedom, 255
  - element, (*see* Element, master)
  - shape function, (*see* Shape function, master)
- Material, 29–36
  - anisotropic, 30, 34, 44, 46, 81, 192–195, 197, 206, 209
  - brittle, 35–36, 42, 161–163
  - carbon fibre composite, 193–194, 196, 200–201
  - composite, 29, 30, 32, 34, 36, 81, 141, 192–209, 231, 246–249
  - orthotropic, 193–194, 201
  - plastic, 29–30, 32, 36, 174–175, 189, 191
  - properties, 20, 29–32, 34–36, 38, 44–45, 81, 92–93, 122–124, 141–142, 151, 193–195, 197, 206, 209, 257, 260
  - specification, 42–43, 141–142, 165, 175–176, 200, 213, 229, 237, 242, 247–248, 250
  - steel, 29–35, 45, 81, 167, 176, 213, 215, 229, 237, 239, 250
- Matrix:
  - damping, 254
  - differential operator, 28, 51, 67
  - element stiffness, 11–15, 28, 51–52, 56–58, 60–68, 70, 72, 74–75, 78–79, 81–83, 124, 195, 257, 259
  - global stiffness, 14, 50–53, 56, 59, 61, 77–78, 82–85, 149, 254–255, 257–258
  - Jacobian, 72
  - mass, 253–255
  - material property, 33, 41, 48, 53, 57, 61–63, 72, 77, 79, 81, 194–195, 258
  - shape function, 51–52, 57–68, 75–76, 79, 253, 260
  - spatial derivative(s) of field variable(s), 51, 53, 57, 60, 62–63, 67, 69–70, 72, 77, 79
  - system matrix, 255
  - Vandermode, 60, 62, 64, 67, 79
- Membrane deformation, 13, 40–41, 62–63, 80, 82, 119–120, 124, 127, 161–174, 177, 184–185, 188, 194–195, 197, 199, 201, 206, 208
  - element, (*see* plane stress/strain or membrane)
- Mesh, 7, 44, 64, 93, 96, 111–139
  - adaption, 136
  - enrichment, 134–136
  - refinement, 53, 56, 109, 120–121, 123, 134–136
  - boundary, 92, 95, 130, 132
  - finding, 137–138
  - checking, 134, 137
  - generation, 44, 71, 73, 81, 92, 95, 112–114, 117–120, 123–125, 128–129, 159, 177, 250
  - algorithms:
    - Delaunay triangulation, 130, 133, 135
    - advancing front method, 133
    - Octree methods, 131, 133
    - Quadtrec methods, 131, 133
  - examples, 11, 56, 82–85, 131–136, 166–167, 177–180, 199–200, 215, 221–222, 234, 237–237, 241–242, 247, 250–251
  - need for, 118
  - simple, 82–86, 114, 136, 145
  - using:
    - commercial software, 92
    - local software, 92
  - instability, 75, 119
  - locking, 108, 119, 122
  - parts:



- mesh (*continued*)
- elements, 53, 56, 63, 77, 92, 94, 103, 112, 114, 117–140, 142–144, 147–148, 151–152, 154, 157, 160–161, 165–166, 169, 174, 177–179, 199–200, 214–215, 221–223, 231, 235, 241, 247, 250, 259, 260
  - nodes, 92, 94, 103, 107, 114, 118, 122–123, 125–127, 130–140, 142–144, 147–148, 152, 157, 159, 166, 174, 178–179, 200, 215, 222, 235, 250, 259
  - refinement, 59, 108, 124, 134–136, 161–191
    - h-, 109, 136, 169, 174, 179, 183, 189
    - hp-, 136
    - p-, 109, 136, 161, 166, 169
  - structure, 125–129, 136
    - comparison of, 56
    - determining, 114, 118, 125–128
    - regular, 10, 125–127, 135
    - irregular, 13, 125–127
  - topology, (*see* Mesh, structure)
  - types:
    - free (and unstructured), 74, 102, 125, 127, 129, 133, 138–139, 154, 160–161, 166, 234
    - mapped (and structured), 10, 125–127, 129, 135, 142–146, 154, 157–160, 174, 177–179, 221–222, 241, 247
- Millions of floating point operations per second (MFLOPS), 100, 106
- Mindlin theory, 79–80, 120, 177, 195, 197, 206
- Minicomputer, 98, 101
- Minimization, 9, 50–53, 256
- Millions of instructions per second (mips), 100, 106
- Mode:
  - failure of, 36, 45, 194
  - of instability, 36
  - of vibration, 255
  - rigid-body, 59
  - shape, 252
- Model checking, (*see* Checking, model)
- Modulus:
  - elastic constants, 20, 29, 30, 33–34, 44, 81, 142, 165, 175, 194–195, 200, 213, 215, 260
  - flexural, 197–198, 206, 209
  - section, (*see* Section, modulus)
  - shear, 34, 40, 194, 197–199, 208–209, 214
  - Young's, 29, 32–35, 40, 44, 92, 141, 175–176, 194, 198, 209, 213, 237, 248
- Mohr's circle, 23, 28
- Moment, 47–52
  - causing bending, 19–20, 40, 45, 79, 194, 198, 212, 214–217, 223, 225
  - curvature expression, 79, 197–198, 204
- Mouse, 153
- Multigrid method, 89
- Multi-point constraint, 108
- National Agency for Finite Element Methods and Standards (NAFEMS), 15, 80
- benchmarks, 16, 71, 120
- Natural:
  - boundary conditions, 14
  - coordinates 64–78
  - frequency, 255
- Need:
  - recognition of, 2
- Network, 97–98, 109, 153
- Neutral files, 97, 149
- Nodal:
  - degree of freedom vector, element, (*see* Element, nodal degree of freedom vector)
- Node:
  - interior, 68–71, 74, 77
  - numbering, 136–137
- Non-dimensional quantities, 162–172
- Nonlinearity, 86, 109, 140, 149, 254
  - of geometry, 7, 19, 44, 191, 259
  - of material properties, 7, 15, 34–35, 44, 102, 168, 162, 251, 253, 259
- Number crunching, 96–98
- Numerical:
  - control parameters, 92, 95, 149, 235, 252
  - error, 56, 64, 70, 74, 81, 90, 108, 117, 122, 124, 130, 135, 166, 178, 180, 185, 209
  - integration, 47, 64, 68–70, 72–76, 253
  - solution process, 82–89, 119, 122, 135, 137, 147
- Non-uniform rational B-spline (NURBS), 115, 129
- Objective function, 256–257
- Objectives, 246
- Octree methods, 131, 133
- Optimization, 13, 101–102, 140, 149, 171, 252, 255–257
- Orthotropic material, (*see* Material, orthotropic)
- Parallel computer, massively, 16, 97–98
- Parent, (*see* Master)
- Partial differential equations, 6–14, 24–25, 36–37, 54, 82, 91, 103, 109, 129, 136, 142
- Pascal's triangle, 63, 71
- Patch test, 59, 80, 119–120, 177
- Pattern search method, 256
- Peripheral devices, 97–100
  - backup devices, 98, 100
  - graphics displays, 97, 100, 134, 152–154
  - hardcopy devices, 100
  - data storage, 98, 106
- Personal computers, 97, 100, 107
- Pixel, 100, 153
- Plane:
  - element, (*see* plane stress/strain or membrane)
  - strain, 10, 13, 41–42

- stress, 13, 40–42,
  - example of, 161–174
- Plastic material, (*see* Material, plastic)
- Plasticity, 7, 15, 34–35, 44, 102, 168, 251
- Plates, 13, 36–37
  - element for bending, (*see* Element, plate bending)
  - element for membrane action, (*see* Element, plane stress/strain or membrane)
- Plotting, (*see* Display, contour plots)
- Point relaxation method, 88
- Poisson's:
  - equation, 260
  - ratio, 29, 32, 44, 92, 175–176, 194, 213, 237, 248
- Polymer, 174–175
  - matrix, 193–194
- Polynomial, 11, 49–50, 54, 57–63, 69–75,
  - 113–115, 136
  - incomplete, 63
  - Legendre, 69
- Post-processing, 16, 94–98, 103, 106, 108, 109,
  - 137, 150, 153, 154, 156, 158, 182, 185–186, 204–207, 226, 238, 241
  - results analysis, 151–159
  - software tools, 94, 96, 103, 153–158
- Potential energy, 9–12, 47–51
  - Principle of minimum, 10–12, 47–50
- Pre-processing, 6, 16, 94–96, 106, 152–153, 160,
  - 193, 200, 214, 241
  - stages in process, 94–95, 129–150
    - geometry generation, 94, 129–130
    - mesh generation, (*see* Mesh, generation)
    - setting boundary conditions, 93, 141–148
    - setting initial conditions, 95
    - setting numerical solution parameters, 95, 149
  - software tools, 94–96
- Preconditioning methods, 89
- Pressure vessel example, 174–191
- Properties of a material, (*see* Material, Modulus, Poisson's ratio, strength)
- Quadrature, (*see* Integration, numerical)
- Quadtree methods, 131, 133
- Quality assurance (QA), 103–104
- Quasi:
  - isotropic, 201, 204
  - static load, 210–211
- Random Access Memory (RAM), 97–100, 106
- Rayleigh–Ritz method, 9, 49–50
- Refinement:
  - mesh, 59, 108–109, 124, 134–136, 161–191
  - model, 94, 159–160, 161–191, 209–231
- Regular structure:
  - geometry, 141
  - mesh, 110, 125–127, 129, 135, 142–146, 154, 157–160, 177–179, 199–200, 222, 241, 247
- Relaxation:
  - method, 9
  - successive over–, 88
  - parameter, 148, 253, 258–259
  - point, 88
  - technique, 258
- Residual:
  - error, 88, 152
  - methods,
    - weighted, 10, 15, 261
  - stress, 48, 81
- Restraints, 6, 39, 43, 44, 84–85, 92, 146–148, 150
  - of examples, 164–165, 175–177, 180–183, 201–202, 215, 222–223, 238, 248, 250
- Results analysis, 43, 53, 78, 81, 93–94, 108–110,
  - 124–124, 135, 141, 152–154, 157–158, from ASCII files, 151–2
  - of examples, 161–250
  - using graphics, 16, 96–98, 103, 108, 109, 137, 150, 153–154, 156, 158, 185–186, 204–207, 226, 238
- Requirements:
  - of the analysis, 42–43, 112, 161, 164, 174–175, 185, 192, 196–197, 209–212, 220, 231, 240, 246, 249
  - of displacement distributions, 58–59
- Rigid-body modes, 59
- Saint–Venant's principle, 38–39, 186, 223
- Search method:
  - direct, 256
  - pattern, 256–257
- Section:
  - modulus, 197–199, 208–209
  - properties, 215
- Semi-discrete form, 253
- Sensitivity analysis, 257
- Shape function, 11, 13, 51–52, 57–80, 253, 260
  - Hermitian, 66
  - Lagrangian, 67–68, 70–72, 77
  - master, 64–67, 70–71, 74–75, 77, 80, 177
  - matrix, (*see* Matrix, shape function)
  - serendipity, 70–71, 74
- Shear:
  - deformation, 78–80, 195–200, 208–209
  - force, 198, 206, 212, 216, 223
  - modulus, 34, 39–40, 194, 197–198, 208–209, 214
  - strain, 25–29, 32–37, 39–42, 206
  - stress, 21–25, 32–37, 39–42, 77, 164, 168–171, 177, 205–206, 216, 225
- Shell:
  - element, (*see* Element, shell)
  - theory, 79–80, 197
    - Mindlin, 80, 120, 177, 195, 206

- Simultaneous equations, 9–10, 52–53, 58, 77
- solution:
  - direct method, 85–86
  - iterative methods:
    - Crank–Nicholson, 253
    - conjugate gradient, 89
    - Gauss–Seidel, 87–88
    - Jacobi, 87
    - line relaxation, 88–89
    - multigrid relaxation, 89
    - point relaxation, 88
    - preconditioning, 89
    - Stone's, 88–89
    - successive overrelaxation, 88
- Singularity, 68, 161–163
- Slender:
  - members, 9, 17, 45, 56
- Software:
  - commercial, (*see* Commercial, software)
  - perpetual licences, 104–105
  - specification, 94–97, 102–106
  - suppliers, 103–110
- Solid element, (*see* Element, solid)
- Solid model, 112, 115–117
  - B–rep, 115–117
  - Constructive Solid Geometry (CSG), 115–117, 233
  - of bicycle frame, 231–234
  - of connecting rod, 240–241
- Solution:
  - accuracy, 36, 77–78, 81, 119–123, 134–136, 142, 152
  - of examples, (*see* Accuracy, of examples)
  - checking, 93–94, 150, 159
  - control, 92, 95, 149–152, 253
  - of linear simultaneous equations, 85–89
    - direct methods, 85–86
    - iterative methods, 85
      - Crank–Nicholson, 253
      - conjugate gradient, 89
      - Gauss–Seidel, 87–88
      - Jacobi, 87
      - line relaxation, 88–89
      - multigrid, 89
      - point relaxation, 88
      - preconditioning, 89
      - Stone's, 88–89
      - successive overrelaxation, 88
  - singular, 82, 151, 260
  - stability, 254
- Solver, 85, 94–97, 103, 107–109, 111, 122, 136, 140, 149–153, 159, 167, 182, 195–196, 204, 252–253, 258–259
  - running, 107–108, 150–151, 167, 182
  - re-running, 159
- Specification:
  - design, (*see* Design, specification)
  - hardware, 43, 56, 96–101, 103, 106, 108
  - geometry of examples, 162, 164–165, 174–175, 177, 199, 211, 214–215, 220–222, 225, 231, 233, 240–241, 247
  - geometry of structure, 44
  - material properties, 42–43, 141–142
  - for examples, (*see* Material, specification)
  - of problem, 2–3, 42–45, 92, 111–112, 162, 171–177, 196–197, 210–212, 232, 240–241, 246, 249
  - software, 102–106
- Speed:
  - of solution, 55–56, 96–103
- Split tensile test example, (*see* Brazilian test example)
- Steel:
  - frame, 9, 209–230
  - material, (*see* Material, steel)
  - members, 45, 198, 209–230
- Stiffness:
  - equations, 13–15, 50–53, 61, 82–85, 98
  - matrix, 11–15, 28, 50–53, 56–58, 60–68, 70, 72, 74–75, 77–79, 81–85, 124, 149, 195, 254–255, 257–259
  - method:
    - direct, 9, 13–15, 85–86
- Stone's method, 88–89
- Strain:
  - axial, 25–29, 32–36, 39–41, 56, 67, 78
  - displacement relationship, 27–28, 51, 64
  - direct, (*see* Strain, axial)
  - energy, 12, 48–51, 57–78, 75
  - engineering, 25–27
  - initial, 13, 48–51, 61, 76–77, 81, 92, 260
  - Lagrangian, 25
  - normal, (*see* Strain, axial)
  - plane, 10, 13, 41, 56, 62, 64
  - principal values, 28
  - shear, (*see* Shear, strain)
  - true, 27
- Strength:
  - yield, 32, 35–36, 45, 160, 213, 222, 228–230
  - ultimate, 35–36, 45, 123
- Stress:
  - at a point, 20–21, 25
  - axial, 21–25, 30–42, 56, 79–80, 216–248
  - concentration, 108, 135–136, 160, 161–174, 223
  - distribution, 10, 57, 123, 260
  - direct, (*see* Stress, axial)
  - engineering, 20
  - experimental, 30–36, 246, 248
  - from elements, 14, 53, 61–63, 75, 77–78, 119, 123, 152, 166, 168, 183–185, 220, 258
  - from isoparametric elements, 77–78
  - functions (Airy), 6, 14, 17, 41–42, 162
  - gradient, 127, 161, 165–166, 168–174
  - hybrid element, 57
  - infinite, 163
  - initial, 48–49, 52, 61, 76–77, 81, 92, 260
  - intensity, 96

- from laminate, 196–197, 204–208
- local, 209
- mean, 6, 244
- normal, (*see* Stress, axial)
- peak, 43, 117, 212, 227
- peel, 205
- plane, 13, 40–41, 61–64, 80, 161–174
- plots, 78, 96, 154, 158–159, 167–173, 184–191, 226–230, 239–240, 244–245, 248
- principal values, 23, 28, 36, 78, 160, 185–189, 206, 227–229
- proof, 35
- range, 6, 183
- residual, 48, 81
- resultants, 194
- shear, (*see* Strain, shear)
- strain relationships, 6, 8, 30–34, 48, 50, 61, 64, 79, 81, 168, 172, 194, 260
- superaccurate, 78
- superconvergent, 78
- tensor, 21
- total, 21
- von Mises', 154, 159, 160, 168, 206, 222, 229–230, 239, 244
- yield, (*see* Strength, yield)
- Structured mesh, (*see* Mesh, mapped)
- Structures:
  - load-bearing, 18–20
- Sub-:
  - region model, 9–13, 69, 92
  - parametric element, 65
  - structuring, 108, 121, 191–192, 210, 215, 218, 220–230
- Successive overrelaxation method, 88
- Supercomputers, 88, 98, 101, 107
  - mini-, 98, 101, 152
- Super-parametric element, 65
- Superposition, principle of 32
- Surface:
  - descriptions, 44, 73–74, 112–117, 128–129, 177, 234–235, 247
  - Bezier, 114–115, 129
  - Coons, 114, 129
  - Non-uniform rational B-spline (NURBS), 115, 129
  - tractions, 37, 48–49, 51–52, 76–77
- Suspension arm example, 246–249
- Symmetry, 108, 117–118, 161, 164–166, 173–174, 176–177, 180, 182–183, 194, 199, 211, 225, 241
  - axial, 118
  - boundary condition, 118, 165, 182, 201–202, 243
  - cyclic, 118
  - mirror, 118, 162, 174, 176, 199, 243
  - repetitive, 118
- Target position, 155–156
- Taylor series, 24, 26–27
- Thermal, 4, 6, 43, 81–82, 102, 127, 160, 260
  - conductivity, 29
  - effects on structure, 4, 81, 109, 252, 260
  - elements, 55, 81
  - Poisson's equation, 260
- Three dimensions:
  - modification from two dimensions, 55–56, 120, 129
  - numerical integration, 72
- Time:
  - dependence, 18, 30, 43, 81, 101–102, 140, 210, 252–255
  - Explicit methods, 253
  - Implicit methods, 89, 253
  - variation, 56, 85, 254–255
- Topology, of mesh, 125–126, 136
- Torsion, 9, 19, 39, 249
  - element, 214
- Tractions, surface, 37, 48–49, 52, 77
- Transformation:
  - axis, 23, 28, 61, 78, 125, 157, 194
  - consistent, 51–52, 61–62, 75–77, 146, 180
- Tresca criterion, 36
- Troubleshooting, 140, 150–151
- Universities, 1, 7, 14, 71, 110
- Unstructured mesh, (*see* Mesh, free)
- Up-direction, 155–156
- User, 96, 98, 100, 107, 137, 145, 150, 200
  - current, 105
  - end-, 110
  - experience, 93–95, 104, 111, 127, 135
  - friendliness, 95, 104–105
  - of graphics, 152–159
  - interface, 96, 104
  - multi-, 97–98
  - single-, 97
  - programmed-, 152
  - successful-, 108–111
  - support, 16, 34, 71, 79, 104–106, 110
- Utility programs, 94, 96–97
- Vandermode matrix, (*see* Matrix, Vandermode)
- Variational formulation method, 9–10, 12, 15
- Variational, Calculus of, 9–10, 12
- Visual Display Unit (VDU), 95, 153
- Vector plots, 96, 154, 158–159, 167
- Vehicle body shell example, 249–251
- Vibration, 4, 43, 81, 101, 109, 127, 210, 213, 227, 249, 254–255
  - mode of, 255
- View area, 156
- Visual display system, (*see* Visual Display Unit)
- Visualization, 108, 117, 134, 139
  - of results, 23, 152–153
- Volume clipping, 157
- Volume fraction, 141, 195

## 276 INDEX

- von Mises':
  - criterion, 36, 78, 154, 160, 168, 229
  - stress, 154, 159, 160, 168, 206, 222, 229–230, 239, 244
- Weight, (*see* Load, dead)
- Weighted:
  - residual method, 10, 15
- Welded joints, 175, 209–231
- Windows, Icons, Menus, Pull-Down Screens (WIMPS), 95
- Workstations, 97–98, 101, 107, 145, 152–153
- Yield, 35–36, 160, 163, 168, 229
  - criteria, 36, 78, 154, 160, 168, 229
  - point, 35–36
  - lower, 35
  - upper, 35
  - strength, (*see* Strength, yield)
  - stress, (*see* Strength, yield)
- Young's modulus, (*see* Modulus, Young's)
- Zooming-in, 153, 156, 227